PERFORMANCE-BASED APPROACH FOR EVALUATING THE FIRE RESPONSE OF PRESTRESSED CONCRETE DOUBLE T-BEAMS

By

Nickolas Robert Hatinger

A THESIS

Submitted to
Michigan State University
in partial fulfillment of the requirements
for the degree of

MASTER OF SCIENCE

Civil Engineering

2012

ABSTRACT

PERFORMANCE-BASED APPROACH FOR EVALUATING THE FIRE RESPONSE OF PRESTRESSED CONCRETE BEAMS

By

Nickolas Robert Hatinger

In recent years precast/prestressed concrete (PPC) double T-beams have gained wide popularity in numerous building applications. Since structural fire safety is a high priority, building codes generally specify fire resistance requirements. The current approach for evaluating fire resistance of structural members, including those of PPC double T-beams, through prescriptive-based methods has numerous drawbacks. The guidelines are limited in scope and restrictive in application, since they were developed based on ASTM E-119 standard fire tests. Furthermore, these guidelines are only valid for a narrow range of beams and do not fully account for realistic fire, loading or restraint scenarios. To overcome these drawbacks, a performance-based methodology is applied to evaluate the fire resistance of PPC beams under realistic fire, loading, and restraint scenarios. SAFIR, a special-purpose finite element program, was used to carry a set of numerical analyses to study the effect of various factors governing the fire resistance of PPC double T-beams. In the analysis, high temperature material properties, various load and restraint levels, and material and geometric nonlinearity were accounted for. A realistic failure criterion was also included to determine failure. Results from the analysis indicate that fire scenario, load level, and failure criterion have significant influence on the fire resistance of PPC double T-beams. The steps involved in undertaking a performance-based fire approach are outlined.

ACKNOWLEDGEMENTS

I would like to acknowledge a number of people whom supported me throughout the completion of this research project:

Precast/Prestressed Concrete Institute for awarding Dr. Venkatesh Kodur the Daniel P. Jenny research fellowship to carry out this research.

Dr. Venkatesh Kodur, my advisor, for this opportunity and for his guidance, patience, and exemplary expertise in the field of structural fire engineering.

Rustin Fike, a Ph.D. candidate and fellow fire group member at Michigan State University, for his technical support with SAFIR and proofreading this thesis.

Lansival Jean-Baptiste, a technical support member of SAFIR at the University of Liege, for his mastery in SAFIR.

Dr. Monther Dwaikat, fellow fire group member at Michigan State University, for his contributions in proofreading this thesis.

Last but not least my parents and wife, Kavita, for their love and support.

TABLE OF CONTENTS

LIST OF TABLES

LIST OF FIGURES

KEY TO SYMBOLS

a	distance from member's bottom face to centroid of bottom strand
a_{mod}	modification for the strand axis distances based the member's cross-section
a_{sd}	average distance from member's side face to axis distance of strand
$a_{sd,mod}$	modified average distance from members side face to axis distance of strand
a_{θ}	temperature reduced depth of equivalent rectangular stress block
A	cross-sectional area
A_{eff}	effective area of member
A_k	unfactored load due to fire effect
A_{ps}	cross-sectional area of prestressing strands
A_s	cross-sectional area of steel truss member
$A_{s,provided}$	area of prestressing steel provided
$A_{s,req}$	required area of prestressing steel
b	width of stem at strand centroid
b	width of member
b_{eff}	effective width of members compression face
b_w	width of member
c	distance from extreme compression fiber to neutral axis
c_{avg}	average concrete cover for side strands

c_{bottom} average minimum concrete cover for bottom strands

c_{min} minimum concrete cover

c_{req} required concrete cover to meet fire resistance rating

c_{side} average minimum concrete cover for side strands

C compressive force in strands

d distance from extreme compression fiber to centroid of prestressing steel in tension

d_p distance from extreme compression fiber to centroid of prestressing steel in tension

D unfactored dead load

DL unfactored dead load pressure

e eccentricity between thermal induced force and center gravity of section

E_s elastic modulus of steel truss member

f'_c concrete compressive strength

f_{ck} characteristic compressive cylinder strength of concrete at 28 days

$\mathrm{f}_{pr\theta}$ stress in prestressed reinforcement at factored resistance under elevated temperatures

$f_{ps\theta}$ temperature reduced stress in prestressed reinforcement at nominal strength of member

f_{pu} ultimate strength of prestressing steel

$f_{pu\theta}$ temperature reduce ultimate tensile strength of prestressing steel

f_{py}	specified yield strength of prestressing steel
f_{se}	effective stress in prestressing steel after losses
FRR	fire resistance rating
G_k	characteristic permanent action
h	concrete slab (topping) thickness
h_s	slab thickness
I	moment of inertia
k_p	coefficient used in calculating critical load
k_s	reduction factor for a strength or deformation property dependent on the material temperature
K	axial stiffness of steel truss member
l	length of steel truss member
l	span length
L	unfactored live load
M	thermal induced restraining moment
$M_{Ed,fi}$	deign value of the applied internal bending moment under fire conditions
$\mathrm{M}_{n\theta}$	nominal moment strength of section at elevated temperatures
$M_{Rd,fi}$	design resistance value of the applied internal bending moment under fire conditions
Q_k	characteristic variable action

R_c	nominal moment resistance of a member under ambient temperatures
R_f	applied moment under fire conditions
S	tensile force in strands, unfactored snow load
S_b	section modulus with respect to the bottom fiber of a cross-section
S_b	section modulus with respect to the top fiber of a cross-section
t_f	flange thickness
T	thermal induced axial force
u	distance from strand centroid to bottom of member
U	ultimate load capacity at ambient temperatures
V/S	volume-to-surface ratio
w	uniform load
$w_{Ed,fi}$	factored uniform load under fire conditions
w_f	factored uniform load under fire conditions
Wt	self-weight
W	unfactored wind load
y_b	distance from the bottom fiber to the center gravity of the section
y_s	distance from the centroid of prestressing strands to the bottom fiber
y_t	distance from the top fiber to the center gravity of the section
α_1	ratio of average stress in rectangular compression block to the specified concrete strength

β_1	compressive stress block factor
ε_c	compressive strain in the top fiber of the section
ε_s	tensile strain in prestressing strand
γ_p	factor for type of prestressing tendon
γ_s	partial factor for prestressing steel
$\gamma_{s,fi}$	partial factor for prestressing steel for material in fire design
θ_c	strength reduction factor under ambient temperatures
θ_{cr}	critical temperature of prestressing strand
θ_f	strength reduction factor under fire conditions
σ_p	ultimate stress of prestressing steel
$\sigma_{pr\theta}$	ultimate stress of prestressing steel at elevated temperatures
η	reduction factor for design load level in fire situation
ω	positive steel reinforcement ratio
ω_{pu}	prestressing steel reinforcement ratio
ω'	negative steel reinforcement ratio

Chapter 1

1. Introduction

1.1. General

In recent years precast/prestressed concrete (PPC) construction has gained wide popularity in buildings, bridges, parking structures, and shopping centers. Precast concrete is a type of construction, where concrete is cast offsite in a reusable mould and then cured in a controlled environment until it is transported to the worksite and erected. A common practice in the precast industry is to prestress the concrete to overcome the concrete's natural weakness to tensile stresses. One method to prestress concrete is by casting concrete around already tensioned high-strength steel strands. Once the concrete has partially cured, the strands are released to induce a net compressive force onto the concrete through friction developed between the concrete and the strands. This clamping or prestressing effect improves the capacity of concrete members and has advantages over traditional reinforced concrete (RC). For example, a PPC double T-beam can be used in applications with longer spans than a heavily reinforced double T-beam with a similar cross-section. Other key advantages that have led to the prevalence of PPC construction in today's structural landscape are its desirable span-to-depth ratios, aesthetics, high quality manufacturing, constructability, low maintenance characteristics, aptitude for seismic applications, acoustics, and fire resistance.

Similar to all types of construction, PPC structures must satisfy minimal safety requirements set forth in design codes, including structural fire safety provisions. The fundamental philosophy behind the structural fire safety design of a building is to protect against death, injury, and property loss during the event of a fire. The two main strategies to provide fire safety are categorized as either active or passive fire protection. Active protection systems include sprinklers, smoke and heat detectors, and fire extinguishers. The primary goals of active protection systems are to either automatically or manually prevent the ignition or growth of a fire. These systems are also intended to ensure the safe escape of buildings occupants from harmful temperatures or smoke inhalation. In contrast, passive fire protection systems refer to the fire resistance measures incorporated into building's structural and nonstructural components. By carefully selecting fire resistant construction materials and proper design of building components, passive fire protection can prevent the spread of fire and collapse of a structure. This thesis focuses on the fire resistance (passive fire protection) of a PPC component, more specifically the fire resistance of PPC double T-beams.

1.2. Fire Resistance of Prestressed Concrete

The primary approach to incorporate passive fire protection measures into a building is through proper selection of fire resistant construction materials, such as concrete. One of the many advantages concrete has over alternative construction materials, such as wood, steel or fiber reinforced polymers, is its inherent fire resistance. The fire resistance of concrete is a product of its' constituents, cement and aggregates. Both of these materials possess a low rate of heat transfer and poor thermal conductivity. Upon chemically combining the components, a high fire resistant construction material (concrete) is produced that is virtually inert, non-combustible, and does not emit smoke, toxic fumes, or molten. Concrete's ability to resist fire is one reason for PPC construction prevalence in residential, warehouse, and industrial buildings, as well as, parking structures, justice facilities, stadiums, and arenas.

To ensure fire safety of PPC facilities and their occupants it is crucial to understand how its constituent materials, such as concrete and prestressing steel, respond to elevated temperatures. When concrete is exposed to prolonged fire exposure the hydrated cement paste composing the matrix binding the aggregates will eventually revert back into its initial components, water and cement. This chemical transformation leads to a slow reduction in the concrete's strength and stiffness. The rate of strength and stiffness loss is dependent on the thermal resistance of a concretes mix design. Variations in concrete mixes, such as aggregate type or content, density, moisture content, permeability, porosity, cement composition, and w/c ratio can dramatically affect the concrete's thermal resistance. Therefore, to ensure fire safety, engineers must understand how variations in concrete mix design affect the fire resistance of prestressed concrete.

Prestressing steel reinforcement is the other primary material used in PPC members. When prestressing steel is exposed to fire, a reduction in strength and stiffness occurs at a much faster rate and lower temperatures than concrete and conventional steel bar reinforcement. Furthermore, it is also more susceptible to permanent strength loss and creep. The fire response of prestressing steel is primarily a result of the cold working process utilized to manufacture the reinforcement and due to the fact that smaller cross-sections are required for the high strength material. The smaller cross-section, in conjunction with the high thermal conductivity of steel, result in faster rise in temperatures of prestressing steel when exposed to fire, hence a lower fire resistance. However, when prestressing steel is encased within concrete an additional insulation barrier is provided which delays temperature rise in the prestressing steel. By designing a PPC member with adequate concrete cover, the concrete thickness between the exposed surface and prestressing strand, a remarkably fire resistant structural member is created.

1.3. Prestressed Concrete Beams under Fire

The fire response of PPC beams is dependent on the behavior of its constituent materials and their interaction. When a PPC beam is exposed to fire conditions the temperatures of concrete and prestressing steel increase due to degradation in thermal properties. As the temperatures rise the concrete expands in the longitudinal direction, but the prestressing steel strands expand at a slower rate due to the reduction of temperatures near the stems' center. This gradient of expansive forces induces a compressive force by the prestressing strands causing the PPC beam to camber under typical service loads. The PPC beam will continue to camber until the prestressing steel strands begin to lose their stiffness and strength leading to excessive sagging and ultimately failure. Initially, the sagging of the PPC beam is a direct result of the reduction in strength and stiffness of its constituents' mechanical properties, but just prior to failure high temperature creep amplifies the sagging. Failure occurs once the capacity of the PPC beam has reduced low enough to be overtaken by the demands of the applied loading. The duration of time, starting from the ignition of the fire until failure is attained in the structural member, is defined as the fire resistance of a PPC beam. Fire resistance of PPC beams is influenced by a number of factors such as fire scenario, load level, and restraint.

Fire scenario influences the fire resistance of PPC beams. According to Magnusson and Thelandersson (1970) the fire scenario for a typical compartment fire is dependent on its fuel load and ventilation conditions. These parameters define the fire scenarios duration and severity for both the growth and decay phases of the fire. Special attention should be given to the decay phase because it is in this stage of the fire that a PPC beam cools and can recover a substantial portion of its lost strength and stiffness.

Load level is another factor which affects the fire resistance of PPC beams. A study undertaken by Selvaggio and Carlson (1964) revealed that when higher loads are applied to a PPC beam the fire resistance of the member decreases, since the decreasing capacity falls below the demand due to applied load at a shorter duration.

Restraint at the end supports also impacts the fire resistance of PPC beams. For PPC beams fire induced restraint is introduced when the longitudinal expansion is constrained by supports leading to fire induced axial forces (Gustaffero and Carlson 1962). When the resultant axial force is eccentric to the beams' center of gravity, hence a thermal induced moment is created. Generally, this moment (restraint) enhances the fire resistance by compensating for the prestressing strands' strength loss. However, if the resulting force is located in the deck of a

PPC beam (above the center of gravity of the section) then the thermal induced moment can have a negative effect and may lead to early failure.

1.4. Fire Resistance Design

Structural fire safety is one of the primary considerations in building applications and hence, building codes generally specify fire resistance rating requirements for structural elements. These fire resistance ratings are generally derived based on standard fire resistance tests or through prescriptive-based approaches. As an illustration, the prescriptive-based provisions in ACI 216.1 (2007) estimates fire ratings based on minimum concrete cover thickness to the reinforcement in PPC beams. These provisions are limited in scope and restrictive in application since they were developed in accordance with ASTM E119 (2008) standard fire tests. Furthermore, the provisions are valid only for narrow range of beams, and do not fully account for realistic fire, loading or restraint scenarios. In addition, simplified rules of thumb cannot be applied to new types of designs (different section configurations) and materials (high strength concrete), which limits designers from taking full advantage of the high fire resistance attributes offered by PPC construction.

1.5. Objectives

This thesis presents results from numerical studies aimed at overcoming the current fire resistance limitations for PPC double T-beams. A performance-based approach is applied in the fire resistance analysis of PPC double T-beams. Two double T-beams were analyzed using a finite element based computer program under different fire scenarios, loading and restraint. High temperature material properties, various load and restraint levels, and material and geometric nonlinearities were accounted for. A realistic failure criterion was also included to evaluate the fire response and determine failure. The design fires were selected to provide a wide spectrum of possible building applications. Results from the parametric studies were used to study the thermal and structural response of PPC double T-beams under realistic fire exposure, restraint, load intensity and failure conditions. To achieve this objective the following tasks were performed to accomplish the intended objectives.

- Conduct a detailed state-of-the-art literature review of experimental and analytical studies, as well as provisions in current design codes on the fire resistance of PPC flexural members.
- Illustrate the differences between United States (US) of America, Canadian, and Eurocode fire design provisions for evaluating fire resistance of PPC double T-beams through a case.
- Validate the numerical model SAFIR using published fire test data on the response of PPC double T-beams from Portland Cement Association (PCA) and Underwriter Laboratories (UL) studies.
- Undertake a parametric study to verify the influence of critical factors on the fire performance of PPC double T-beams.
- Outline a performance-based approach to undertake fire resistance analysis on PPC double T-beams.

1.6. Layout

This thesis is divided into six main chapters, followed by a series of appendices. Chapter 1 provides the background on the fire resistance of PPC beams and objectives for this thesis. The intent of Chapter 2 is to identify the critical factors affecting the fire resistance of PPC beams through a state-of-the-art literature review highlighting the details and findings of fire tests and numerical studies. In addition, an overview of current provisions provided in US, Canadian, and Eurocode codes/standards is discussed. Chapter 3 presents the details regarding capabilities, features, and analysis procedures of the finite-element based SAFIR computer program. A sensitivity analysis investigating the level of refinement required to discretize the model is also presented in this chapter. Also, the validation of the model is presented by comparing fire resistance predictions with data from fire tests and finite-element analyses. Chapter 4 presents details and results of the parametric study on the effect of critical factors on the fire resistance of two PPC double T-beams. These results are used in Chapter 5 to develop guidelines for a performance-based approach for PPC beams. The guidelines outline the specific requirements for the selection of the fire scenario, material model, numerical model, and failure criteria. The final chapter, Chapter 6, presents conclusions from the study recommendations for future work.

Chapter 2

2. Literature Review

2.1. General

Since the 1950's a number of experimental and analytical studies have been carried out to study the response of precast/prestressed concrete (PPC) members under fire conditions. Typically, these studies were based on standard fire exposure and focused strictly on the behavior of single elements such as beams, slabs, etc., and neglected any structural interactions such as beam-slab assemblies and framed structures. Through these studies, many of the key factors affecting fire resistance of PPC members have been identified. Many of these findings are the basis of prescriptive fire provisions offered in design codes and standards. A brief overview of a state-of-the-art literature review of experimental and analytical studies is presented to investigate the behavior of PPC beams and its constituents under fire exposure. In addition, provisions in US, Canadian, and Eurocode design fire codes/standards and high temperature material properties influencing the fire resistance of concrete, prestressing steel, and reinforcing steel are reviewed. The discussion provided for each material property is accompanied with high temperature material models used to predict the fire resistance of PPC beams.

2.2. Design for Fire Resistance

The fire resistance of a structural member is defined as the time to reach failure under a given fire exposure. In the US, failure of a roof/floor beam correlates to the time when the beam, which is subjected to an ASTM E119 fire exposure, has either exceeded a predefined unexposed slab or critical strand temperature, or when the strength limit state is reached. For a structural element to be deemed acceptable in a building application, the fire resistance time must be equal to or exceed the required fire rating. The fire rating is the minimal time required by building fire codes and is dependent on the type of structural element, the occupancy of the building and the building characteristics. The most common method to establish fire resistance of a concrete beam is through tabulated data based on cross-sectional area, aggregate type, and concrete cover. These fire ratings are derived from standard fire tests. The problem with this approach is that these tabulated fire ratings are based on standard fire tests for a few select beams and cannot be extended to other types of beam cross-sections. The following literature review highlights many of the fire tests carried out to establish the current fire resistance requirements and is intended to reveal the limitations of their application.

2.2.1. Fire Resistance Tests

Numerous fire resistance tests have been performed on PPC beams primarily to derive fire resistance ratings. The majority of these tests have been based on scaled specimens subjected to standard fire exposure. Some of the notable experimental studies are discussed below:

Woods (1960) conducted one of the first fire tests on a PPC beam at the Portland Cement Association (PCA) Fire Research Center in USA. A full sized, 14.26 m (43 ft 6 in.), I-shaped bridge girder, illustrated in Figure 2.1, was tested in a massive furnace to determine its structural behavior and fire resistance rating under an ASTM E119 (2008) standard fire exposure. This PPC beam achieved a high fire resistance of 4 hr 31 min and this was attributed to massive concrete cross-sectional area capable of absorbing substantial amounts of heat. Further, Woods concluded that concrete cover thickness to steel strands has significant impact on fire resistance of PPC beams.

Results of 47 standard fire tests on precast PPC building components (beams and slabs), conducted by several organizations were compiled by Gustaferro and Carlson (1962). These fire tests were conducted by National Bureau of Standards, Underwriters Laboratories, PCA, and Fire Prevention Research Institute to assess the critical factors affecting fire performance. An assortment of span lengths, insulation thicknesses, aggregate types and member cross-section shapes, such as I-shaped, double-tee, and single-tee beams, as well as flat hollow-core, solid, and stemmed floor assemblies, were tested in accordance with ASTM E119 (2008) standard test provisions. Using the data from 43 beam and 4 slab fire tests, a prescriptive-based table of fire ratings for 1, 2, 3, and 4 hours are shown in Table 2.1 was developed for beams and slabs in terms of concrete cover and cross-sectional area. Based on the analysis of test data the authors concluded that restraint effect, which develop during fire exposure, improves the fire resistance of PPC elements, but this effect is difficult to account for in fire resistance calculations due to complexities associated with this concept. This comprehensive test data resulted in establishing critical factors that govern fire resistance of PPC elements. Accordingly:

- Lightweight aggregate concrete has better thermal resistance than normal weight aggregate concrete.
- Type of aggregate (siliceous or carbonate) has minimal effect on fire performance of structural members.
- Higher moisture content (exceeding 70 percent of relative humidity) in PPC members leads to fire induced spalling.
- Addition of insulation layers increases fire resistance of PPC components.
- Failure of unrestrained PPC members generally occurs when strand temperatures exceed critical limiting temperature, while in the case of restrained members failure occurs through heat transmission criteria.

Selvaggio and Carlson (1963) undertook fire tests on six PPC double T-beams exposed to standard fire conditions to study the effect of fire induced restraint. The cross-section used for all six T-beams is shown in Figure 2.2. All the beams were of 5.45 m (17 ft 10½ in.) span and loaded with 7.8 kPa (163 psf) of live load computed based on $U=1.8(D+L)$ (where U = ultimate load at ambient temperatures, D = dead load and L = live load). Different degrees of restraint were incorporated through limiting axial deformation (expansion) from resulting fire exposure. The series of tests provided an insight into the effects of degree of restraint. The tests confirmed that moisture content plays an important role in determining the fire performance of T-beams. More specifically, over drying during fabrication reduces fire resistance times, while excessive moisture leads to fire induced spalling in stems near supports. Also the test data revealed that strand temperatures and midspan deflections do not govern the fire resistance of restrained members, if adequate restraint is provided. However, it is unlikely that the thermal restraint developed to resist the thermal expansion is greater than most buildings can provide. Thus, restraint improves the fire resistance of PPC T-beams through plastic flow (compressive deformations without an increase in stress) and fire induced thermal moments.

Selvaggio and Carlson (1964) performed fire tests to study the influence of aggregate type and load intensity on the fire resistance of restrained and simply supported PPC I-beams under standard fire exposure. All tested beams had a span of 6.10 m (20 ft) and three different aggregates, normal weight (dolomite and siliceous) and lightweight (expanded shale's) were investigated. The beams were loaded with a live load of 35.8, 28.5, and 21.2 kN/m (2455, 1950, and 1450 lb/ft), with the larger two loads computed based on $U=1.2D+2.4L$ and $U=1.8(D+L)$, respectively. The lower load was arbitrarily selected. The test results revealed that aggregate type has a significant influence on the midspan deflection, thermal thrust, and heat transmission characteristics in PPC beams. It was found that lightweight aggregate concrete provides better fire resistance than normal weight aggregate concrete. The authors concluded that the load intensity has significant effect on the fire resistance, with higher loads leading to lower fire resistance. The shape and size of the compression zone has a significant impact on the fire performance of simply supported PPC T-beams. Restrained beams exhibited 22% better fire performance than unrestrained beams.

Abrams et al. (1971) conducted fire tests on multiple concrete joist floor and roof assemblies to compare the results of unexposed surface temperatures with five RC double T-beams. Figure 2.3 illustrates the cross-section of the joist assemblies tested, while Figure 2.4 show the cross-sections of the T-beams used in the comparison. A span of 5.49 m (18 ft) was used for floor joist fire tests, while the T-beams had spans of 5.41 m (17 ft 9 in.) and 5.45 m (17 ft 10½ in.), respectively. Different aggregate and insulation types were included, as well as various degrees of longitudinal and lateral restraint. The specimens were subjected to ASTM E119 (2008) standard fire exposure and were subjected to a load in the range of 3.9 to 5.3 kPa (82 to 110 psf). The test data indicated that fire resistance of slabs depends on unexposed surface temperatures, rather than on structural (strength) considerations. Furthermore, it was concluded that unexposed surface temperatures can be determined strictly through testing slabs with no considerations for assembly type. Intermediate degrees of restraint improved fire resistance of concrete floor/roof assemblies. A series of thermal interaction diagram envelopes were developed from the test results and proved to be an excellent measure of structural integrity of PPC beams.

Abrams and Gustaferro (1972) conducted tests on four PPC double T-beams coated with spray-applied insulation, by exposing them to ASTM E119 (2008) standard fire to assess the fire resistance. Figure 2.5 illustrates the cross-sections and dimensions of each test specimen. All of the specimens had spans of 6.10 m (20 ft) and were loaded with a live load ranging from 4.1 to 4.8 kPa (85 to 100 psf). Two types of cross-sections were considered in the test program and vermiculite acoustical plastic, as well as mineral fiber insulation was applied independently to the beams. Results from the fire tests indicated that both types of insulation are effective and maintained adhesion during fire exposure. Therefore, spray-applied insulation is a feasible alternative to improving the fire resistance of PPC beams. Overall, vermiculite insulation provides slightly better fire resistance than mineral fiber insulation. These findings were used to develop a prescriptive-based tabulated approach for 2 and 3 hour ratings, based on stem width, concrete cover, insulation type and thickness of PPC beams.

Lin et al. (1981) performed a series of fire tests on RC beams of rectangular cross-section and PPC double T-beams to study the effect of shear and moment redistribution of continuously supported flexural members. Both simply and continuously supported beams were tested under ASTM E119 (2008) standard fire exposure. The cross-sections of the RC beams are illustrated in Figure 2.6 and the reinforcement schemes (top, bottom, and stirrup reinforcements) for each cross-section are tabulated in Table 2.3. The details for the T-beam at the midspan and the supports are shown in Figure 2.7, respectively. All of the beams were loaded with a series of 37.8 kN (8.5 kip) point loads to represent a uniformly distributed load. Based on the test results, the authors concluded that the fire resistance of simply supported concrete beams can be estimated by accounting for reduced strength in steel and concrete. However, to accurately determine the fire performance of continuous members, redistribution of moments has to be considered. The fire test data on indeterminate beams revealed that the additional intermediate supports restrain rotation and thus cause an increase in negative moments, hence a reduction in positive moments. This redistribution of moments enhances the fire performance of continuously supported beams as compared to that of simply supported beams.

Franssen and Bruls (1997) tested two PPC double T-beams to develop a proprietary fire rating for a precast manufacturer. Both specimens were scaled to a total length of approximately 7.0 m (23 ft) and subjected to ISO 834 (1975) standard fire exposure. Two point loads of 233.8 kN (52.6 kips) were applied to the T-beams, with equidistant spacing between the loads and supports. In order to assure that 2 hour fire rating could be achieved, an initial design of the double T-beam, shown in Figure 2.8(a), was tested. During the fire test, this double T-beam developed vertical cracking resulting in loss of bond and failed in 79 minutes. An improved section of the double T-beam, shown in Figure 2.8(b) was designed and tested. The improvements included modifying the strand pattern into two columns, hooped shear reinforcement, and reduced aggregate size to maximize bond strength. The modified beam when tested achieved a 2 hour fire rating. The test proved that a single column of vertically aligned prestressing strands are susceptible to hairline cracks that promote bond failure. Furthermore, this study proved that bond failure can be minimized with appropriate detailing of prestressing strands, shear reinforcement, and concrete mix design.

Anderson and Lauridsen (1999) conducted fire tests to investigate the effect of fire induced spalling on fire resistance of three PPC double T-beams made with high strength concrete (HSC). Figure 2.9 shows the generalized cross-section used for all three T-beams and the three different strand arrangements. The simply supported beams had a span of approximately 6.12 m (20 ft 1 in.) and were exposed to ISO 834 (1975) standard fire exposure. Four point loads ranging from 364 to 374.8 kN (81.8 to 84.3 kips) were applied on the T-beams. Based on the test results the authors concluded that HSC is prone to explosive spalling within the first 20 minutes of fire exposure, especially at the junction of the stem and bottom surface of the slab. Another observation was that scaled specimens are more prone to bond failure because of the dramatic increase in the shear envelope.

The experimental studies presented above have proven to be invaluable in identifying key factors governing fire resistance of PPC beams and also common failure modes under fire conditions. These tests indicate that the primary factors affecting fire performance of PPC beams are moisture content, aggregate type, concrete density, restraint, insulation, continuity, and load intensity. The typical failure in simply supported beam is dictated by its strand temperatures, while in continuous beams the failure is governed by unexposed slab temperatures. Many of these studies have been utilized to establish proprietary fire ratings, as well as prescriptive design provisions. The design provisions are typically based on concrete cover thickness, aggregate type, and either cross-sectional area or beam width. The fire ratings are prescriptive since these ratings were derived based on standard fire conditions, without full consideration for load, restraint or design fire scenario. Although, some studies did incorporate restraint, much work is still required to quantify its influence in practical scenarios.

2.2.2. Analytical Studies

The review of literature indicates that there is limited number of analytical studies relating to the fire performance of PPC beams. The reported analytical studies range from applying simple empirical methods to advanced calculation approaches for evaluating fire resistance of PPC beams. This section provides an overview of the analytical studies:

Boon and Monnier (1976) developed an analytical approach for evaluating fire resistance of PPC beams based on shear and flexural failure criterion. This approach, developed utilizing available data from fire tests on PPC beams, is applicable to simply supported beams exposed to standard fire scenarios and subjected to service loads. Fundamentally, the approach is similar to generic gravity load design with the exception that ambient strength properties of concrete, reinforcement, and prestressing steel are reduced to account for the degradation of strength and stiffness associated with elevated temperature. The reduced material properties in prestressing steel at a given time is based on the temperature of each strand relative to its location from the surface. For shear reinforcement, strength is computed based on actual fire temperatures. To estimate such temperatures in the prestressing steel, time-temperature profiles based on concrete cover thickness is provided. Similarly, plots are also supplemented to estimate the reduced material properties for a given temperature. The reduced material properties are used to evaluate the reduction in the beams' shear and flexural capacity at a given fire exposure time. At any given time, if applied loads (moments) exceed the member's capacity, failure is said to occur due to loss of prestressing strength, horizontal cracking of the stem and bond degradation.

Franssen and Bruls (1997) performed finite-element analysis on a PPC double T-beam to evaluate its fire response. SAFIR (2004), a special purpose computer program, was utilized to evaluate fire resistance based on flexural considerations only. To verify the results of the analysis, a beam was tested under ISO 834 (1975) standard fire conditions. Contrary to author's assumption that flexural strength would govern, the beam failed in the fire test due to shear considerations. Since SAFIR cannot handle shear considerations, Eurocode 2 (2004) provisions were applied to determine ultimate shear capacity of the beam. The analysis indicated that shear failure occurred in the beam at about 80 minutes, which coincided well with the Eurocode predictions of 79 minutes. Results from this analysis were utilized to redesign the beam section to enhance its shear resistance at both ambient and fire conditions. The analysis of the revised section indicated that the fire resistance improved to 135 and 130 minutes based on shear and flexural considerations, respectively. This upgraded beam when tested in the laboratory yielded a fire resistance time of 144 minutes. This study clearly illustrated the usefulness of detailed finite-element analysis to improve the member's design for enhancing fire resistance.

Fellinger et al. (2001) attempted to develop an elasto-plastic bond slip model for 7-wire prestressed strands embedded in concrete at ambient and elevated temperatures. The analysis was carried out using a 2D finite-element computer program, named DIANA. The cross-section, discretized into concrete, prestressing strand, and bond interface components, was represented with plane stress triangular, truss, and plane stress quadrilateral elements, respectively. The model captured changes in bond stress due to slip, Poison's effect, concrete confinement, pitch, splitting of concrete, and differential thermal expansions of steel and concrete. The mechanical properties of the constituent materials were in accordance with Eurocode 2 (2004) relationships and due consideration was given to thermal elongation, transient creep, plasticity, and fracture energy. The model was validated by comparing the results with test data on hollow-core slabs. The ambient temperature results indicated that the development of prestress, effect of shrinkage and creep, and change of steel stress after development of flexural cracks can be predicted reasonably well. However, under elevated temperatures, the model proved to be inconsistent due to lack of temperature dependent input parameters (high temperature material properties such as bond). Nonetheless, this study identified that the two key parameters, friction coefficient and bond strength, have significant influence on fire performance of prestressing strands.

The above analytical studies indicate that both simplistic and advanced finite-element methods can be applied in evaluating fire resistance of PPC beams. It should be noted that the models used for analytical studies were validated only under standard fire conditions, without due consideration to realistic load, restraint, and fire scenarios.

2.2.3. Provisions in Codes/Standards

In USA fire design provisions for concrete and masonry elements are specified in ACI 216 (1997), PCI Design Handbook (2004), ASCE/SEI/SFPE 29-05 (2007) and International Building Code (2006). These codes and design standards offer three different alternatives to assess fire ratings of PPC double T-beams exposed to three-sided standard fire exposure. The simplest and quickest procedure consists of tabulated fire ratings based on minimum concrete cover thickness to prestressing strands. The specified concrete cover thickness is based on a combination of aggregate type (carbonate, siliceous, lightweight, semi-lightweight, or all), restraint (restrained or unrestrained), and beam width or area considerations. These concrete cover thickness provisions were derived from fire test data and assumes that failure occurs in the beam when temperature in the strand reaches a limiting temperature of 427°C (800°F).

The PCI (2004) design standard offers an alternative to the tabulated fire ratings approach through the use of simplified calculations. This approach is similar to ambient temperature calculations in that flexural resistance is evaluated to determine if the beam can withstand the load effects at a specified fire exposure time. The reduced capacity at any given fire exposure time is evaluated by taking into consideration the loss of strength in prestressing steel, reinforcing steel, and concrete. The strength loss is estimated using temperature-strength relationships (graphs) derived from high temperature material test data. The strand temperatures are estimated from temperature profiles (graphs) given for different beam dimensions and aggregate type. If the computed capacity is less than the applied moment, failure is said to occur and this fire exposure time is termed as "fire resistance." One advantage in using this approach, as compared to tabulated ratings, is that it accounts for the effect of load intensity.

In addition to flexural strength considerations, PCI (2004) design standard also require PPC double T-beams to satisfy insulation (heat transmission) criteria, since the member acts as a floor/roof (barrier) assembly. Accordingly, failure is said to occur when the unexposed temperature on the slab exceeds 181°C (325°F) at any one point or an average of 139°C (250°F). This limiting temperature ensures compartmentation functionality and corresponds to a critical temperature required to ignite cotton waste. The tabulated fire ratings for the heat transmission criterion of RC (PPC) slabs are expressed in the PCI Design Handbook as function of aggregate type and concrete thickness. Additional heat transmission fire ratings are provided for insulated and built-up concrete floor/roof assemblies based on slab thickness, insulation type (sprayed mineral fiber, vermiculite cementitious material, mineral board, and glass fiber board), and insulation thickness. Once both heat transmission and strength fire ratings are evaluated the minimum of these two values represents the fire rating of PPC double T-beam and is generally assigned to be as 1, 1½, 2, 3, or 4 hours ratings.

In Canada, the National Building Code of Canada (2005) and CPCI Design Manual (2007) are two main guidance documents which set forth fire provisions for PPC structures. These provisions are very much similar to those in US codes/standards. The tabulated fire ratings are based on concrete cover to prestressing strands, but the specified cover thickness is only based on aggregate type in concrete and beam area. Three aggregate types namely type S, N, and L represent concrete composed of siliceous, calcareous, or lightweight aggregates, respectively. No consideration for restraint is included because it is assumed that the unrestrained member governs and will suffice for restrained conditions. Except for minor difference in tabulated fire ratings, the simplified calculation method is virtually identical to provisions in US code provisions. The only other significant difference in Canadian fire provisions is that heat transmission criteria for insulated concrete floor/roof assemblies' utilize multiplying factors rather than tabulated data. The multiplying factors modify the effective thickness of the insulation material (multiple types of plaster, gypsum wallboard, cellular concrete, vermiculite and perlite concrete, portland cement with sand aggregates, and terrazzo) to determine a equivalent concrete thickness based on its thermal properties. This equivalent thickness is then used to determine the tabulated fire rating, similar to US fire provisions. Based on these three criteria a fire rating, corresponding to a minimum value, is assigned for PPC double T-beam as ½, ¾, 1, 1½, 2, 3 or 4 hours.

In Europe fire provisions for PPC structures are specified in the Eurocode. The tabulated fire ratings for PPC beams set forth in Eurocode 2 (2004) are similar to US and Candian fire provisions, except they are based on combinations of web width and axis distance to strand centroid for both simply and continuously supported beams. An additional set of tabulated fire ratings is provided for four-sided exposure (in addition to three-sided exposure) in beams. Neither set of tabulating fire ratings in the Eurocode take in to consideration the influence of aggregate type on fire resistance. In addtion to these prescriptive-based approaches, Eurocode fire provisions also permit the use of advanced analysis for evaluating fire resistance of PPC members. Application of these advanced analysis techniques require detailed thermal and mechanical analysis with due consideration to realistic fire scenarios, actual load intensities, and restraint conditions to evaluate fire resistance under performaced-based codes. Fire rating provisions specified in US, Canadian, and European fire codes and standards are tabulated in Table 2.4.

To illustrate the variation in US, Canadian, and Eurocode fire provisions, fire ratings were evaluated for two PPC double T-beams (10DT24+2 and 12DT32+2). Ratings computed based on tabulated data, simplified calculation, and heat transmission approaches are shown in Table 2.5. The detailed calculations for these results are in Appendix A. The tabulated fire ratings of both beams yield 1½ hour as per US standards, while Canadian and Eurocode fire provisions produce 1½ hour for 10DT24+2 and 2 hour rating for beam 12DT32+2. This variation in fire ratings is mainly due to the consideration given to different factors in each code such as the use of effective flange thickness in Canadian code and neglecting aggregate type in Eurocode.

Further deviations are observed in simplified calculation fire ratings, where Eurocode and Canadian provisions result in a 1½ hour fire rating for both beams. However, the US fire provisions produce 1½ and 2 hour fire ratings for beam 10DT24+2 and 12DT32+2, respectively. The main reason for these differences in fire ratings is due to the load combinations utilized in standard fire tests. In heat transmission criteria US and Canadian fire provisions yield 1 hour fire rating for both beams, while the Eurocode provisions result in 1½ hour fire rating for both beams and this is due to the lack of consideration for aggregate type in Eurocode. It should be noted that all these provisions are based on the standard fire exposure without any consideration for realistic fire, loading, and restraint scenarios.

2.3. High Temperature Material Properties

2.3.1. General

The fire resistance of PPC beams is dependent on the high temperature material properties of its constituent materials, namely concrete, mild reinforcing steel and prestressing steel. The three properties that influence fire response of structural members are thermal, mechanical, or deformation properties. Thermal properties (specific heat, thermal conductivity, and density) influence heat transfer characteristics, mechanical properties (compressive strength, yield strength, and elastic modulus) affect strength and stiffness attributes, and deformation (thermal elongation, creep, and transient strain) properties control the deflections of a material. In addition to these inherent material properties, physical characteristics, such as fire-induced concrete spalling or bond strength, also affect the fire resistance of PPC beams.

In today's technology driven society it is common practice to utilize computer software to predict the fire resistance of PPC beams. These software programs require high temperature constitutive models as input for each unique material type included in the analysis. Generally, these material relationships are developed based on an exhaustive number of high temperature material tests. Two widely accepted sources for high temperature constitutive models are ASCE Manual of Practice No. 78 (1992) and Eurocode 2 (2004). The following sections provide an overview of these high temperature constitutive models for normal strength (conventional) concrete, high strength prestressing steel, and mild reinforcing steel. To view the empirical relationships for these constitutive models refer to Appendix A.1. In addition, the findings of several studies used to establish similar material relationships are highlighted.

2.3.2. Concrete

High temperature material properties which influence the fire resistance of concrete are thermal, mechanical, and deformation properties. Fire induced spalling is a physical characteristic which also impacts the fire resistance of concrete.

2.3.2.1. Thermal Properties

Thermal properties which influence concrete temperatures are specific heat, thermal conductivity, and density. Limited research (Saad et. al 1996, Kodur and Sultan 2003, Arioz 2007, Shin et. al 2007, Kodur et. al 2008, and Kodur and Harmaty 2008) has been performed to quantify high temperature relationships for normal strength concrete due the difficulty associated with measuring these properties under fire. In addition, the results of these studies reveal large discrepancies due to differences in test methods, procedures, conditions, and measurement techniques (Kodur et. al 2008). Despite these complications, ASCE (1992) and Eurocode (2004) provide relationships for thermal properties of normal strength concrete.

Thermal Conductivity

Thermal conductivity characterizes the heat transfer rate for a solid material. Figure 2.10 illustrates the variation of thermal conductivity for normal strength concrete according to ASCE (1992) and Eurocode (2004) models. The ASCE model offers more options than the Eurocode model because it is a function of temperature and aggregate type, rather than temperature alone. Four different types of aggregates (siliceous, carbonate, pure quartz, and expanded shale) are provided for the ASCE model. Although, the Eurocode model does not differentiate between aggregate type, it does offer an upper and lower limit, relying on the users discretion. The upper limit was derived from tests on steel/composite structures, while the lower limit is suggested to give more accurate results since it is based on fire tests from a variety of different types of concrete structures. Therefore, the Eurocode model could provide misleading temperature results, especially if utilized for concrete containing siliceous or pure quartz aggregates.

Specific Heat and Density

Thermal capacity is the product of specific heat and density. This property defines the amount of energy required to raise a unit volume of a material by a unit temperature. Figure 2.11 illustrate the variation of thermal capacity for normal strength concrete according to ASCE (1992) and Eurocode (2004) models. Once again, the temperature-heat capacity ASCE model is a function of temperature and aggregate, but the Eurocode model is dependent on temperature alone. Therefore, Eurocode model cannot account for differences between aggregate type that ASCE model can, such as the large increase in thermal capacity that occurs during the range of 600-800°C (1112-1472°F) in carbonate (limestone) aggregates. These discrepancies could lead to significantly different outcomes when used to predict the fire resistance of PPC beams, especially under increasing temperatures.

2.3.2.2. Mechanical Properties

High temperature mechanical properties that influence fire resistance of concrete are tensile strength, compressive strength, and elastic modulus. To date, few studies have focused on the effects of fire on concrete's tensile strength, due to the standard practice of neglecting the tensile resistance of concrete in design. However, the latter two material properties have been extensively researched. These studies (Saad et. al 1996, Arioz 2007, Kodur et. al 2008, Kodur and Harmathy 2008, Li et. al 2004, and Husem 2006) have focused on developing high temperature relationships (i.e. stress-strain curves) for normal strength concrete based on two approaches, either high temperature or residual material testing. Both testing techniques are similar in that they are performed incrementally at a series specified temperatures by loading the specimen until failure. The difference between these techniques is that the high temperature tests are loaded during fire exposure, while residual tests are loaded once the concrete specimen has been cooled (after exposure to high temperatures) under either ambient, air, or water jet conditions. Although the residual properties of a concrete are important in a post-fire assessment, only high temperature relationships are considered in the following review.

Stress-Strain Curve

Stress-strain curves define a material's mechanical response to an applied force or deformation. Since concrete's mechanical response is temperature dependent, a unique curve is necessary for every temperature encountered. Figure 2.12 illustrates a series of stress-strain curves for a normal weight concrete at various temperatures according to ASCE (1992) and Eurocode (2004). The Eurocode model provides a curve for carbonate and siliceous aggregate types, while ASCE model utilizes a single curve for siliceous, carbonate, and expanded shale aggregate types. Both models initially behave similar, until the maximum stress is reached. Beyond this point, both curves begin their descent, but the Eurocode model incorporates a linear trend, while the ASCE model utilizes a nonlinear relationship that is much more prolonged. Although not illustrated in the figure, the Eurocode model does offer a nonlinear option that is comparable its linear alternative. The Eurocode model reveals that concrete members made of carbonate aggregates possess a greater fire resistance than those made of siliceous aggregates. At lower temperatures the ASCE model envelopes the Eurocode model, but as temperatures rise the ASCE model eventually provides a lower fire resistance than the Eurocode model. These models are further examined in the following discussion on elastic modulus and compressive strength.

Elastic Modulus

Elastic modulus describes how a solid material elastically deforms under stress. In solid mechanics, it is defined mathematically as the initial slope of the stress-strain curve and can be easily identified for each stress-strain curve in Figure 2.12. Figure 2.13 illustrates the variation of elastic modulus of concrete with respect to temperature, according to ASCE (1992) and Eurocode (2004) models. The ASCE model initially degrades at a slower rate than the Eurocode model, until approximately 800°C (1472°F). The greatest difference between these models occurs at temperatures below 300°C (572°F). The elastic modulus curves for the Eurocode model further reinforces the fact that carbonate aggregate concrete provides better fire resistance than siliceous aggregate concrete.

Compressive Strength

Compressive strength of concrete corresponds to the limiting stress at which the failure of concrete occurs due to a uniaxial crushing load. This limit is defined numerically as the maximum compressive stress along a stress-strain curve and is clearly illustrated in Figure 2.12. Figure 12.4 illustrates the variation of compressive strength of concrete with respect to temperature, according to ASCE (1992) and Eurocode (2004) models. The ASCE model retains 100% its strength until temperatures reach 450°C (842°F), at which point it begins to linearly decrease until all of the concretes strength is exhausted at a temperature of 874°C (1605°F). In the Eurocode model the onset of strength loss occurs at a temperature of 200°C (392°F) and as temperatures rise loses continue to accumulate nonlinearly until zero strength remains at a temperature of 1200°C (2192°F). Based on these empirical relationships, the ASCE model provides better fire resistance than the Eurocode model for temperatures below approximately 700°C (1292°F). However, it is not until temperatures exceed 800°C (1472°F) that the Eurocode model exhibits a better fire performance than its counterpart, due to the fact that the Eurocode model distinguishes between aggregate type. Similar to the previous results, the Eurocode model depicts that carbonate aggregates perform better under fire conditions than siliceous aggregates.

Tensile Strength

Tensile strength of concrete refers to the critical stress when concrete fails under uniaxial tension. A general rule of thumb, under ambient temperatures, is the tensile strength is one tenth of concrete’s compressive strength. As mentioned previously, it is common practice to neglect the tensile resistance of concrete. Consequently, many design guides, such as ASCE, do not provide high temperature relationships for tensile strength of concrete. Despite this practice, the

Eurocode does provide a relationship and is shown in Figure 2.15. This model provides a single curve for all aggregate types. For temperatures up to 100°C (212°F), the concrete retains full tensile strength, but for temperatures in excess of 100°C (212°F) the tensile strength reduces at a rate 0.2%/°C (0.06%/°F) until zero strength remains at a temperature of 600°C (1112°F).

2.3.2.3. Deformation Properties

The four types of deformation properties that influence the fire resistance of concrete are mechanical, thermal, creep, and transient strain. Engineers rely on strain to measure the relative deformation of a material. Strain is defined as the change in length over its original length. Hence, it is the accumulation of these four types of strain that lead to the net deformation of concrete, under both ambient and fire conditions. Although, these properties are discussed individually, they have a very complex interrelationship that can make it difficult to distinguish one type of strain from another, especially under fire conditions. It should be noted, although mechanical strains contribute to the deformations of concrete, this property is generally classified as a mechanical property and is already presented in the previous section. The discussion below highlights the concretes deformation properties and their response to fire conditions.

Thermal Expansion

Thermal expansion (contraction) of concrete refers to the change in volume of concrete due to an increase or decrease in temperature. Thermal expansion, also known as thermal strain, is defined as quotient of the change in length over its original length. Although at first glance this mathematical relationship appears trivial, when trying to measure this property to quantify a material relationship it can be very difficult to distinguish the difference between thermal strain and shrinkage. Despite this fact, many researchers (Kodur and Sultan 2003, Naus 2005, Harmathy 1967, Petterson 1965, Saito 1965, and Anderberg and Thelandersson 1976) have conducted studies to develop high-temperature relationships for numerous concrete types. Most of the studies relied on commercially available dilatometric equipment to measure the volume changes, while other simply mounted radial and longitudinal strain gauges to a specimen and place in a furnace. Several factors that have been identified to influence this parameter are aggregate type, cement type, water/cement ratio, and moisture content.

Figure 2.16 illustrates variation of concrete thermal expansion as a function of temperature according to ASCE (1992) and Eurocode (2004) models. These models reveal that with increasing temperatures the thermal strain increase. The ASCE model provides a single curve for all aggregate types and gradually increases as a function of temperature. The Eurocode model provides two separate curves, one for carbonate aggregates and another for siliceous aggregates. Both of these curves tend to increase at a faster rate until they plateau around 700 or 800°C (1292 or 1472°F), depending on the aggregate type. The Eurocode model reveals that carbonate aggregates are much more sensitive to temperature than siliceous aggregates. Another, interesting feature of this model is that for high temperatures, thermal expansion no longer increases with temperature for neither type of concrete.

Creep Strain

Creep refers to the time-dependent plastic deformations of a material. More specifically, creep is when a material deforms permanently from a stress that is less than its yield point. Under ambient conditions, this type of deformations occurs very slowly, over a long period of time, and as a result of high stress levels. However, in the presence of fire, it only takes moderate stress levels to rapidly generate large creep strains in concrete. One reason for this behavior is that high temperature creep in concrete is caused by the migration of water within its microstructure and upon heating this movement of moisture is accelerated. Another reason is that with increasing temperatures, materials degrade and lend themselves to be more susceptible to the effects of creep. High temperature creep influences the fire resistance of concrete, because it can lead to large defections, a redistribution of stresses, and/or relieve unwanted tensile stresses.

Literature reveals that the main factors influencing high temperature creep in concrete are composition, load duration and intensity, temperature and exposure time. The composition, such as aggregate type, mix proportions and type of cement, have been found to influence the creep of concrete at high temperatures. As for the remaining factors, creep has proven to increase with larger loads applied for longer durations, as well as under higher temperatures for longer exposure times. Despite these findings, limited research has been undertaken to develop practical high temperature creep curves due to its complexity. This lack of data is one reason why the effects of high temperature creep are not generally explicitly included in manual or computer-based fire resistance calculations. However, part of high temperature creep is still accounted for in fire resistance calculations implicitly through the use of stress-strain curves which have built-in allowances for typical amounts of creep strain encountered in fire tests of concrete members.

Transient Strain

Transient strain is an irrecoverable strain that develops the very first time, and only the first time when loaded concrete is exposed to elevated temperatures. This type of strain is very complex, it accounts for deformations resulting from concretes' chemical decomposition and thermal instability under fire conditions. Two examples of the type of chemical decomposition that occur in concrete is the breakdown of hydration products in the cement paste and phase changes that aggregates undergo. Whereas, the thermal instabilities in concrete are caused by a variance in the thermal expansion of aggregates and cement paste. The combined effects of the deterioration and varying thermal expansion induce stress-concentrations that lead to micro-cracking and deformations. This behavior provides a degree of relaxation and is one reason why concrete does not degrade completely when heated.

Research (Gernay & Franssen 2011, Anderberg and Thelandersson 1976, Fletcher, et. al. 2007, Bastami and Aslani 2010) to study the behavior of transient strain in different types of concrete has been limited. One of the reasons for this is that there is no direct test procedure to measure transient strain. In fact, commonly, transient and creep strain are measured together by measuring the total strain and deducting both mechanical and free thermal strain. This lumped measurement is often called, transient creep strain. Although neither the ASCE (1992), nor the Eurocode (2004) models provide a direct relationship for transient strain or transient creep strain. As mentioned previously, these effects are included implicitly by providing an allowance for such behavior in the stress-strain relationships. This approach has been argued by some Anderberg and Thelandersson 1976) to have implications on the elastic modulus of concrete.

2.3.2.4. Physical Properties

The primary physical property that influences the fire resistance of concrete is fire-induced spalling. Fire-induced spalling refers to the act of large and/or small pieces or layers of concrete breaking off during a fire as a result of temperature effects. Of the four types of spalling (explosive, surface, aggregate, and corner), explosive spalling has the potential to be the most damaging, because it occurs suddenly in a violent fashion and results in large voids of missing concrete. One of the consequences of fire-induced spalling is that it directly exposes the steel reinforcement to the deleterious effects of fire, causing a rapid decay in strength and stiffness. In addition, the missing concrete also contributes to a reduction in stiffness and load bearing capacity. Fire-induced spalling can also trigger bond loss between the concrete and reinforcement. All of these effects can be detrimental on the fire resistance of concrete.

A review of literature (Khoury and Anderberg (2000), Husem (2006), Fletcher et. al. (2007), Naus (2005), Jansson (2008), and Kodur and Dwaikat (2008)) reveals that numerous studies have been undertaken to study fire-induced spalling. These studies indicate the factors that influence fire-induced spalling are heat rate, heating profile, section size, section shape, moisture content, pore pressure, permeability, age of concrete, concrete strength, restraint, type of aggregate, aggregate size, cracking, reinforcement, concrete cover, supplementary reinforcement, steel fibers, polypropylene fibers, and air-entrainment. Despite these findings, fire-induced spalling is still quite unpredictable. This is in part due to the complexity associated with the phenomenon and also to lack of high temperature material properties and calculation methodologies. Therefore, neither the ASCE (1992), nor the Eurocode (2004) models provide a high-temperature relationship to predict the fire-induced spalling.

2.3.3. Prestressing and Mild Reinforcing Steel

Similar to concrete, the high temperature material properties which influence the fire resistance of steel reinforcement are thermal, mechanical, and deformation properties. At any temperature, the material properties of steel reinforcement are greatly influenced by composition, forging procedure, and heat treatment employed during creation. In the following sections, two types of steel reinforcement are presented, prestressing steel and mild reinforcing steel. Prestressing steel is produced by cold working the steel, while reinforcing steel is formed through a hot-rolling process. As a result of the different techniques used to manufacture these products, their behavior and response to high temperature varies. To compare and contrast these differences, the material properties for both types of steel reinforcement are presented simultaneously in the following sections.

2.3.3.1. Thermal Properties

Thermal conductivity and specific heat are thermal properties that influence heat distribution and temperature rise in reinforcing and prestressing steel. A number of studies (Yafei et. al 2009, Kodur and Harmathy 2008, Harmathy 1988) have been undertaken to study the behavior of these material properties under fire conditions. These studies reveal at ambient temperatures, thermal properties are influenced by metallurgical composition, type of reinforcement, and temperature, but under fire conditions, temperature is the only variable which has a significant influence. At any temperature, all types of steel possess a relatively high thermal conductivity and low specific heat compared to other construction materials. Despite the minor variation in thermal properties due to temperature, the thermal response of the both types of steel reinforcement lead to rapid temperature rise and uniform distribution of heat. In the case of PPC members, this temperature rise in the steel reinforcement is further exemplified by the slender cross-sections. Therefore, when predicting the fire resistance of PPC members the thermal properties of reinforcing steel or prestressing steel are ignored and idealized as a perfect conductor. In essence, the temperature of the steel reinforcement is equivalent to the surrounding concrete. Based on this assumption, design guides do not readily provide constitutive models for the thermal properties for either type of steel reinforcement.

2.3.3.2. Mechanical Properties

Yield strength, ultimate strength, and elastic modulus are temperature dependent mechanical properties which influence the strength and stiffness characteristics of steel reinforcement. Generally, these material properties are provided in the form of a series of stress-strain curves. Many high temperature material tests (Abrams and Cruz 1961, Atienza and Elices 2009, Elghazouli et. al 2009, Harmathy 1970, Harmathy 1988, Holmes et. al 1982, Kodur and Harmathy 2008, Neves et. al 1996, Schneider et. al 1981, and Wenzhong et. al 2007) have been carried out to develop empirical relationships for stress-strain curves of prestressing and mild reinforcing steel under fire conditions. Most of these tests were carried out utilizing static loading and steady-state heating conditions. The studies identified heating rate, strain rate, type of reinforcement, and temperature as several factors that influence the mechanical properties of steel reinforcement. Another conclusion drawn from these studies was that prestressing steel is much more sensitive to high temperatures then reinforcing steel. According to Hill and Ashton (1957), prestressing steel loses half of its strength around 400°C (752°F), while mild steel reinforcing loses half its strength when temperatures approach 600°C (1,112°F).

Stress-Strain Curve

Stress-strain curves provide a means to predict the mechanical behavior of steel reinforcement when subjected to stress or strain. When steel reinforcement is exposed to fire conditions, a unique stress-strain curve is required at every temperature encountered to define its mechanical behavior. For example, Figure 2.17 illustrates a series of stress-strain curves at several temperatures for prestressing steel according to Eurocode (2004) model. Each curve initially behaves linear elastic until the proportional limit has been reached. Beyond this point, the prestressing steel begins to undergo irreversible deformations and the relationships become rounded until the ultimate strength is reached and the strain increases without an increase in stress. These curves reveal that with increasing temperatures the strength and stiffness of prestressing steel decreases. It is noteworthy to mention that the ASCE (1992) model only provides high-temperature material relationships for reinforcing steel and not prestressing steel.

Similarly, Figure 2.18 illustrates a series of stress-strain curves for mild reinforcing steel at various temperatures according to Eurocode (2004) and ASCE (1992) models. Like prestressing steel, an increase in temperature results in a decrease in strength and stiffness. Contrary to the other relationships, the Eurocode model for reinforcing steel exhibits a nearly idealized elasto-plastic stress-strain relationship at ambient temperatures, with a discrete yield and ultimate strength. This model does not capture the ductile behavior of mild steel reinforcing, because it assumes that strain hardening is negligible at all temperatures. Hence the maximum stress level is treated as effective yield strength. Some (Elghazouli et al. 2009) argue that this assumption is not valid until temperatures exceed 400°C (752°F). As a result of this assumption, the model maintains a 100% of its ultimate strength for temperatures up to 400°C (752°F), whereas the other relationships for reinforcing and prestressing steel are continuously degrading as temperatures rise. Excluding the stress-strain curves shown for 600°C (1,112°F), the two mild steel reinforcing models correlate poorly. These differences and more are further emphasized in the following discussion regarding the high temperature relationships for ultimate strength, yield strength and elastic modulus of steel reinforcement.

Ultimate Strength

Ultimate strength of steel reinforcement corresponds to the maximum stress along a stress-strain curve. Figure 2.19 illustrates the variation of ultimate strength of prestressing and mild reinforcing steel as a function of temperature according to Eurocode (2004), PCI (2004), and ASCE (1992) models. With the exception of the ASCE model for mild reinforcing steel, all of the ultimate strength relationships exhibit an S-shaped curve, common amongst materials degrading under elevated temperatures. Although, these three models behave similar, the prestressing steel curves begin to lose strength at 100°C (212°F), compared to 400°C (752°F) according the Eurocode model for reinforcing steel. In contrast, the ASCE model for mild reinforcing steel decays in a bilinear fashion. It immediately begins to lose strength linearly until it reaches approximately 20% of its strength at 900°C (1,652°F) and then completely degrades once 1,000°C (1,832°F) is reached. When comparing the models for each material, a strong correlation between the Eurocode and PCI prestressing steel models exist. However, significant differences can be observed when comparing the Eurocode and ASCE mild reinforcing models and is partly due to assumptions inherent to the Eurocode model. This figure reiterates the fact that prestressing steel is more susceptible to high temperatures than reinforcing steel.

Yield Strength

The yield strength of steel refers to the stress at which the steel begins to undergo permanent deformations. Under ambient temperatures, the stress-strain curve for mild reinforcing steel has a well-defined yield strength characterized by the onset of deformations without an increase in stress or by the sharp change in direction of the stress-strain curve. When mild steel reinforcement exposed to elevated temperatures this distinct point along the stress-strain curve loses its definition as deleterious effects of fire cause the relationships to become more rounded. This same effect is common in prestressing steel under both ambient and fire conditions. Therefore, to quantify the yield strength of steel reinforcement of a soft curve, it is common practice to utilize the concept of proof strength. This approach defines the yield strength as the intersection of stress-strain curve and a line drawn parallel to the linear elastic portion of the curve starting at a specified strain. A proof strain of 0.2% is commonly used and widely accepted as a reasonable starting point.

Figure 2.20 illustrates the variation of mild reinforcing and prestressing steel yield strength as a function of temperature according to Eurocode (2004) and ASCE (1992) model. All three curves reveal that with increasing temperatures the yield strength of steel reinforcement decreases. However, the Eurocode model for prestressing steel immediately forms and continues to maintain the lower bound for all three curves until temperatures reach 700°C (1,292°F). A similar trend is observed for the Eurocode model for mild reinforcing steel, except that it does not begin to lose strength until 100°C (212°F). Lastly, the ASCE model for mild reinforcing steel trend is nearly identical to that of its ultimate strength, the yield strength linearly decreases until it is all of it strength has been depleted.

Elastic Modulus

As mentioned previously, elastic modulus describes how a solid material elastically deforms under stress and is defined mathematically as the initial slope of the stress-strain curve. Figure 2.21 illustrates the variation elastic modulus for mild reinforcing and prestressing steel as a function of temperature according to Eurocode (2004) and ASCE (1992) model. Once again, the Eurocode models for both types steel reinforcement exhibit an S-shaped trend. With increasing temperatures, the two relationships crisscross several times until temperatures reach 700°C (1,292°F) when they begin coincide as temperatures continue to rise. In contrast, the ASCE model for mild reinforcing steel illustrates a steady reduction in stiffness from ambient temperatures until temperatures reach 1,000°C (1,832°F). When compared the Eurocode models, the ASCE model also exhibits greater relative losses in stiffness until temperatures reach 600°C (1,112°F).

2.3.3.3. Deformation Properties

The three types of deformation properties that influence the fire resistance of steel reinforcement are mechanical, thermal, and creep strain. As mentioned previously, strain is used to measure the relative deformation of a material and is defined as the change in length divided by its original length. Therefore, the net deformation or strain of steel reinforcement is the summation of these three types of strain. Although, these properties are discussed individually, they have a very complex interrelationship that can make it difficult to distinguish one type of strain from another, especially under fire conditions. The mechanical strains contribute to the deformations of steel reinforcement, but this property is generally classified as a mechanical property and is presented as one in the previous section. The discussion below highlights the deformation properties and their response to fire conditions for prestressing and mild reinforcing steel reinforcement.

Thermal Expansion

The thermal strain of mild steel reinforcement is characterized by the deformation property known as thermal expansion. Thermal expansion (contraction) of steel reinforcement refers to the change in volume of steel due to an increase or decrease in temperature. Many studies (Schneider et. al 1981, Elghazouli et al. 2009, Anderberg 1986, and Harmathy 1988) have been undertaken to establish high temperature relationships for both mild reinforcing and prestressing steel. Generally, these high temperature material relationships were on developed based unloaded specimens and under transient heating regimes. The test results revealed only minor differences between minor reinforcing and prestressing steel. Types of steel and strength have no bearing on the thermal expansion of either type of steel reinforcement.

Figure 2.22 illustrates the variation of mild reinforcing and prestressing steel thermal expansion as a function of temperature according to the ASCE (1992) and Eurocode (2004). In general, all three relationships primarily exhibit a linear increase in thermal strain with increasing temperatures. Furthermore, the two curves for reinforcing steel also tend to produce higher strains than that of the prestressing steel. One variation between these relationship occurs between the temperatures of 800°C (1,472°F) and 860°C (1,580°F) when the Eurocode reinforcing steel strains flatten and maintain a constant value until temperatures exceed this range. This sudden change in behavior is a result of an austenitic transformation of steel, where the crystalline structure of steel transforms from ferrite into austenite. This transformation requires large amounts of energy and consequently has a direct influence on the materials' physical properties of steel. Despite this minor inconsistency, all three curves correlate well. Furthermore, these curves prove to be representative of how well the different studies correlated amongst one another, hence the reason why design guides commonly prescribe a constant value of $14x10^{-6}$/°C for the coefficient of thermal expansion.

Creep Strain

Creep strain in steel reinforcement refers to the irrecoverable strains that result from high stress levels sustained over long periods of time and/or from exposure to high temperatures. Typically, high temperature creep does not influence the fire resistance of prestressing steel until temperatures exceed approximately 250°C (482°F) (Anderberg, 2008), while in reinforcing steel the effects of creep do not come into play until temperatures are around 400°C (752°F) to 500°C (932°F) (Elghazouli et. al, 2009). Creep is characterized by three distinct phases: a primary, secondary, and tertiary phase. In the primary phase, the creep strain increases parabolically at decreasing rate with respect to time and temperature. Next, the secondary phase exhibits constant rate of increase in strain over time and temperature. Lastly, the tertiary phase leads to an accelerated increase in strain until rupture, better known as runaway strain. According to Leir (1993), it is not essential to capture the tertiary phase of creep strain in steel reinforcement because creep strains in the later part of the secondary phase produce a structural response that is deemed unacceptable.

Numerous studies (Williams-Leir 1983, Harmathy and Stanzak 1970, Harmathy 1988, Dwaikat and Kodur 2008) have been undertaken to develop to high temperature material relationships for creep strains in prestressing and reinforcing steel. These relationships are based on a variety of factors, such as stress, temperature, activation energy, and duration of stress. Historically, Harmathy's model based on Dorn's (1955) creep theory has been the most widely accepted approach for predicting high temperature creep. Despite its acceptance, it has several drawbacks. For example, it assumes constant stress, which does not hold true for restrained members. Also, it is based on the assumption that the material remains physiochemically stable, but between the temperatures of 371°C (700°F) and 704°C (1,300°F) carbon steel begins to soften and the assumption is no longer valid. In lieu of these arduous relationships, code-based equations avoid the complexities associated with predicting creep strain in fire resistance calculations by implicitly including through the stress-strain relationships based on strength and stiffness as a function of temperature.

2.3.3.4. Physical Properties

Bond strength is a physical property of steel reinforcement that is based on the adhesion and friction developed between steel reinforcement and concrete. The characteristics of steel reinforcement that influence these mechanisms are reinforcement type (smooth bars, ribbed, strands, and tendons), diameter, coating (none or epoxy), size and spacing of ribs, and whether the reinforcement is in compression or tension. In concrete, it is the proportions and ingredients included in the concrete mix design (cement type, admixtures, and water-cement ratios), as well as shrinkage when present, that impact bond strength. In addition to these factors, under fire conditions, fire-induced spalling of the concrete immediately in the vicinity of steel reinforcement can cause the bond to degrade rapidly or can result in complete bond loss. In the event of bond loss, the steel reinforcement slips, leading to an increase in concrete stress and reduction in capacity and often pursued by structural failure.

The bond strength of mild reinforcing and prestressing steel under ambient temperatures is well studied, but under elevated temperature research has been limited. In a literature review developed by Naus (2005) the findings of a small collection of studies reveal that the bond strength of steel reinforcement decreases with increasing temperatures, but significant losses are not sustained until temperatures exceed 400°C (752°F). Also, prestressing steel provides better bond strength at higher temperatures than mild reinforcing steel. Furthermore, when comparing the bond attributes different types of mild reinforcing steel, ribbed reinforcing provides better fire resistance than plain round bars. Despite these findings, current codes and standards do not provide any guidance or consideration for failure due to bond loss. Rather it assumed that the loss of strength and stiffness will occur first and govern the fire resistance of PPC beams.

2.4. Summary

This chapter presented a state-of-the-art literature review on the fire resistance of PPC beams. First, begins a description of the current approach for the design for fire resistance of PPC beams was provided. Next, a review of experimental and analytical studies identified some of the key factors governing the fire resistance PPC Beams, common failure modes, and basis of current prescriptive-based design provisions. The main drawback of these studies is that they are based on standard fire conditions, without full consideration for load, restraint or design fire scenario. Also, an overview of US, Canadian, and Eurocode design fire codes/standards is presented. This review confirmed that the current prescriptive-based approach is limited in scope and restrictive in nature. Furthermore, these guidelines are only valid for a narrow range of beams and do not fully account for realistic fire, loading or restraint scenarios. Lastly, a review of literature on the high temperature material properties of concrete, mild reinforcing steel and prestressing steel were highlighted. Included in this section are high temperature material models according to the ASCE (1992) and Eurocode (2004) models. Large variations are observed when comparing each model. Based on this literature review it is evident to overcome these drawbacks further research is required to develop a rational approach to predict the fire resistance of PPC beams.

Table 2.1 – Tabulated Fire Ratings for PPC Building Components (Gustaferro and Carlson 1962)

Concrete cover for various fire resistance, mm					
Type of unit	Cross-sectional area, cm^2	Recommended rating, hr			
		1	2	3	4
Girders, beams, and joists	258 to 968	51	n.d.	n.d.	n.d.
	968 to 1935	38	64	n.d.	n.d.
	Over 1935	38	51	76*	4*
Slabs: solid or cored	n.a.	25	38	51	n.d.

Note: 1 in. = 25.4 mm; n.d. = no data (missing); n.a. = not applicable.
*Adequate provisions against spalling shall be provided by means of wire mesh.
In computing the cross-sectional area for joists, the area of the flange shall be added to the area of the stem, and the total width of the flange, as used, shall not exceed three times the average width of the stem.

Table 2.2 – Tabulated Fire Ratings for PPC T-beams with Spray-applied Insulation developed by Abrams and Gustaferro (1972)

Stem width at steel centroid, b, mm	Concrete cover, u, mm	Thickness of insulation, mm			
		Vermiculite Type MK		Sprayed mineral fiber	
		2, hr	3, hr	2, hr	3, hr
64	25	25	n.d.	25	n.d.
76	32	19	32	19	32
102	38	13	25	13	25
127	44	10	19	10	16
152	44	6*	13	10*	16
203	44	6*	10*	10*	13*
203	70	0	6	0	10

Note: 1 in = 25.4 mm.
*Governed by requirements for u

Table 2.3 – Reinforcement Details of RC Beams used in Lin et al. (1981) Study to Investigate the Effects of Shear and Moment Redistribution of Continuously Supported Flexural Members

(a) Top Reinforcement Details

Specimen type and designation	Top bar					
	Design	A	b	c	d	e
I - AAA	A	2 #19 9.7 m	2 #19 2.8 m	2 #19 8.0 m	n.a.	n.a.
II - ABA	A	2 #19 9.7 m	2 #19 2.8 m	2 #19 8.0 m	n.a.	n.a.
III - AAB	A	2 #19 9.7 m	2 #19 2.8 m	2 #19 8.0 m	n.a.	n.a.
IV- ABC	A	2 #19 9.7 m	2 #19 2.8 m	2 #19 8.0 m	n.a.	n.a.
V - BCD	B	n.a.	n.a.	n.a.	5 #25 9.6 m	2 #25 4.0 m
Note: 1 in. = 25.4 mm; 1 ft = 0.3048 m; n.a. = not applicable. Top reinforcement bars begin 38 mm (1½ in.) from each end. Roman numeral designates type. First letter refers to top steel, second to bottom steel and third to stirrups. All bars of Grade 413 (60 ksi).						

Table 2.3 (cont'd)

(b) Bottom Reinforcement Details

Specimen type and designation	Bottom bar				
	Design	F	g	h	i
I - AAA	A	2 #19 9.7 m	2 #19 3.6 m	n.a.	n.a.
II - ABA	B	2 #19 9.7 m	2 #19 9.7 m	n.a.	n.a.
III - AAB	A	2 #19 9.7 m	2 #19 3.6 m	n.a.	n.a.
IV- ABC	B	2 #19 9.7 m	2 #19 9.7 m	n.a.	n.a.
V - BCD	C	n.a.	n.a.	2 #19 9.6 m	5 #25 3.3 m

Note: 1 in. = 25.4 mm; 1 ft = 0.3048 m; n.a. = not applicable. Bottom reinforcement bars are symmetric about centerline. Roman numeral designates type. First letter refers to top steel, second to bottom steel and third to stirrups. All bars of Grade 413 (60 ksi).

Table 2.3 (cont'd)

(c) Stirrup Reinforcement Details

Specimen type and designation	Stirrups						
	Design	Size	Spaces (mm)				
I - AAA	A	3	19 @ 152 = 2.9 m	5 @ 305 = 1.5 m	n.a.		
II - ABA	A	3	19 @ 152 = 2.9 m	5 @ 305 = 1.5 m	n.a.		
III - AAB	B	3 & 4	10 @ 114* = 1.1 m	19 @ 64* = 4.0 m	7 @ 76 = 0.5 m	7 @ 152 = 1.1 m	2 @ 305 = 0.6 m
IV- ABC	C	3	7 @ 152 = 1.1 m	18 @ 76 = 1.4 m	3 @ 152 = 0.5 m	6 @ 305 = 1.8 m	n.a.
V - BCD	D	3 & 4	10 @ 114* = 1.1 m	16 @ 76 * = 1.2 m	5 @ 102 = 1.7 m	8 @ 152 = 0.9 m	3 @ 305 = 0.9 m

Note: 1 in. = 25.4 mm; 1 ft = 0.3048 m; n.a. = not applicable.
*Designates # 4 bar stirrups; all other stirrups #10 (#3) bar
Shear stirrups reinforcement begin 76 mm (3 in.) from each end. Roman numeral designates type. First letter refers to top steel, second to bottom steel and third to stirrups. All bars of Grade 413 (60 ksi)

Table 2.4 – Comparison of Design Provisions Specified by US, Canadian, and Eurocode Design Provisions

Code/Standard	United States	Canadian	Eurocode
Methodology			
Tabulated	X	X	X
Simplified calculations	X	X	X
Heat transmission	X	X	X
Performance-based			X
Design factors			
Aggregate type	X	X	
½ hr fire rating		X	X
¾ hr fire rating		X	
Fire proofing (insulation)	X	X	
Restraint	X	X*	X
Four-sided exposure			X
Spalling			X
*Restraint is included implicitly			

Table 2.5 – Fire Resistance Ratings (hrs) for 10DT24+2 and 12DT32+2 as per Different Codes of Practice

Tabulated data			
Code/standard	United States	Canadian	Eurocode
10DT24+2	1 ½	1 ½	1 ½
12DT32+2	1 ½	2	2
Simplified calculations			
10DT24+2	1 ½	1 ½	1 ½
12DT32+2	2	1 ½	1 ½
Heat Transmission			
10DT24+2	1	1	1 ½
12DT32+2	1	1	1 ½

Figure 2.1 – Details of Bridge Girder Tested by Wood's (1960) to Establish a Fire Rating

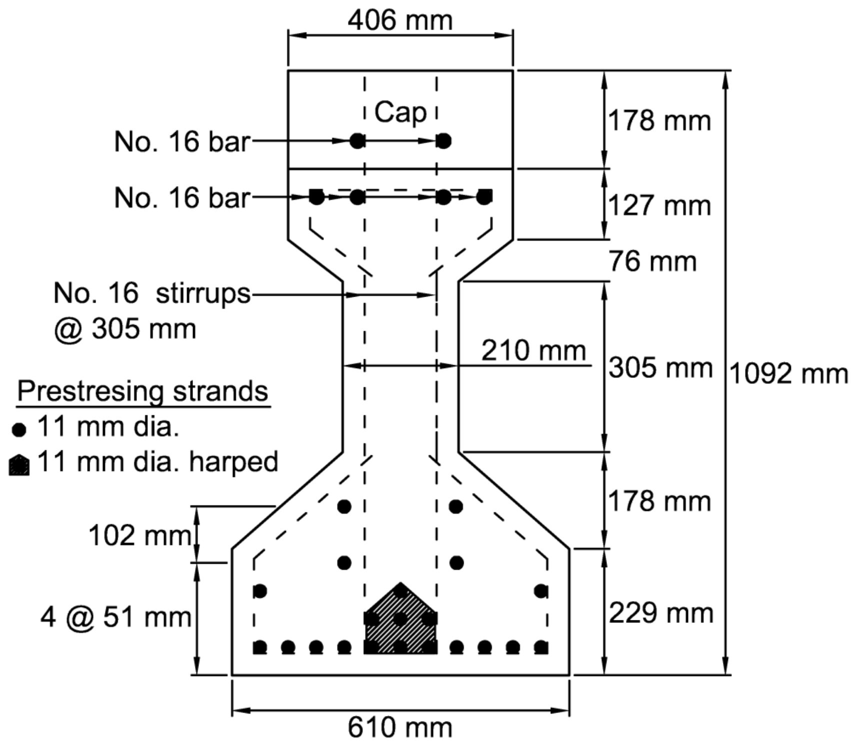

Figure 2.2 – Details of T-beams Tested by Selvaggio and Carlson (1963) to Study the Effect of Restraint

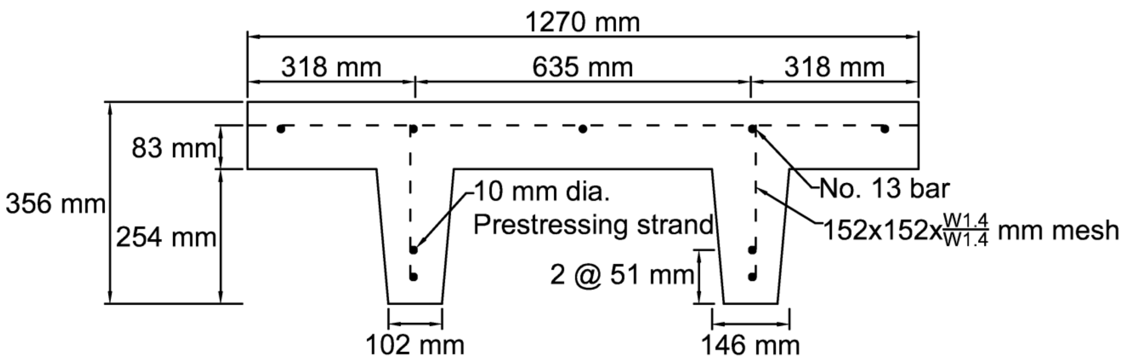

Figure 2.3 – Details of Concrete Joist Floor and Roof Assembly Tested by Abram et al. (1971) to Evaluate Unexposed Surface Temperatures

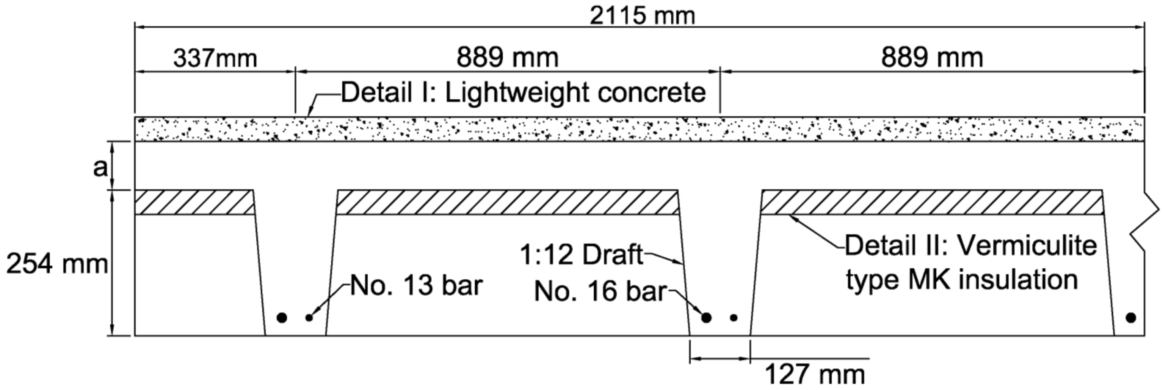

Figure 2.4 – Details of T-beam's Tested by Abram et al. (1971) to Compare the Unexposed Slab Temperatures

(a) First Test Specimen

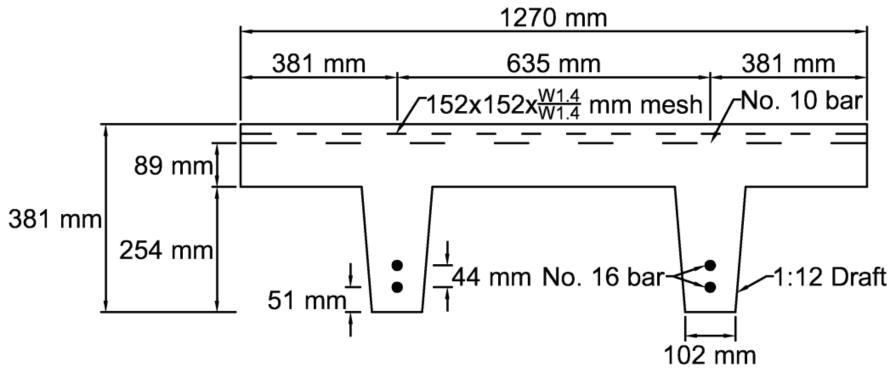

(b) Second Test Specimen

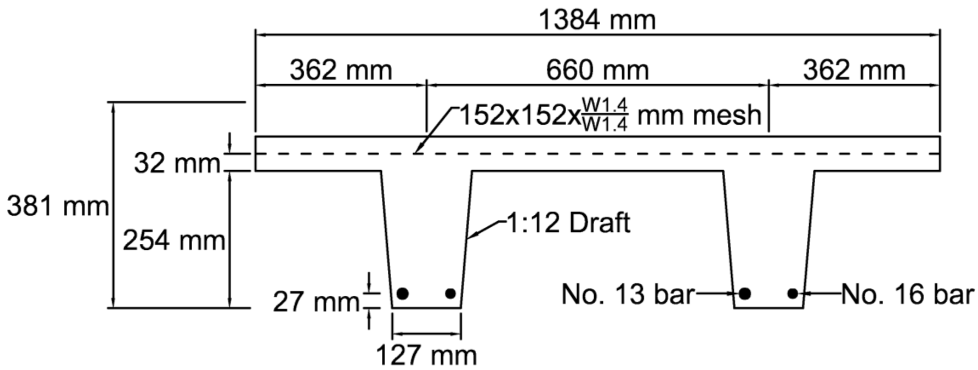

Figure 2.5 - Details of Insulated T-beam's Tested by Abram's and Gustaferro's (1972) Study to Assess the Effect of Spray-applied Insulation on Fire Ratings

(a) Non-insulated T-beam

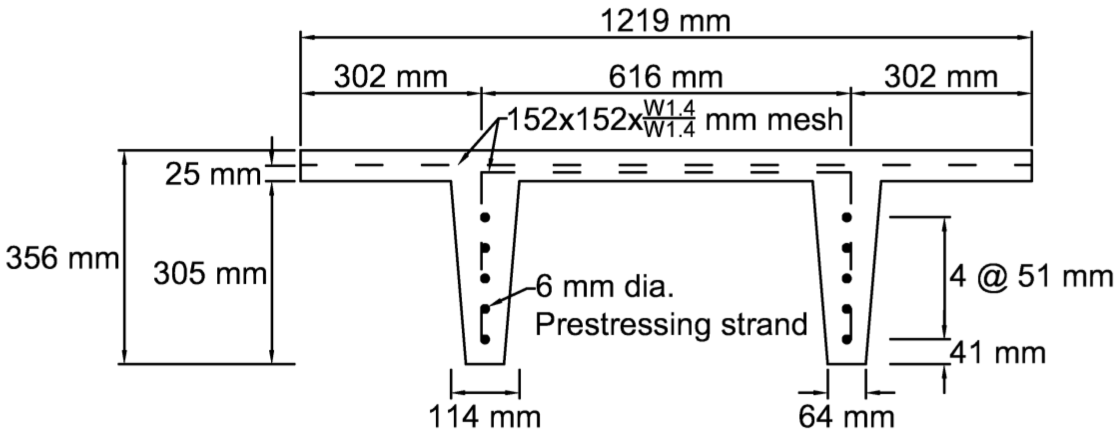

(b) ½ in. Vermiculite Acoustical Insulation Protected T-beam

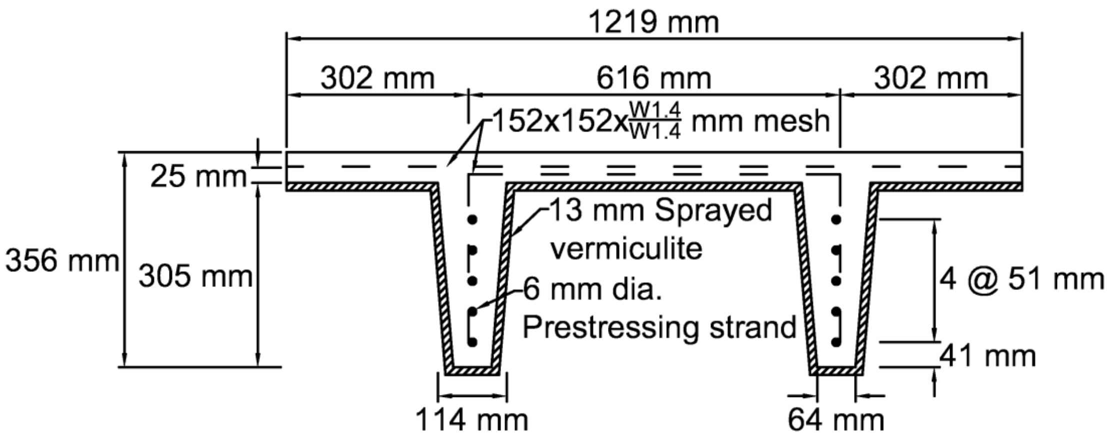

Figure 2.5 (cont'd) - Details of Insulated T-beam's Tested by Abram's and Gustaferro's (1972) Study to Assess the Effect of Spray-applied Insulation on Fire Ratings

(c) 1 in. Vermiculite Acoustical Insulation Protected T-beam

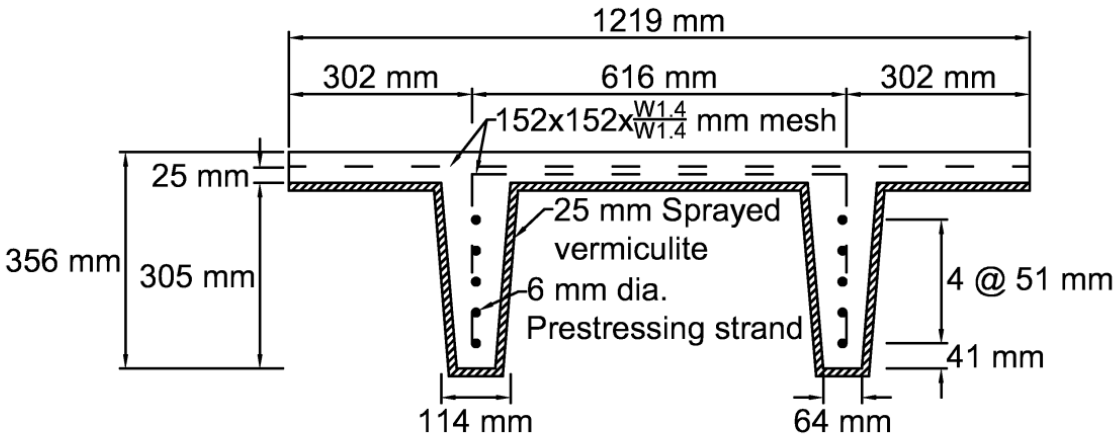

(d) ½ in. Mineral Fiber Insulation Protected T-beam

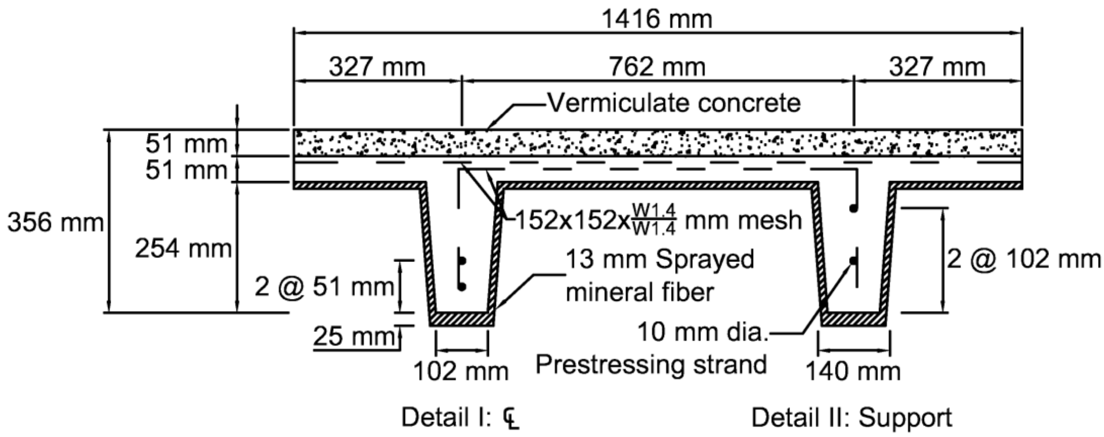

Figure 2.6 – Details of Continuous RC Beams Tested by Lin et al. (1981) to Investigate the Effects of Shear and Moment Redistribution on Fire Performance

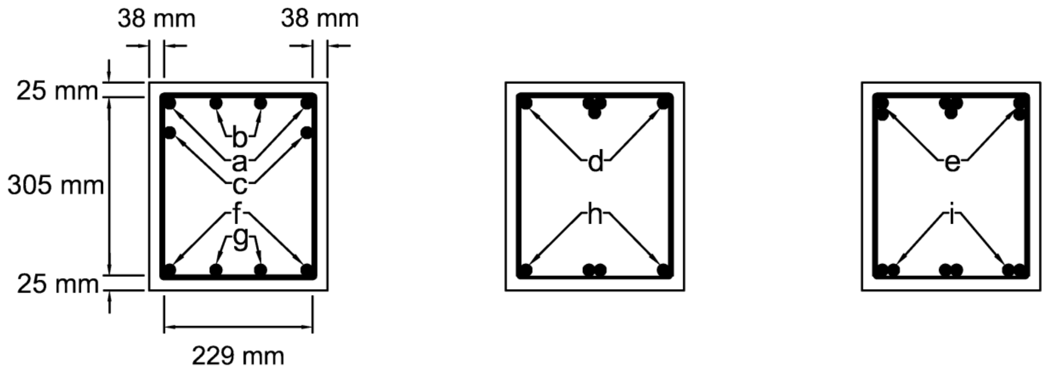

Figure 2.7 – Details of Continuous T-beam Tested by Lin et al. (1981) to Investigate the Effects of Shear and Moment Redistribution on Fire Performance

(a) Midspan Section

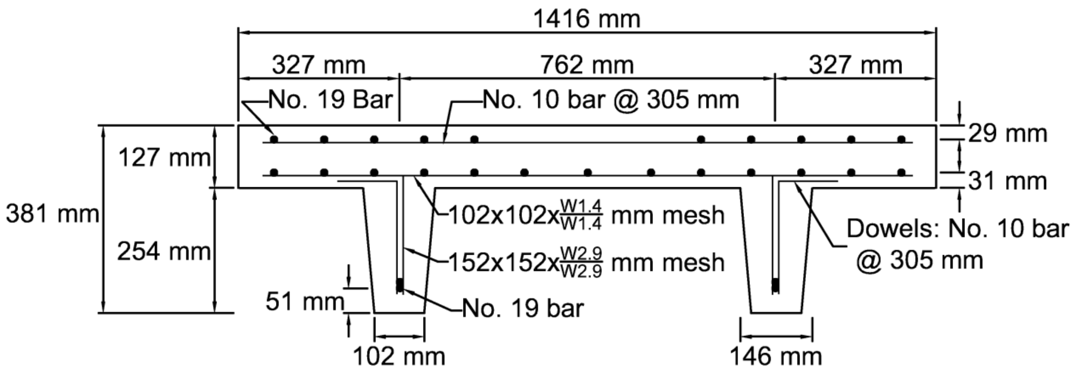

(b) Support Section

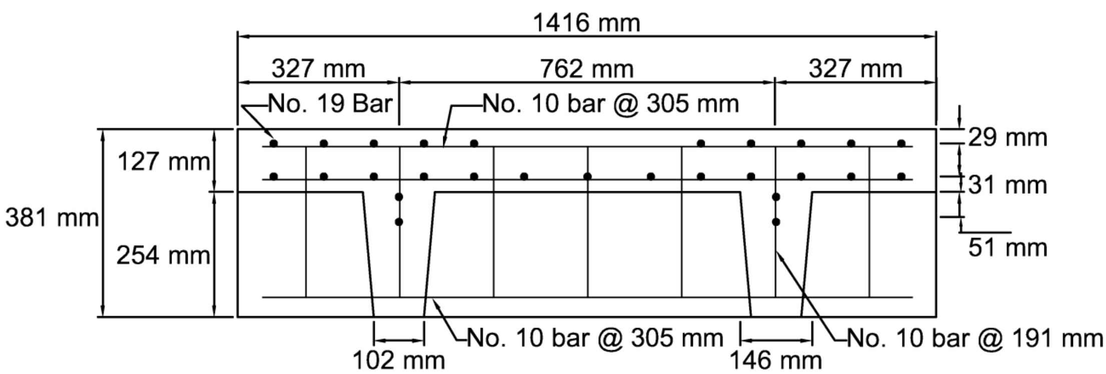

Figure 2.8 – Cross-sectional Details of Double T-beams Tested by Franssen and Bruls (2007) to Develop a Proprietary Fire Rating

(a) Original Section

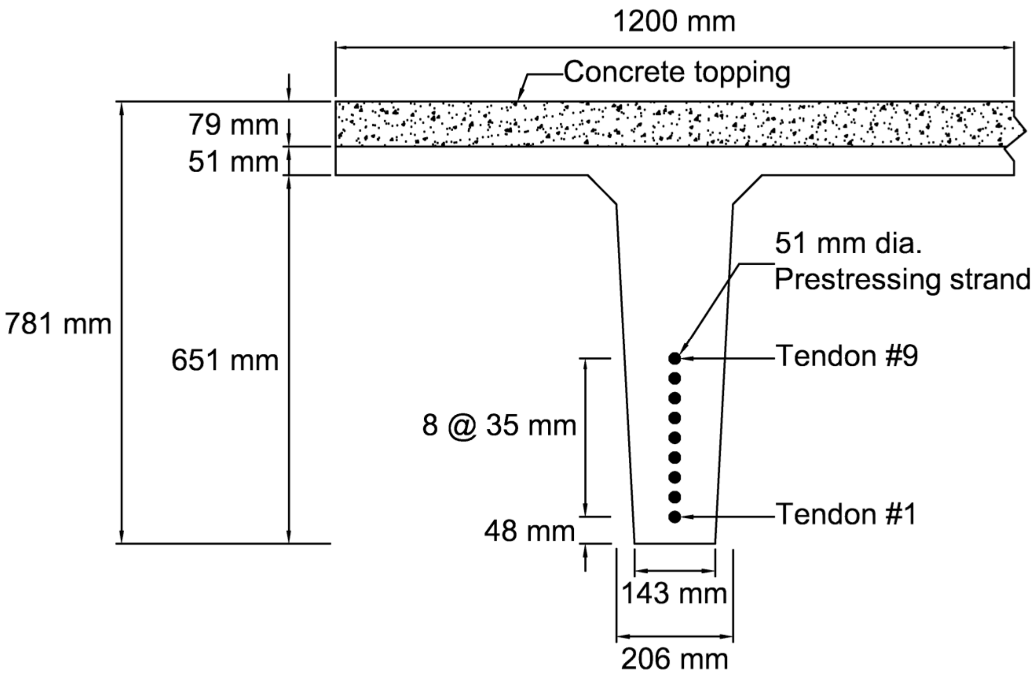

(b) Improved Section

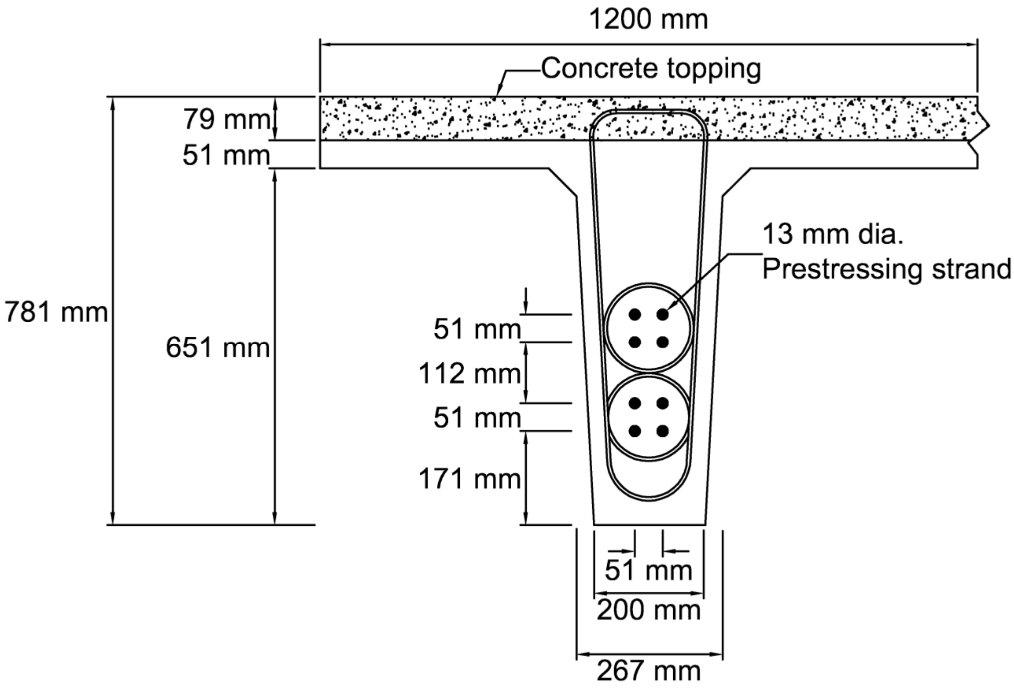

Figure 2.9 – Details of Double T-beams Tested by Anderson and Lauridsen (1999) to Study the Effects of Fire Induced Spalling

(a) Cross-sectional Details

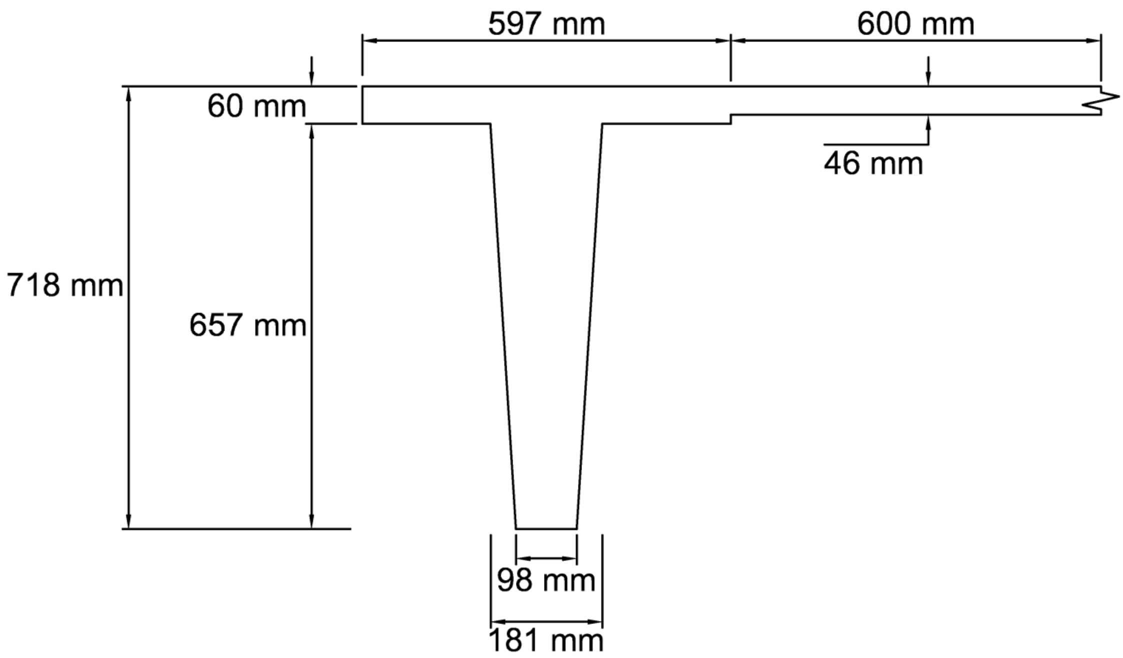

(b) Strand Arrangements in the Beams

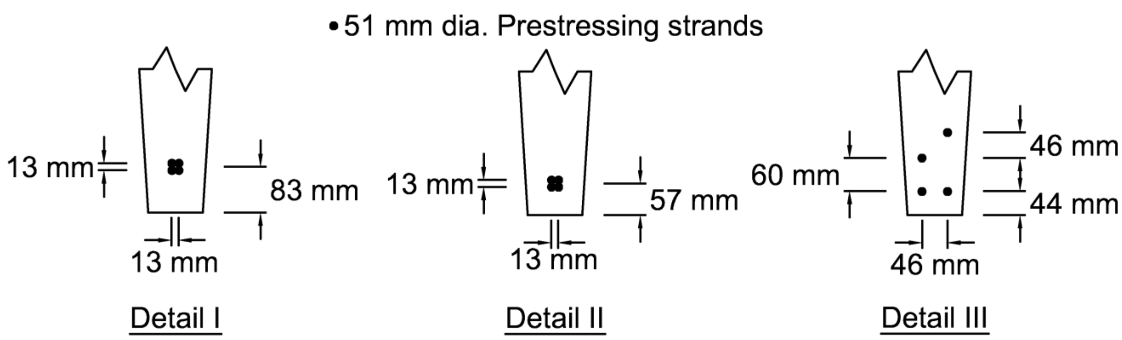

Figure 2.10 – Variation of Thermal Conductivity of Concrete as Function of Temperature according to Eurocode (2004) and ASCE (1992)

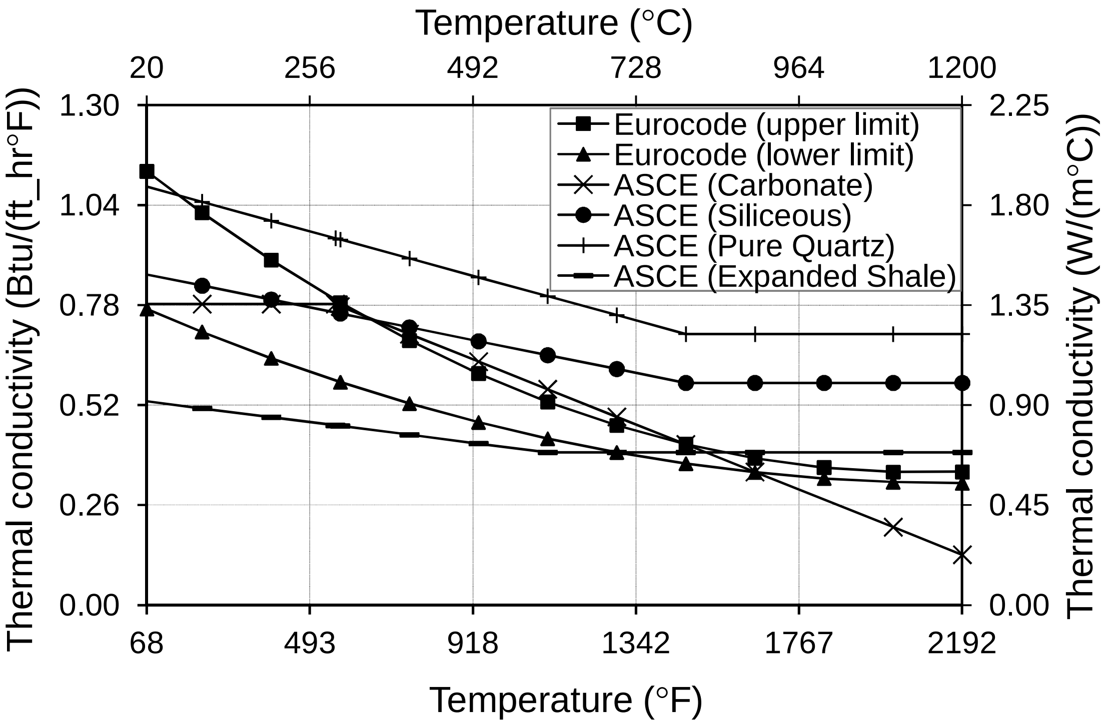

Figure 2.11 – Variation of Thermal Capacity of Concrete as a Function of Temperature according to Eurocode (2004) and ASCE (1992)

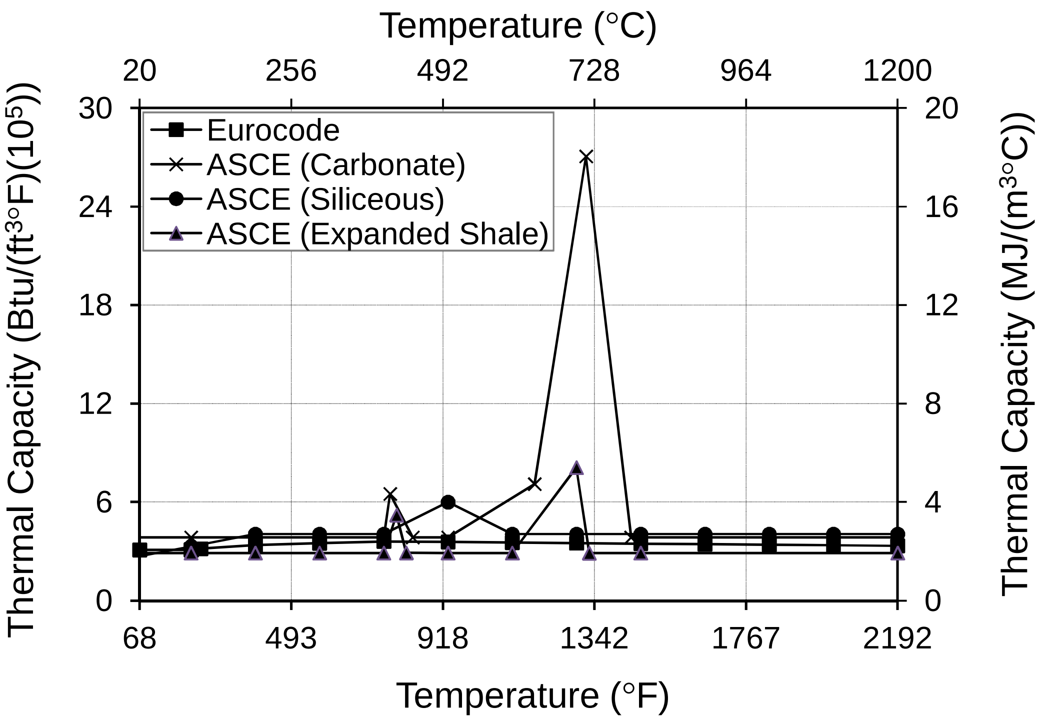

Figure 2.12 – Variation of Concrete Stress-Strain Curves as a Function of Temperature according to Eurocode (2004) and ASCE (1992)

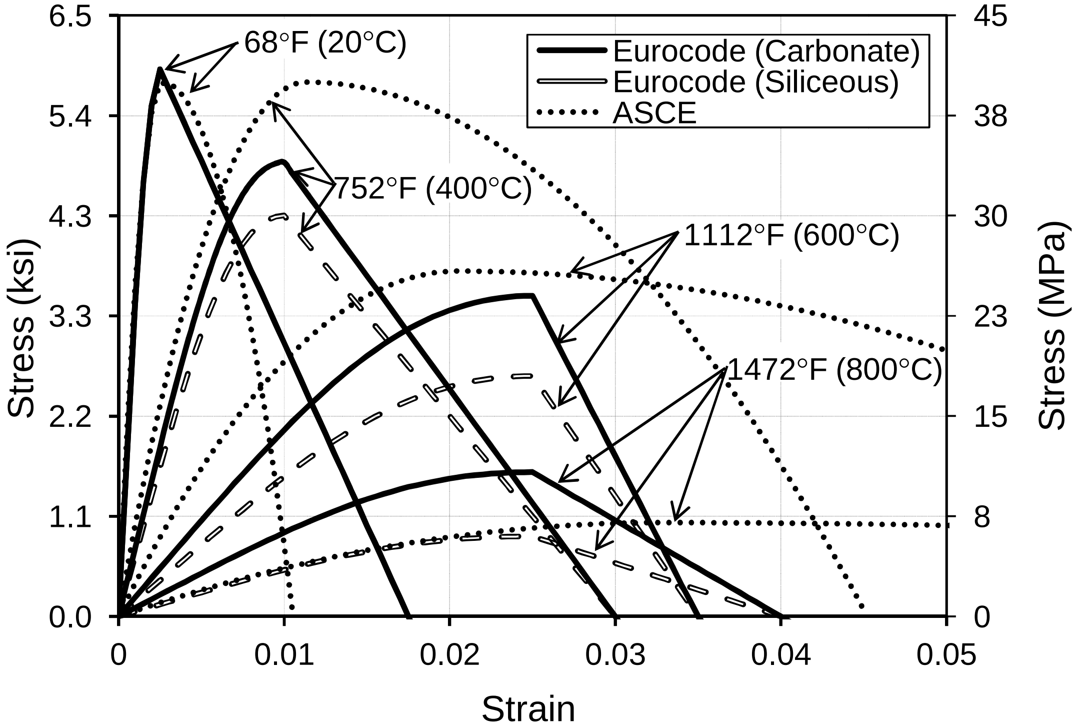

Figure 2.13 – Variation of Elastic Modulus of Concrete as a Function of Temperature according to Eurocode (2004) and ASCE (1992)

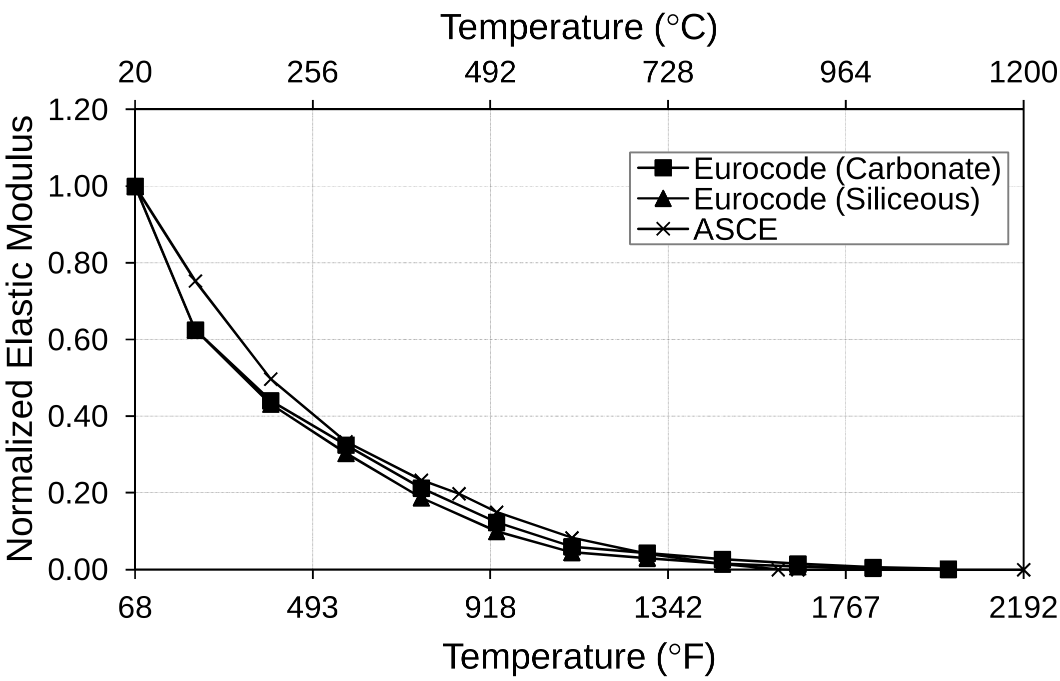

Figure 2.14 – Variation of Concrete Compressive Strength as a Function of Temperature according to Eurocode (2004) and ASCE (1992)

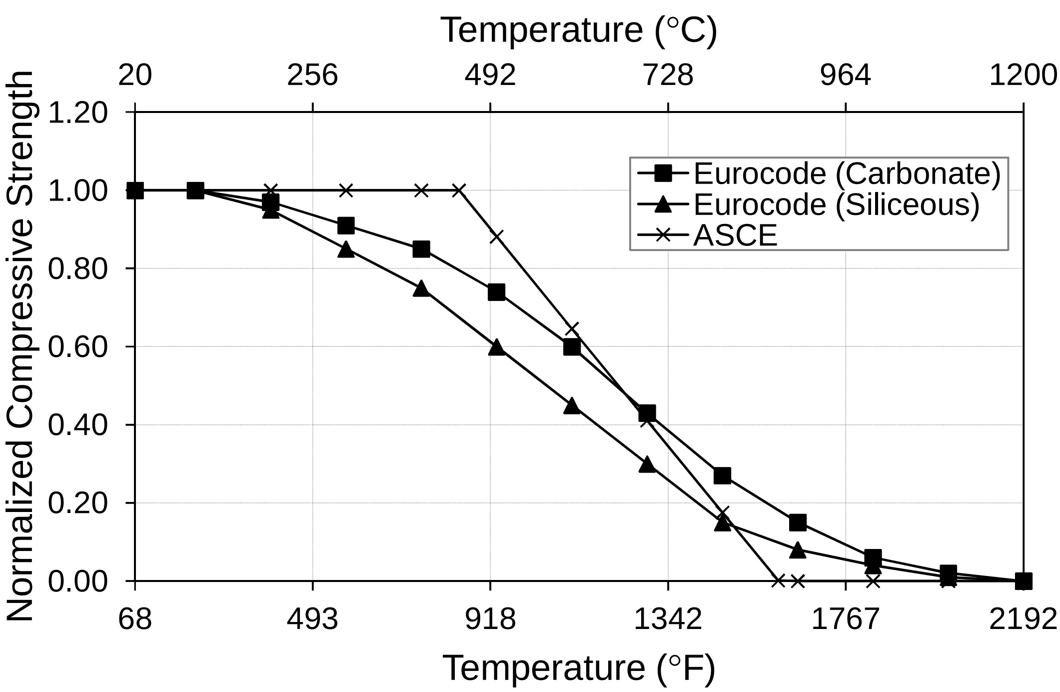

Figure 2.15 – Variation of Concrete Tensile Strength as a Function of Temperature according to Eurocode (2004)

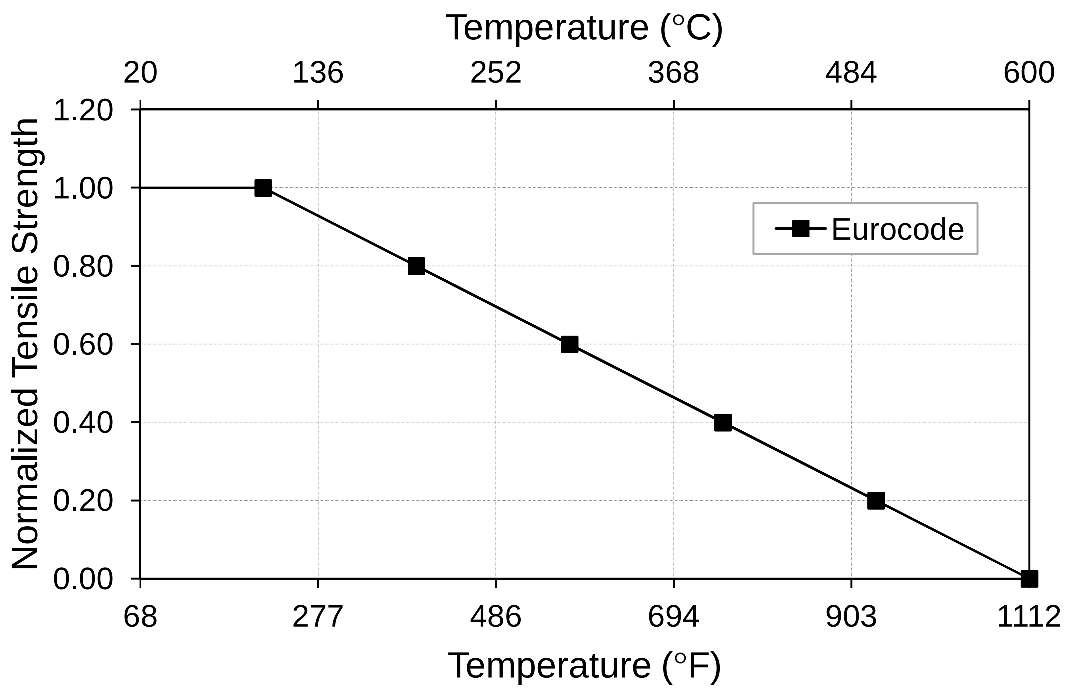

Figure 2.16 – Variation of Concrete Thermal Expansion as a Function of Temperature according to Eurocode (2004) and ASCE (1992)

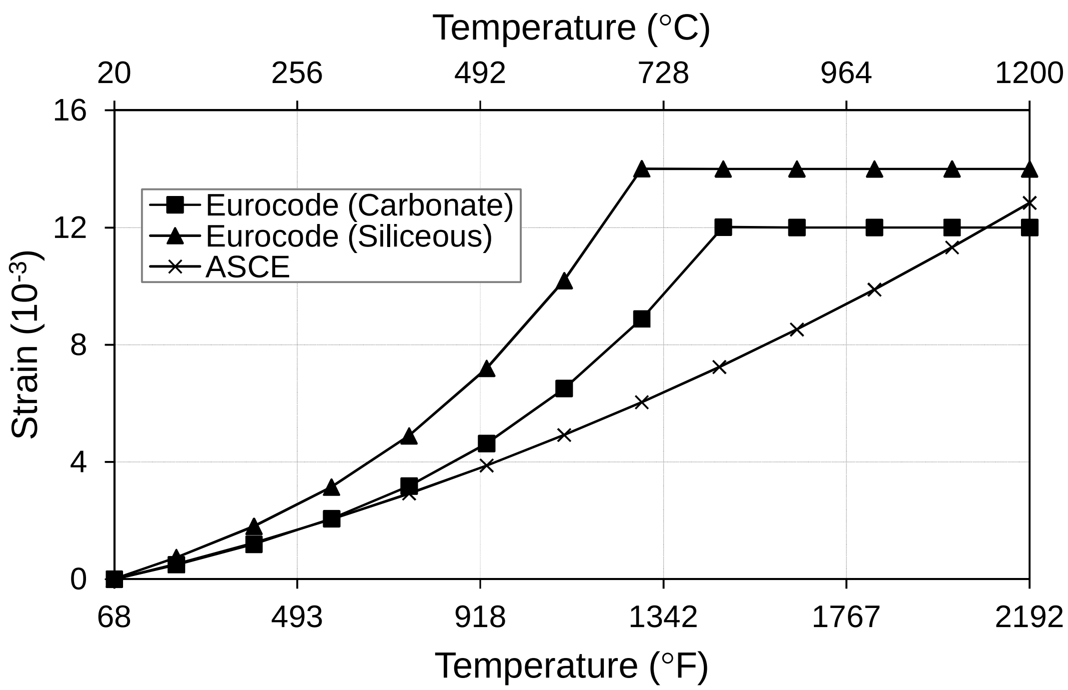

Figure 2.17 – Variation of Prestressing Steel Stress-Strain Curves as a Function of Temperature according to Eurocode (2004)

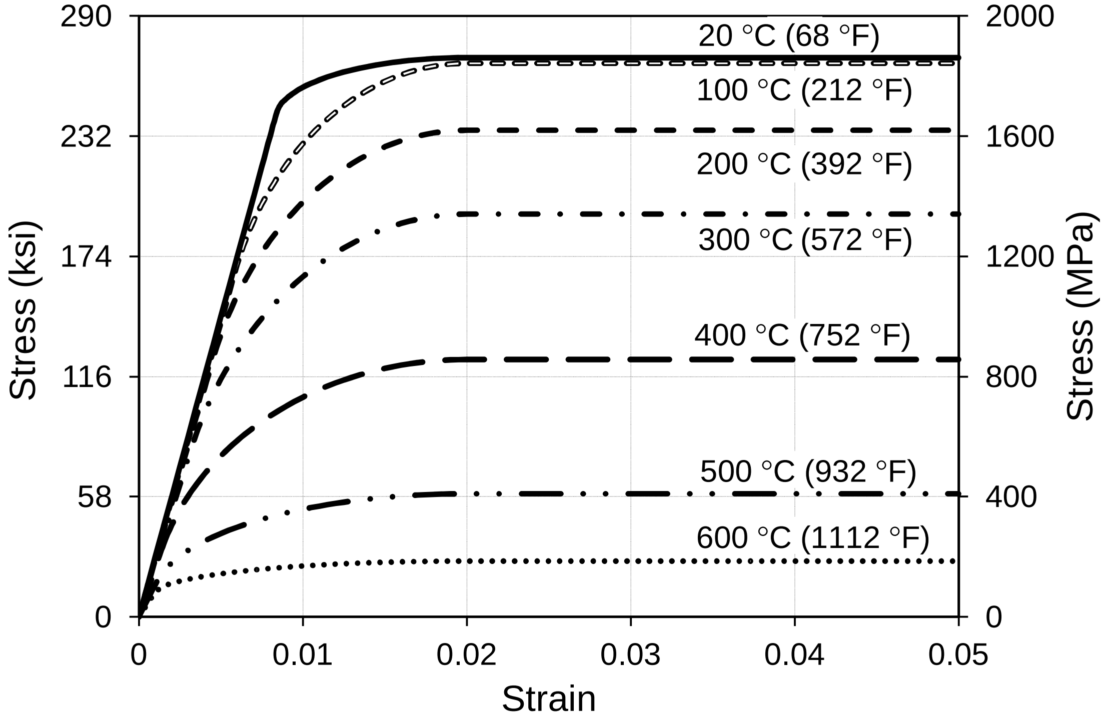

Figure 2.18 – Variation of Mild Reinforcing Steel Stress-Strain Curves as a Function of Temperature according to Eurocode (2004) and ASCE (1992)

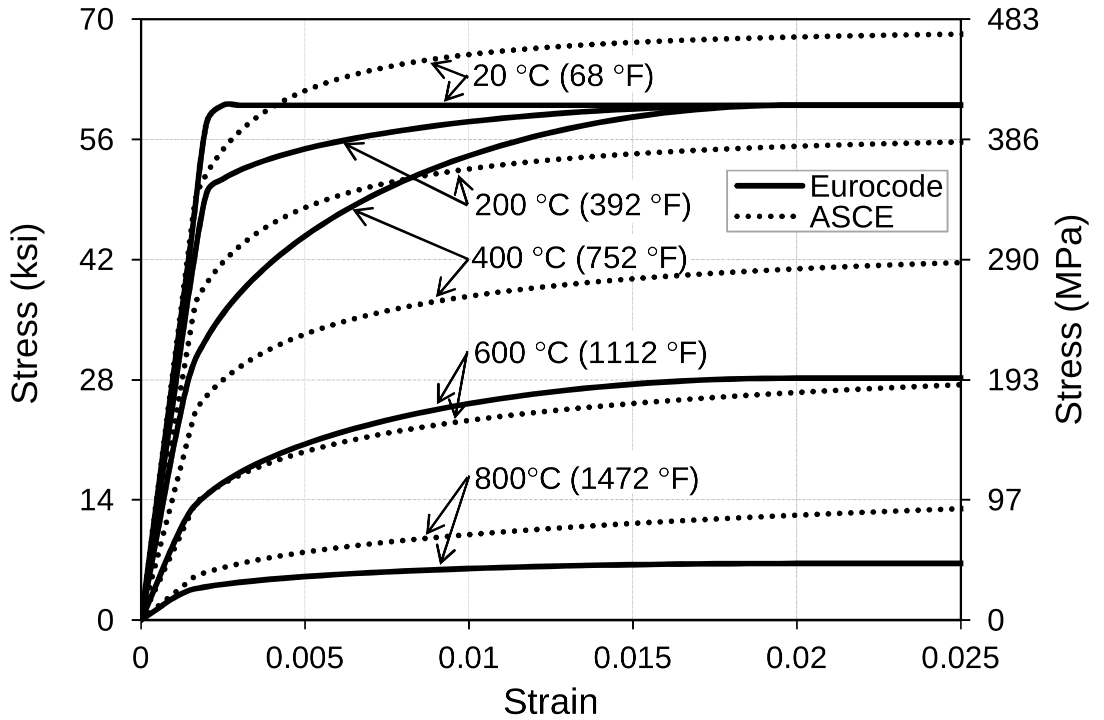

Figure 2.19 – Variation of Mild Reinforcing and Prestressing Steel Ultimate Strength as a Function of Temperature according to Eurocode (2004), PCI (2004), and ASCE (1992)

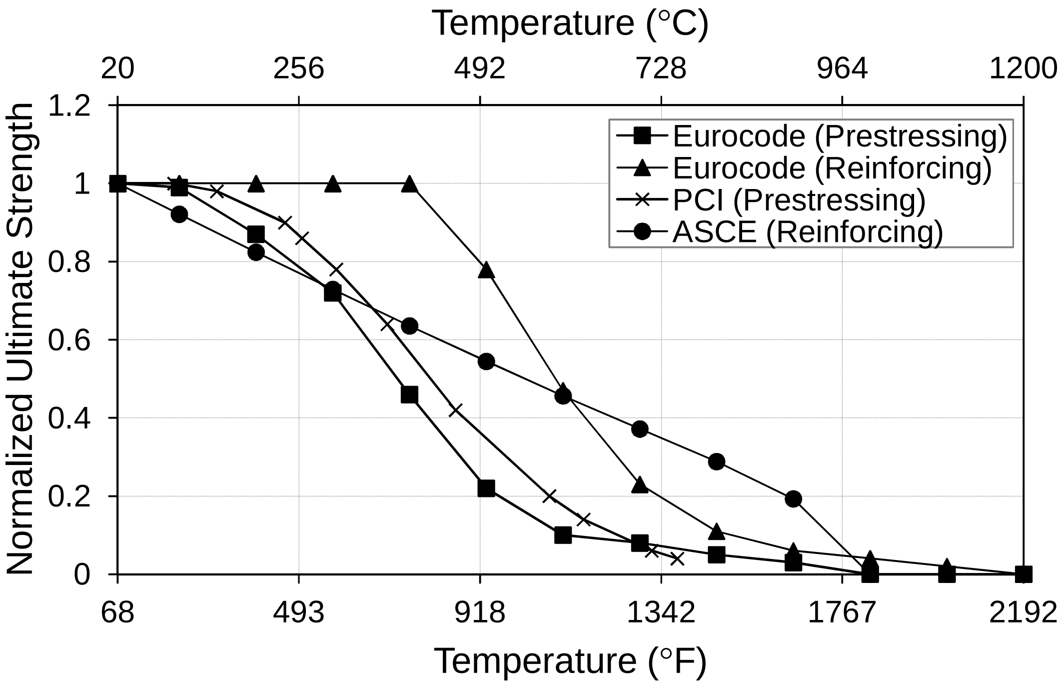

Figure 2.20 – Variation of Mild Reinforcing and Prestressing Steel Yield Strength as a Function of Temperature according to Eurocode (2004) and ASCE (1992)

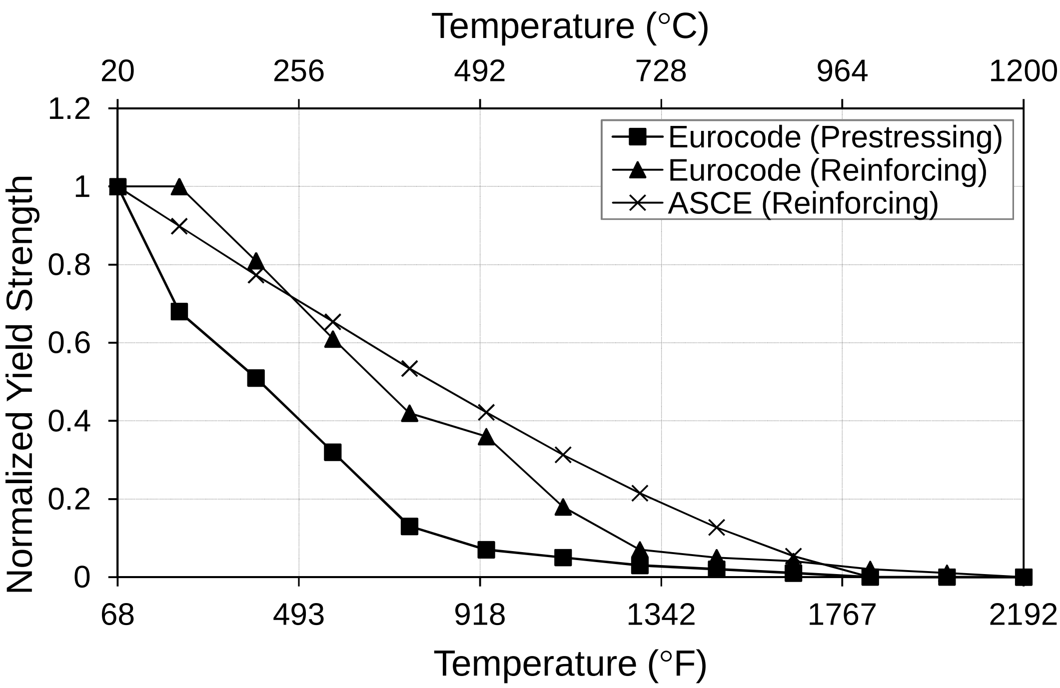

Figure 2.21 – Variation of Mild Reinforcing and Prestressing Steel Elastic Modulus as a Function of Temperature according to Eurocode (2004) and ASCE (1992)

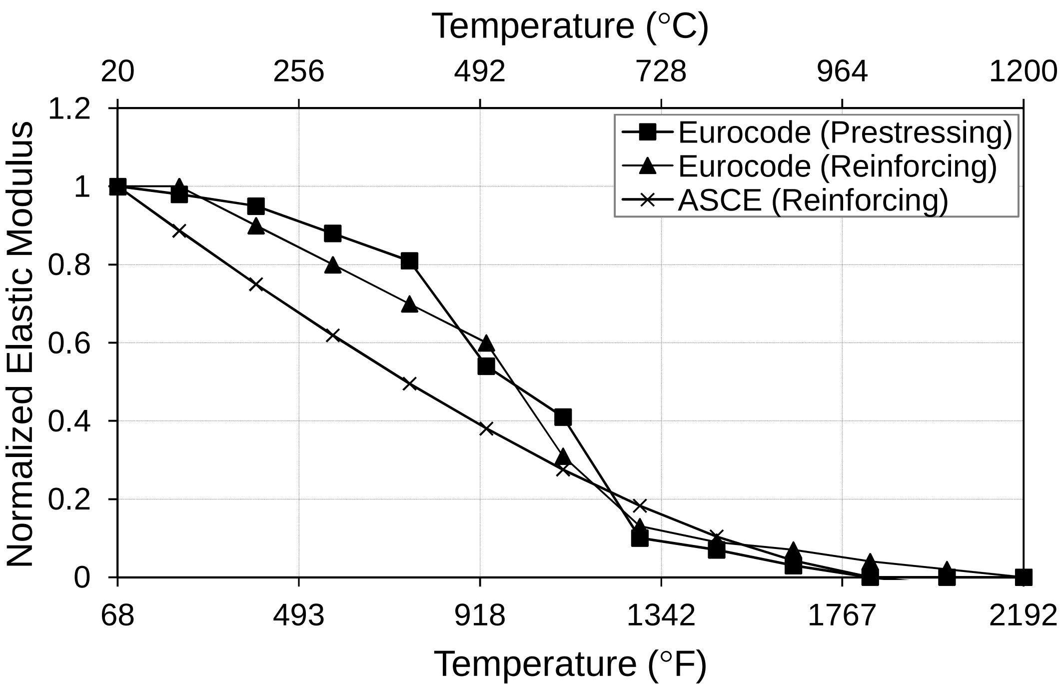

Figure 2.22 – Variation of Mild Reinforcing and Prestressing Steel Thermal Elongation as a Function of Temperature according to ASCE (1992) and Eurocode (2004)

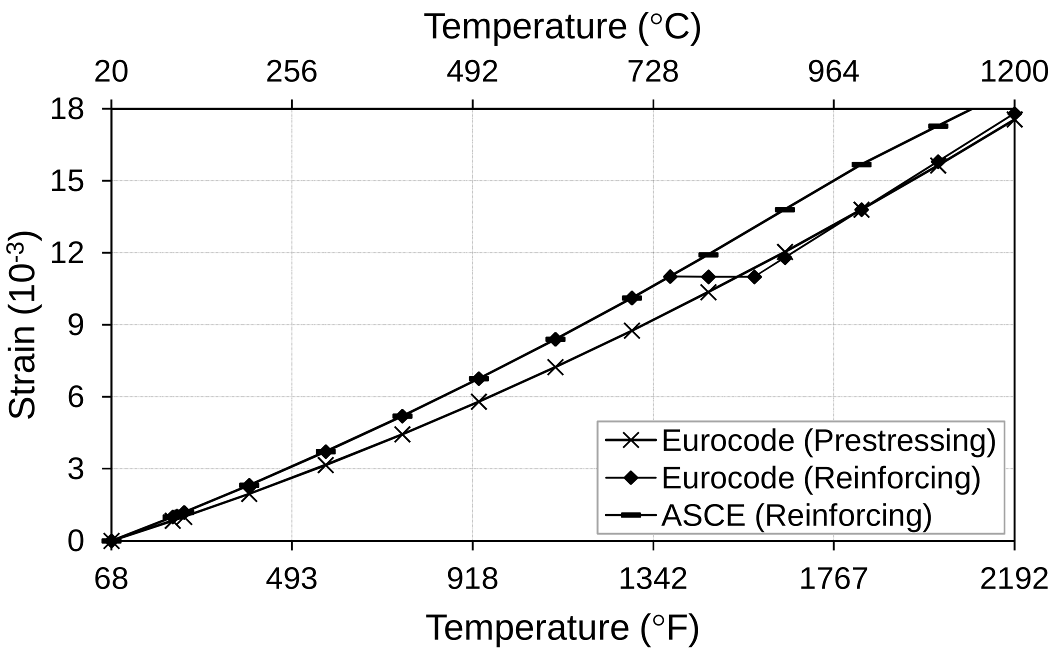

Chapter 3

3. Numerical Model

3.1. General

In this chapter, details of SAFIR, the finite-element computer program utilized to carry out numerical studies on precast/prestressed concrete (PPC) double T-beams, is presented. The chapter begins with a discussion on the rationale behind why SAFIR was selected to perform the fire resistance analysis. Next, a brief overview of SAFIR is presented, followed by a detailed description of the general analysis procedure. Also, the specifics of both the thermal and structural analysis procedures are highlighted, as well as the material properties used in each analysis. A summary of SAFIR's software features are mentioned and the findings of the sensitivity analysis to investigate the influence of mesh density and element length on the accuracy of thermal and structural models are provided. At the conclusion of this chapter two separate studies are presented to validate the model and the information is summarized.

3.2. Selection of Computer Model

SAFIR, a special-purpose, finite-element program was selected to perform the numerical studies for this research. The reason why SAFIR (2004) was selected, rather than other commercially available finite-element software packages, such as ANSYS (2011) or ABAQUS (2011), is because this program has been developed for the sole purpose of modeling structures in fire. Although, these other highly sophisticated programs are more than capable of achieving the same goal, they can require a significant amount of effort to develop a working model, as well as to validate the model. In contrast, SAFIR has been well validated for modeling the fire response of numerous types of members and materials. Furthermore, the program has reached a level of refinement where even the subtle nuances that require years of experience are already accounted for in the model. In addition, SAFIR offers the convenience of a library of predefined high temperature material models and fire curves. It also, limits the number structural element to only the most relevant elements required to model the types of structures encountered in civil applications.

3.3. Computer Program SAFIR

As mentioned, numerical studies of PPC double T-beams are carried out using a special-purpose finite-element computer program SAFIR (2004), developed at the University of Liege in Belgium, which is capable of predicting the fire response of structural systems. This software is well validated for evaluating fire resistance of steel and RC members. However, SAFIR is utilized to assess the fire resistance of PPC members in a limited way (Franssen and Bruls 1997 and Franssen 1993). In this computer program, the fire resistance of a structural system is analyzed through a two-fold thermo-mechanical analysis. For thermal analysis, the cross-section is discretized into triangular and quadrilateral solid elements in 2-dimensions or prismatic (6 or 8 nodes) elements in 3-dimensions. For structural analysis, the member is discretized into truss, beam, frame, shell, or prismatic beam elements. The elements can be discretized into irregular-shaped cross-sections with multiple materials. Any fire exposure (design or standard) scenario can be incorporated in the analysis by providing relevant time–temperature data. In the analysis the computer program accounts for high-temperature material properties, large displacements, both heating and cooling phases of a fire, torsion, and residual stresses.

3.3.1. General Analysis Procedure

The thermal mechanical analysis utilized in SAFIR is based on a time-step approach. Figure 3.1 illustrates a flowchart of the iterative step-by-step procedure utilized in SAFIR. At the beginning of every analysis and iteration, the exposure temperatures are calculated based on the time-temperature relationship. These exposure temperatures are then applied to the thermal model as boundary conditions. Next, the thermal analysis is performed based on the exposure temperature, residual temperature, and high temperature thermal properties to determine the new temperatures within the structure. The temperature results from the thermal analysis are then used in the structural analysis to evaluate the temperature reduced mechanical properties for the structural model. Based on the structural models' mechanical properties, support conditions, and applied loading a structural analysis is undertaken to evaluate the stresses, strains, internal forces, and deflections of the structure. At the end of every iteration failure is checked. If failure occurs, then the analysis procedure ends, if failure does not occur another iteration begins and analysis procedure repeats itself.

3.3.2. Thermal Analysis

The thermal analysis model used in the numerical studies is based on fundamental heat transfer principles to generate temperature profiles within a two/three-dimensional nonlinear geometric cross-section. The PPC beams' cross-section is modeled as composed of three different materials (concrete topping, member, and steel prestressing strands) and discretized into triangular and quadrilateral solid elements, as illustrated in Figure 3.2. The Eurocode temperature-dependent thermal properties (thermal conductivity, specific heat, density, and thermal expansion) of concrete, prestressing steel, and mild reinforcing steel are built into the program and as an illustration are reproduced in the Appendix C. In thermal calculations, energy required to evaporate moisture within the concrete is considered, but the effect of fire-induced spalling that occurs in concrete is neglected.

3.3.3. Structural Analysis

The structural analysis model utilizes large deflection theory for tracing the mechanical response under fire conditions. The thermal analysis is linked to structural analysis by assuming that each triangular or quadrilateral element formed in the thermal analysis is represented as a fiber-based beam element. Each fiber is assigned a nonlinear temperature-dependent material property (Poisson's ratio, compressive strength, tensile strength, elastic modulus, and yield strength) in accordance with Eurocode 2 (2004) and is constant along the length of the beam element. The material properties incorporated in the model are reproduced in the Appendix C. The culmination of these fibers determine the stiffness of the beam elements and mechanical response at a given time step. Therefore, for a given time increment, the temperatures of all the fibers are generated from the thermal analysis and utilized in the structural analysis to estimate the reduction in strength and stiffness of that beam element.

For the analysis of a PPC beam, the discretization is a series (single line) of beam elements, as illustrated in Figure 3.3. Each beam element utilizes two integration points to assess the internal forces resulting from the applied loading. For simulating restraint effects, a truss element is incorporated and various degrees of restraint are simulated by modifying the cross-sectional area of the member. The output parameters at each time step include temperatures, support reactions, internal forces, and longitudinal and midspan deflections. Failure is defined as a loss of stiffness in the member or when the material strains are exceeded which typically corresponds to the strength limit state. The Newton–Raphson procedure is applied to solve the system of nonlinear equations. Although the structural model has numerous advantages, it cannot account for shear effects, fire-induced spalling in concrete, and bond degradation between prestressing strands and concrete.

3.3.4. Material Models

As mentioned, the material properties incorporated in both the thermal and structural analysis model are based on Eurocode 2 (2004). The empirical relationships and material models are reproduced in the Appendix C. The specific behavior of each these material properties has been discussed in detail in Chapter 2.

3.3.5. Software Features

SAFIR has numerous software features and its developers are continuously adding new features to the programs' repertoire. To mention a few, SAFIR provides the user with a easy to use graphical user interface pre-processor (depending on type of section) and post-processor allowing the user to visualize the models geometry, temperature isotherms, internal forces, and deflections, graphically. It also offers the user the option of matrix optimization, a feature that shortens the time required for analysis by renumbering the system of equations in a more efficient manner. Another feature is the option to include master-slave relations by imposing identical displacements and temperatures between nodes. SAFIR is also capable of torsional analysis, dynamic analysis for the local failure of members, and 3D thermal analysis. It also has the ability to model composite members.

3.4. Sensitivity Analysis

In a finite element model, the level of refinement used to discretize the model influences the accuracy of the results. In general, the finer the discretization, more accurate the results will be. Therefore, to assure an acceptable level of accuracy when assessing the fire resistance of PPC Beams in SAFIR, a sensitivity analysis was undertaken to study the influence of mesh density and element length in thermal and structural analyses, respectively. The study consisted of developing three models for each type of analysis. To investigate the influence of mesh density in the thermal analysis, a base model was discretized under the premise that a single quadrilateral element would represent one prestressing strand; hence the dimensions for the square element were derived from the strands cross-sectional area. The discretization utilized for the remaining elements were of similar size and proportion. As for the other two models, they were developed by either decreasing or increasing the mesh density by a factor of two. Figure 3.4 illustrates the three cases considered and are labeled as I, II, and III. The first case, model I, corresponds to the model with the coarsest mesh, while model III has the finest mesh. To investigate the influence of element length in the structural analysis, the original model was discretized into twenty 0.61 m (2 ft) long elements (model II). Similarly, two more models were discretized, one with ten 1.22 m (4 ft) (model I) and another with forty 0.30 m (1 ft) long elements (model III). The following discussion presents the finding of the sensitivity analysis.

Figure 3.5 illustrates strand and average slab temperature results from the three thermal models (I, II, and III). The strand temperatures are based on the lowest strand and were arbitrarily selected for the purpose of comparison. The results reveal that a finer mesh density produces higher temperatures. When comparing the results the average percent difference between the models range from 0.6 to 2.0% for the strand temperatures and 0.9 to 4.4% for the average slab temperatures. The greatest difference observed was between model I and III. The largest difference in individual data occurs within the first 20 minutes for the strand temperatures and between 20 and 50 minutes for the average slab temperatures with a maximum percent difference ranging from 7.9 to 27.3% and 4.3 to 19.6%, respectively. Based on these results it evident that model I produces the least accurate results. As for case II and III the results are nearly identical, excluding the difference of 7.9% that occurs early on in the fire and is short lived.

Figure 3.6 shows the midspan deflections for the three structural models developed to investigate the influence of beam length on fire resistance of PPC beams. As mentioned previously, the longest elements are utilized in model I and shortest elements in model III. In general, the three models correlate well with one another until the deflections begin to increase significantly at approximately 50 minutes, just prior to failure. The average percent difference between the deflections for each model range from 0.3 to 7.1%. When comparing failure times, model I fails first at 53 minutes with corresponding deflection of -0.46 m (-18.2 in.). Models II and III fail at 56 and 57 minutes with corresponding deflections of -1.12 m (-44.3 in.) and -1.39 m (-54.9 in.), respectively. These results indicate that model I provides the least accuracy, while only minor variations exist between models II and III. Based on the findings of the sensitivity analysis, model II will be used as the basis for discretization of the thermal and structural models used in the parametric study to investigate the factors that influence the fire resistance of PPC beams.

3.5. Model Validation

The numerical model, SAFIR (2004), was validated by comparing predictions from the model with measured data from fire tests on two PPC double T-beams. There is very limited experimental data on fire performance of PPC double T-beams. Due to lack of comprehensive test data (such as temperatures and deflections) for any one tested beam, test data from the first beam was utilized to compare the predicted unexposed slab temperatures, while the data from the second beam was utilized to compare strand temperatures and deflections.

The first beam selected for validation is a PPC double T-beam tested at Underwriter's Laboratories (UL) (1996) to establish proprietary fire ratings under ASTM E119 (2008) standard fire exposure. The cross-sectional details of the tested beam are shown in Figure 3.7. In the tests failure occurred when the unexposed surface temperature exceeded the limiting temperature criterion, which is 181°C (325°F). Results from fire tests were used to generate fire ratings of 30, 60, 90, 120, and 180 minutes by increasing the slab thicknesses (*h*) from 51, 76, 102, 121, and 152 mm (2, 3, 4, 4¾, and 6 in.). This beam was analyzed using SAFIR with various slab thicknesses. For the analysis, a normal weight concrete comprising carbonate aggregate with a moisture content of 3% by weight was assumed. High temperature properties, as specified in Eurocode, are used in the analysis. These properties are similar to those in ASCE manual of practice and are reproduced in Appendix C.

The unexposed slab temperatures predicted by SAFIR are plotted in Figure 3.8 as a function of fire exposure time for varying slab thicknesses. Also plotted in the figure is the limiting heat transmission temperature of 181°C (325°F). In all cases the temperatures in the unexposed side of the slab initially rises slowly in a linear fashion until all of the free moisture has completely evaporated. After this point, the temperatures increase at a higher rate and follow a similar trend as that of ASTM E119 fire curve. These temperature trends reveal that a thicker slab delays the temperature rise in the unexposed slab's surface than a thinner slab. Figure 3.9 shows a comparison of predicted fire resistance ratings with that of UL listed ratings for beams with different slab thicknesses. The predicted fire resistance values are close to UL listed ratings over the entire range with the data points lying within 10%. These comparisons indicate that the unexposed slab temperatures can be predicted reasonably well with SAFIR if relevant high temperature thermal properties (concrete type, moisture content, and density) are accounted for in the analysis.

The second beam selected for validation was the one tested by Gustaferro et al. (1962) to study the response of a simply supported PPC double T-beam under ASTM E119 (2008) fire exposure. In the test a uniform live load of 4.8 KN/m^2 (100 psf) was applied over the 6.1 m (20 ft) span of the beam whose cross-section is shown in Figure 3.10. A summary of test data namely, strand temperatures, midspan deflections, and fire resistance time, is listed in Table 3.1. This beam was analyzed using SAFIR computer program. In the analysis the moisture content within the concrete was assumed to be 3% by weight. The strand temperatures generated from SAFIR analysis are plotted in Figure 3.11, where strands 5 and 1 correspond to the strand with the greatest and least concrete cover, respectively. In all strands the temperatures gradually increase, with temperatures in strand 1 rising more rapidly than strand 5. Also, shown in Figure 3.11 are the minimum, average, and maximum strand temperatures at failure as measured in the test. The results indicate a strong correlation between the model and test data, with average strand temperatures falling within 9% of each other. The difference in the strand temperatures can be attributed to variation of the concrete moisture content and thermal properties of concrete used in the analysis. These values had to be assumed based on best guess estimates, since they are not provided in the test report.

The predicted midspan deflections are compared with measured deflections from the test in Figure 3.12. The deflections gradually decrease with time up to about 40 minutes due to deterioration of the members' stiffness. After 40 minutes, the measured deflections increase at a faster rate compared to predicted deflections. This can be primarily attributed to faster degradation of strength and also to the fact that high temperature creep plays significant role and the model accounts for only part of this creep. The predicted deflections are within 24% of measured values and this kind of variation is not uncommon in fire resistance analysis. The failure times (fire resistance) match well with only a difference of 4 minutes. The strand temperature, midspan deflection and failure time results indicate that SAFIR is capable of reasonably predicting thermal and structural response of PPC beams exposed to fire.

3.6. Summary

This chapter provided a comprehensive explanation of the finite element analysis program SAFIR used in the numerical studies of chapter 4 to predict the fire response of PPC double T-beams. It began with a discussion describing rationale behind the selection of the program, compared to other commercially available programs. Next, an overview of the program and general analysis procedure was presented, followed by a detailed description of the thermo-mechanical analysis. A number of the programs software features were also highlighted. Based on the sensitivity analysis, the level of refinement to be used in the finite element models to produce accurate results was established. To conclude the chapter, the findings of the two PPC double T-beams used to validate the model were presented. These studies revealed, the temperatures, deflections, and fire resistance times predicted with SAFIR show a strong correlation with the results of real fire tests.

Table 3.1 – Summary of Results from Fire Resistance Test on Simply Supported PPC Beam.

Time (minutes)	30	45	62	Strand temperatures (°C)		
Midspan deflection (mm)	58	124	381	**Minimum**	**Average**	**Maximum**
Fire endurance (minutes)		62		366	521	632

Source: Gustaferro et al. October 1962. Note: 1 in. = 25.4 mm; T(°C) = 5/9*(T(°F) - 32).

Figure 3.1 – Overview of SAFIR's General Analysis Procedure

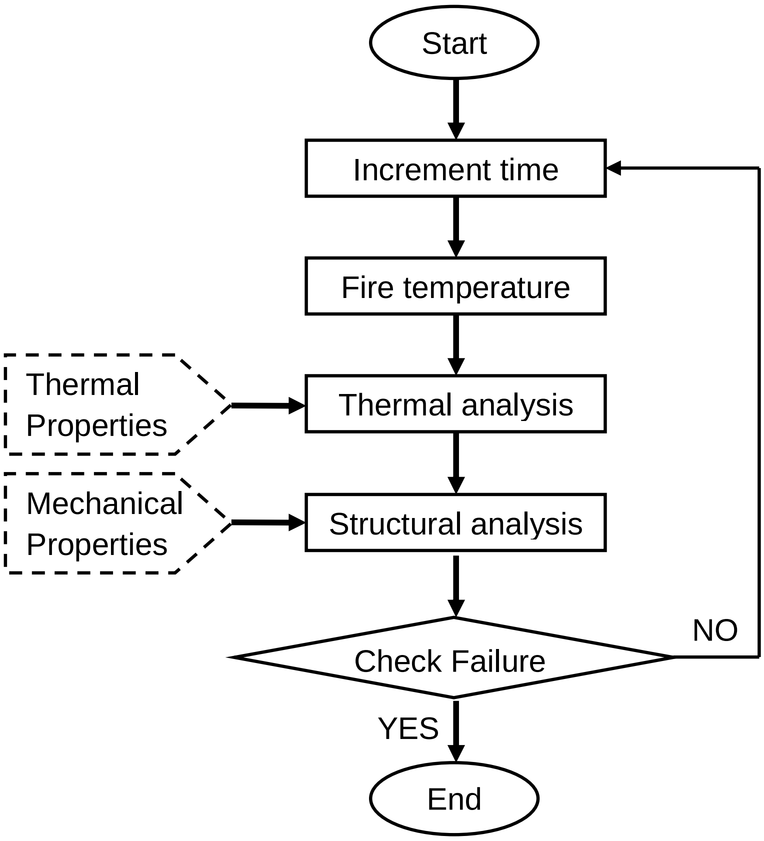

Figure 3.2 – 10DT24+2 Thermal Model for Temperature Analysis of PPC T-beam. For interpretation of the references to color in this and all other figures, the reader is referred to the electronic version of this thesis.

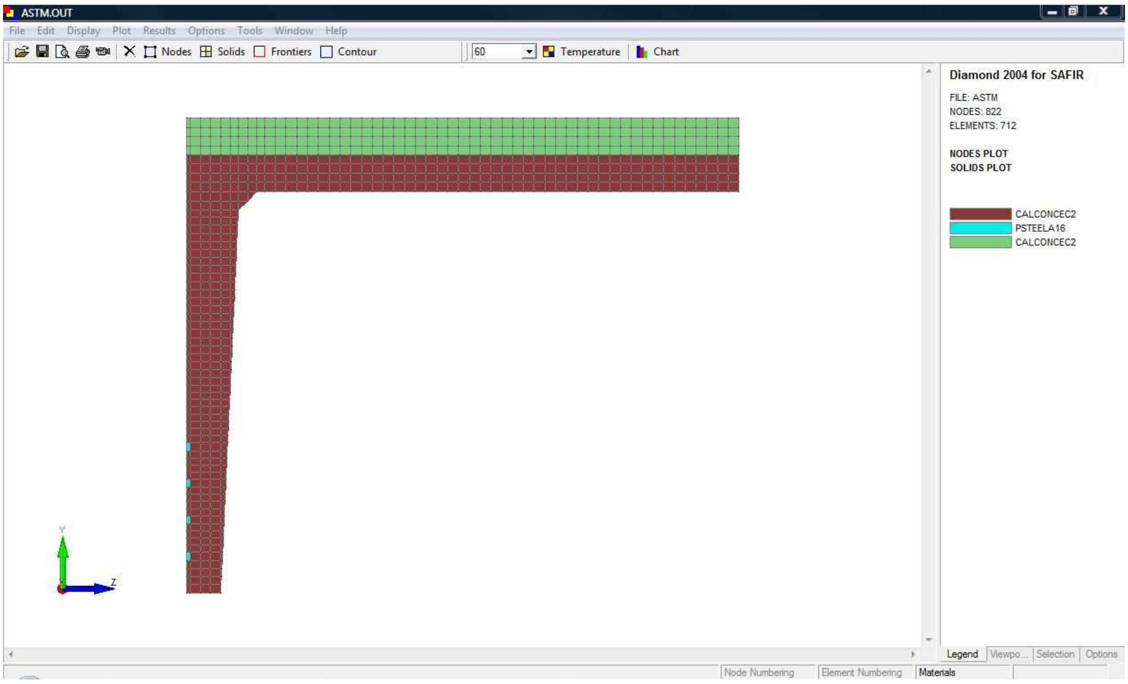

Figure 3.3 – 10DT24+2 Structural Model for Strength Analysis of PPC T-beam.

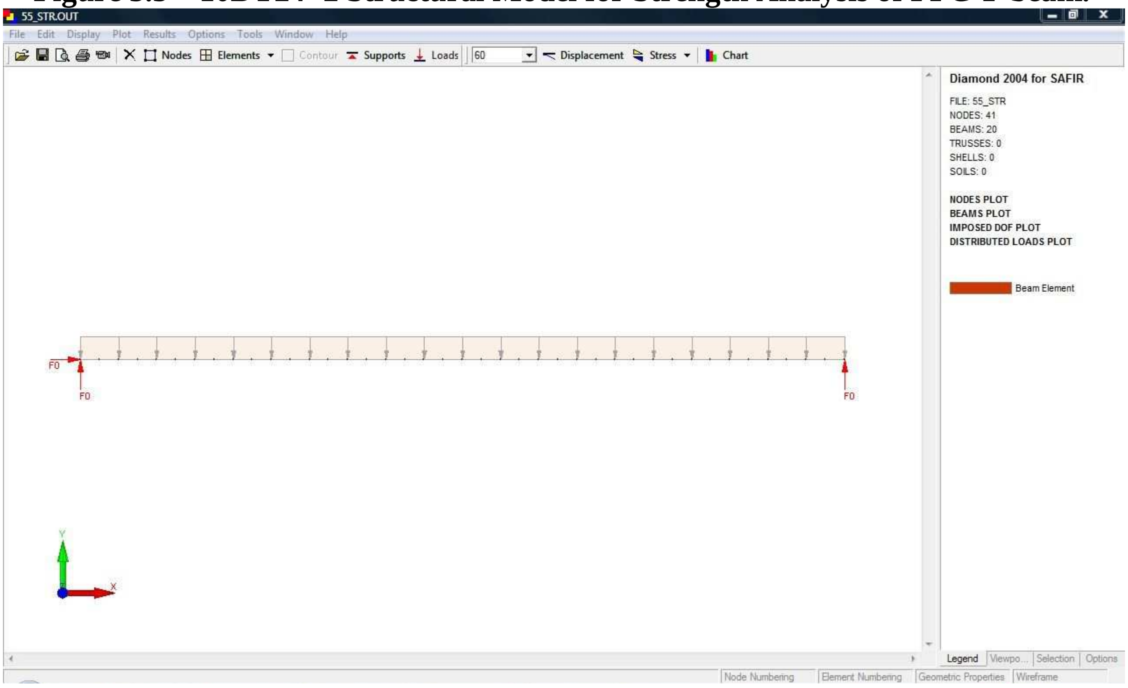

Figure 3.4 – Thermal Model I, II, and III for Temperature Analysis of PPC T-beam.

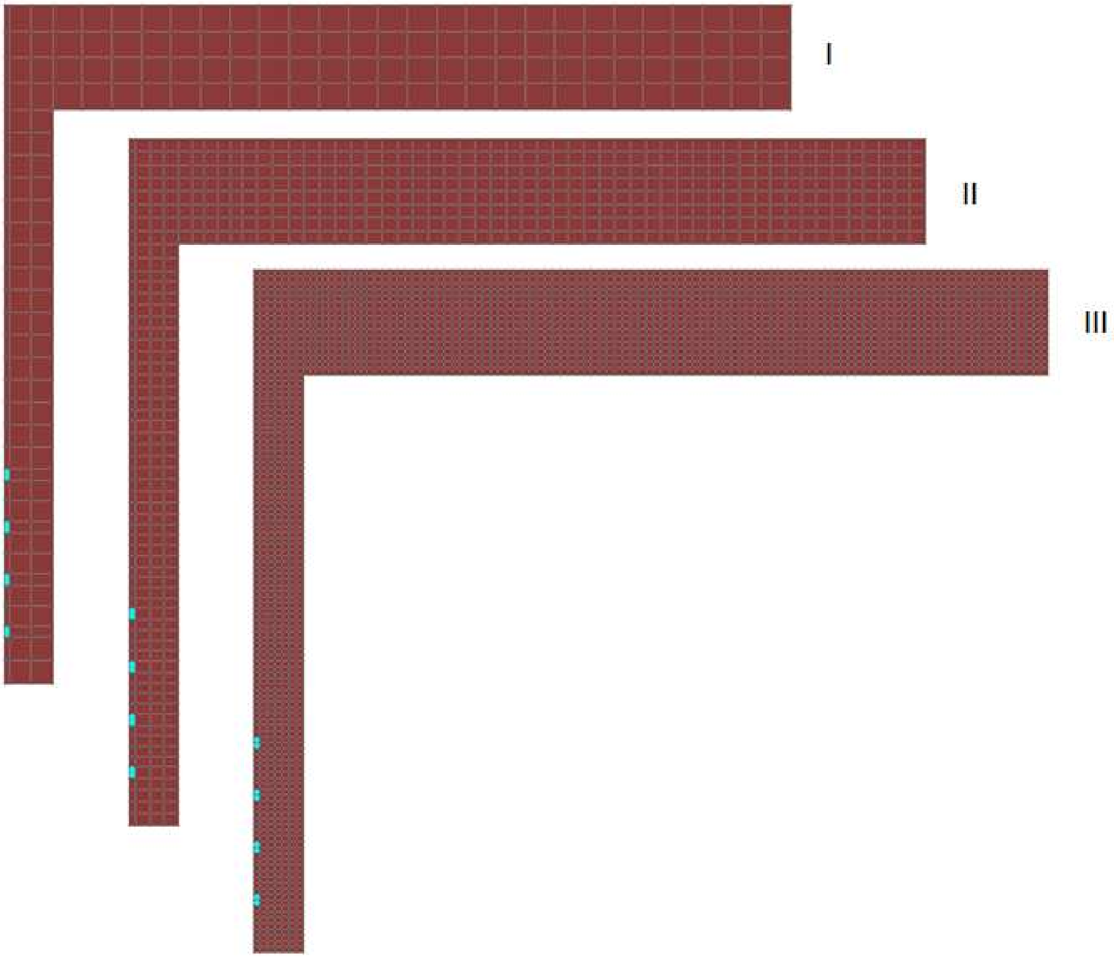

Figure 3.5 – Variation of Strand and Average Slab Temperatures as a Function of Time for Model I, II, and III.

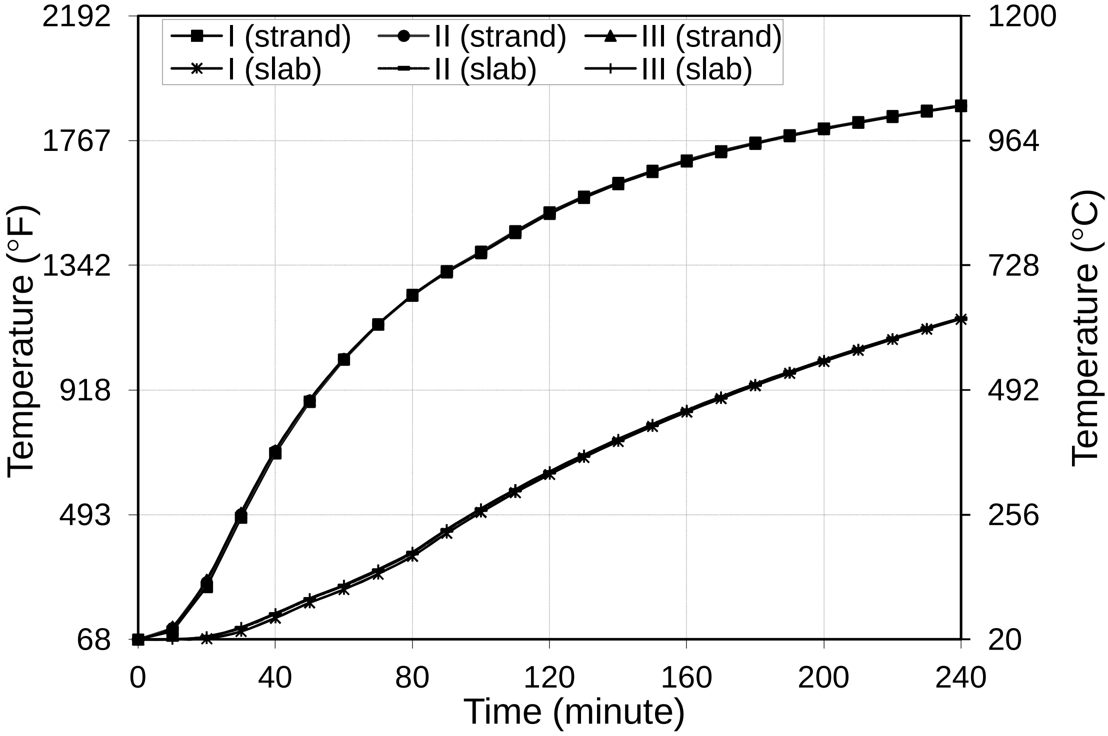

Figure 3.6 – Midspan Deflection as a Function of Time for Model I, II, and III.

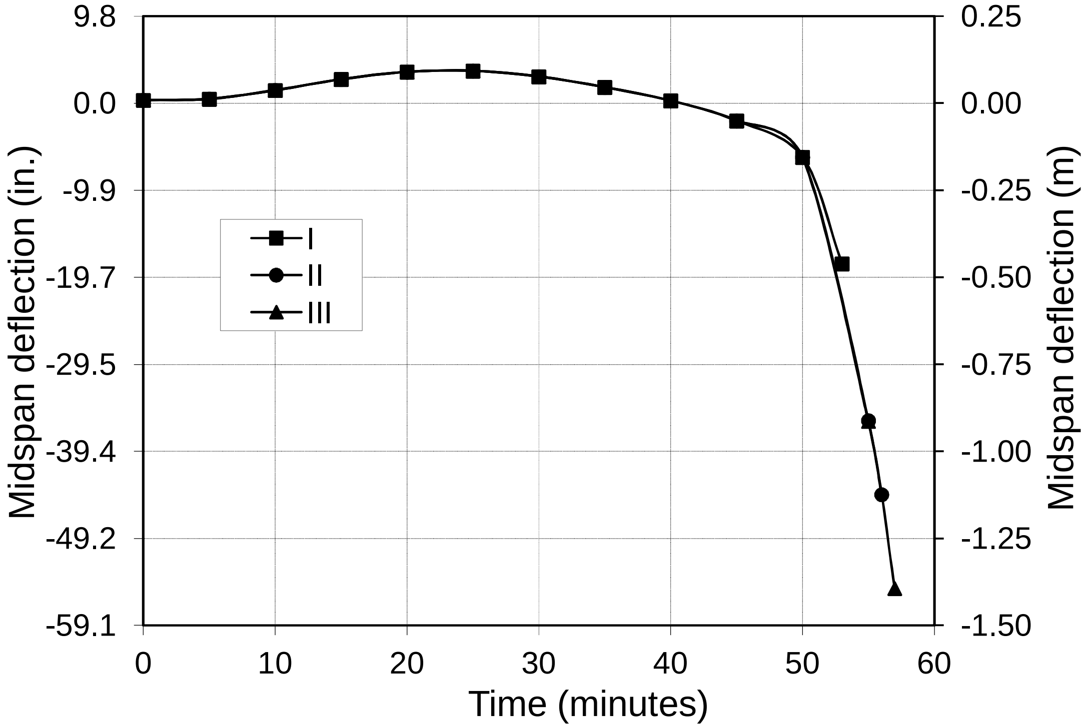

Figure 3.7 – Cross-sectional Details of the Beam Tested by UL for Establishing Fire Ratings

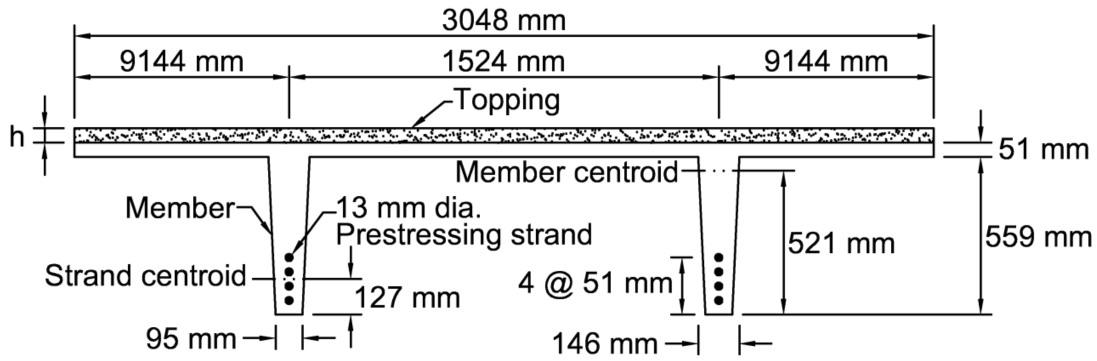

Figure 3.8 – Unexposed Slab Temperatures as a Function of Time for Various Slab Thickness for UL Beam

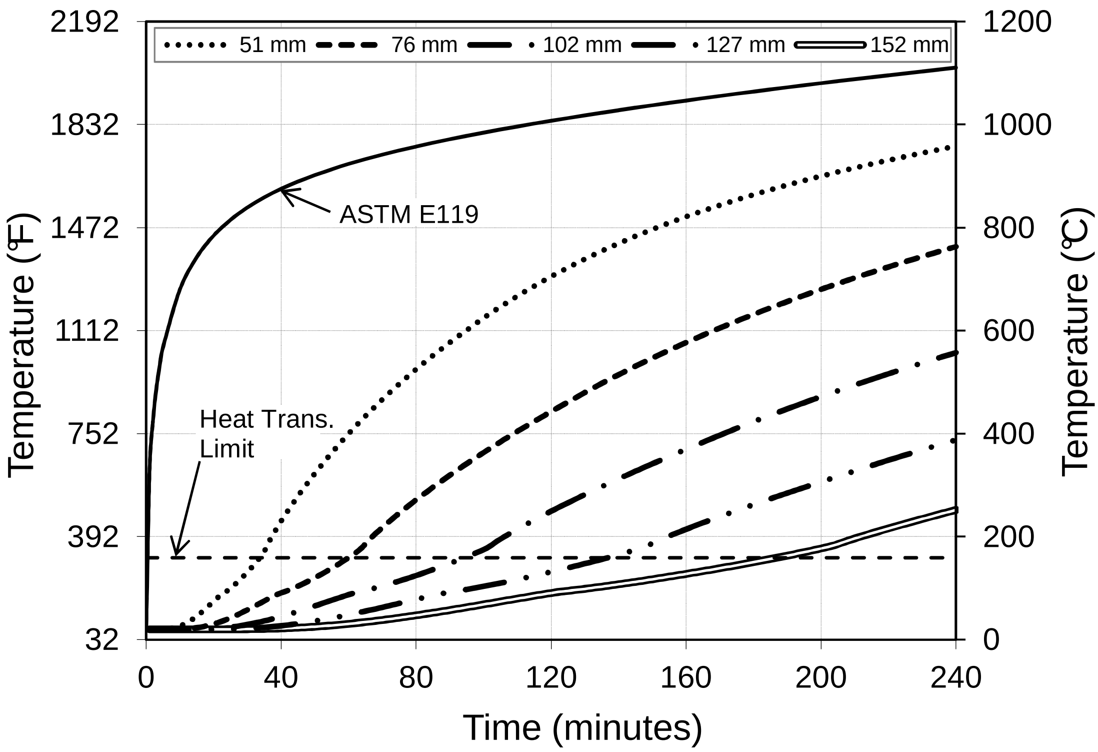

Figure 3.9 – Comparison of Predicted Fire Resistance (SAFIR) with Measured Test Data.

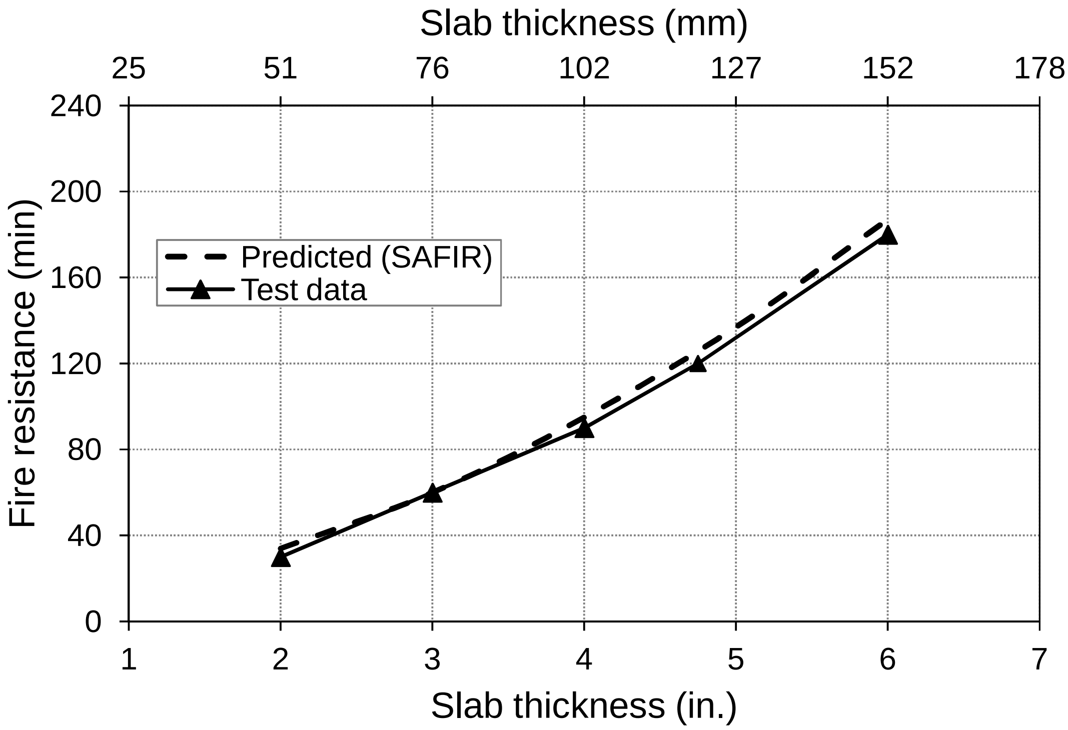

Figure 3.10 – Cross-sectional details of Gusaferro et. al. Beam used in Validation Study.

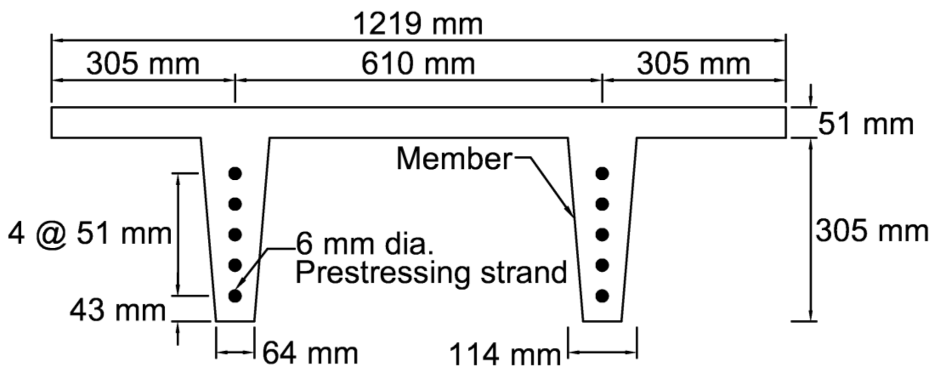

Figure 3.11 – Variation of Strand Temperature as a Function of Time for Gustaferro et al. PPC beam.

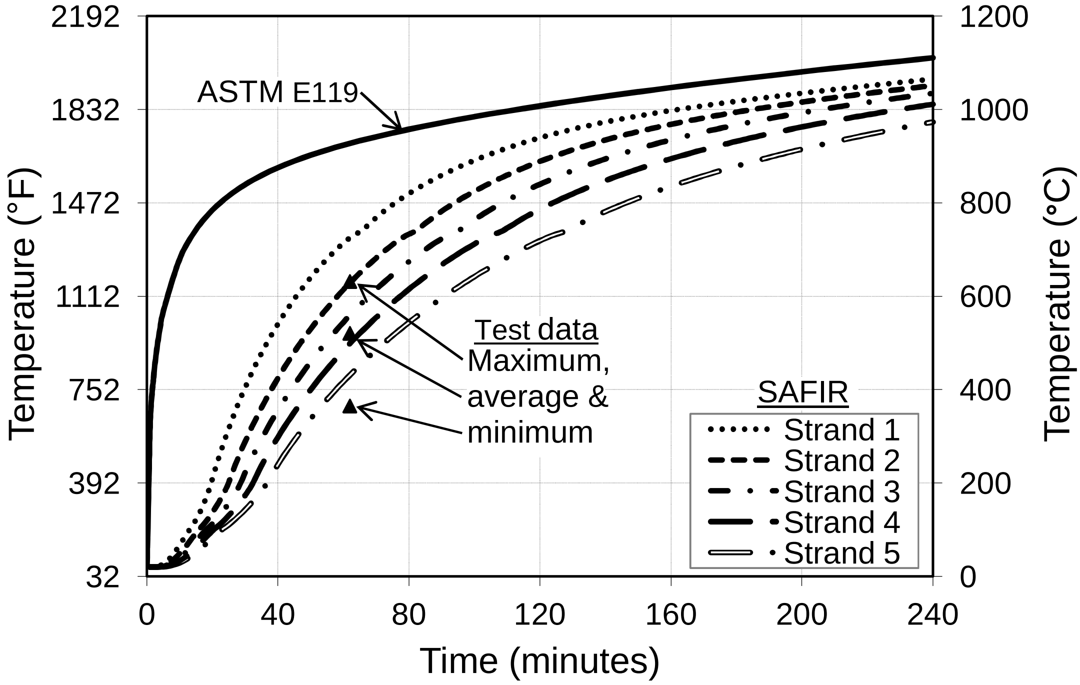

Figure 3.12 – Comparison of Predicted Midspan Deflections with Test Data for Gustaferro et al. PPC Beam.

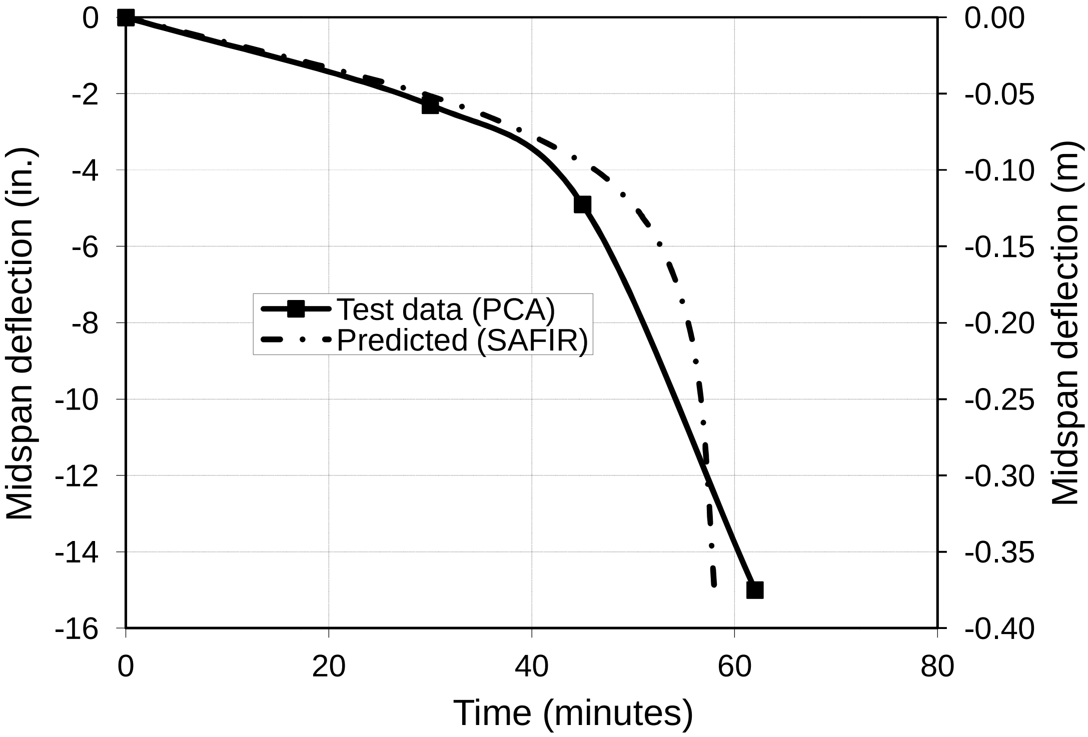

Chapter 4

4. Parametric Studies

4.1. General

To study the influence of various factors on the fire response of precast/prestressed concrete (PPC) double T-beams, a parametric study was carried out using SAFIR. For the study, two cross-sections, namely 10DT24+2 and 12DT32+2, were selected from the PCI Design Handbook (2004). The sections were selected to represent a typical PPC beam found in a parking garage/building structure. The factors considered in the parametric study are fire scenario, concrete compressive strength, axial restraint, load intensity, aggregate type, and failure criteria. Results from the SAFIR analysis were applied to evaluate failure and the time to failure was taken as fire resistance. For all parameters, except when the failure criterion was the focus, flexural strength limit state was applied to define failure. The following sections present the analysis details of the parametric study and in-depth discussion on the various effects of each parameter on the fire resistance of PPC beams.

4.2. Analysis Details

4.2.1. Beams

As mentioned, the two cross-sections selected for the parametric study were taken from the PCI Design Handbook (2004) were a 10DT24+2 and 12DT32+2, with spans 12.2 and 15.2 m (40 and 50 ft), respectively. The elevation and cross-sectional details of the 10DT24+2 and 12DT32+2 are shown in Figures 4.1 and 4.2, respectively. The sectional and material properties for both members are tabulated in Table 4.1. As illustrated in Figure 4.1, and can be deduced from the sections' name, 10DT24+2 is a 3.048 m (10 ft) wide double T-beam with a 610 mm (24 in.) deep precast section topped with additional 51 mm (2 in.) of concrete. Likewise, the 12DT32+2 is a 3.658 m (12 ft) wide double T-beam with a 813 mm (32 in.) deep precast section topped with additional 51 mm (2 in.) of concrete. Both beam–slab assemblies (including the topping) were assumed to be fabricated with normal weight concrete composed of carbonate aggregate having a compressive strength of 40 MPa (5.8 ksi), excluding the studies where aggregate type or concrete compressive strength were under consideration.

Per PCI's nomenclature, an 88-S and 128-S strand pattern was used for the 10DT24+2 and 12DT32+2 PPC beams, respectively. In other words, 8 (4 per stem) and 12 (6 per stem) prestressing strands with a straight profile were incorporated in the 10DT24+2 and 12DT32+2 PPC beams, respectively. The diameter of the prestressing strands for both the PPC beams were a special, 13 mm (1/2 in.) diameter, 1,860 MPa (270 ksi)-grade, low-relaxation cold-drawn steel.

Each prestressing strand was assumed to be stressed to 1,172 MPa (170 ksi) to account for the initial jacking force (0.75 f_{pu} where f_{pu} is the ultimate tensile strength of strand) and minimum stress loss 207 MPa (30 ksi) as per the provisions specified in PCI Design Handbook (2004) to account for all losses.

The 10DT24+2 and 12DT32+2 PPC beams were subjected to a uniformly distributed live load of 2.4 kPa (50 psf). This load was selected in accordance with the ASCE 7-05 (2005) design loads for a parking garage/building. The uniformly distributed dead load for each beam was comprised only of the self weight of concrete and calculated to be 3.4 and 4.1 kPa (72 and 85 psf) for the 10DT24+2 and 12DT32+2 PPC beams, respectively. The loads were evaluated based on a load combination of U = 1.2D + 0.5L under fire conditions. The loading resulted in load ratios 37% and 41% for the 10DT24+2 and 12DT32+2, respectively. See Appendix D for the load ratio calculations.

4.2.2. SAFIR Models

In this section, the specifics (discretization, boundary conditions, and pertinent assumptions) regarding the SAFIR models used to predict fire response of 10DT24+2 and 12DT32+2 PPC beams for the parametric study are divulged. The general procedure used to perform the thermal-structural analysis in SAFIR is as described in Chapter 3. In addition, the level of refinement for the discretization of these models is based on the finding s of sensitivity analysis, which is also presented in Chapter 3. Below, is a brief overview of thermal and structural analysis models, including the underlying assumptions, developed to capture the fire response of the PPC beams in the parametric study.

In the thermal model, the PPC beams' cross-section is modeled with three different materials (concrete topping, member, and steel prestressing strands) and discretized into triangular and quadrilateral solid elements, as illustrated for 10DT24+2 PPC beam in Figure 3.2 of Chapter 3. A total of 712 elements and 822 nodes were used for the 10DT24+2 thermal analysis and 1078 elements and 1209 nodes were used to discretize the 12DT32+2 thermal model. A concrete moisture content of 1% by weight was assumed for the normal weight concrete comprised of carbonate aggregates. Three-sided fire exposure was utilized for every fire scenario considered to emulate a PPC beam that is placed side-by-side with other beams in a structure that is exposed to a burning fire from below. Therefore, the boundary conditions for the thermal model are based on ambient temperatures at the top and side surfaces of the top slab, while the remaining surfaces were subjected to a constant uniform temperature distribution based on the time-temperature relationship.

The structural models for 10DT24+2 and 12DT32+2 PPC beams were discretized into 20 beam elements, each with two integration points, for a total of 41 nodes. The PPC beams were modeled as simply supported, with a pin support (vertical and horizontal translations restrained) at one end and a roller support (vertical translations restrained) at the other end. In addition to these boundary conditions, when investigating the influence of axial restraint, a truss element was introduced into the analysis to provide variable axial restraint. It was assumed the concrete topping and member act monolithically, based on the assumption that adequate shear reinforcement is provided to tie the topping to the member. A residual stress is applied in the thermal model to include the effects of prestressing, which is translated into the structural model through longitudinal strains based on a fiber based approach.

4.2.3. High Temperature Material Properties

For the analysis, high temperature properties of concrete and prestressing steel, per Eurocode 2 (2004), are used. These constitutive material models are preprogrammed into SAFIR. Details regarding the nature of these properties are presented in chapter 2 where in-depth discussion is provided on each individual material property. In addition, Appendix C provides empirical relationships for each material property and Appendix D provides an illustration of the thermal (thermal conductivity, specific heat, density, and thermal expansion) and mechanical properties for both materials accounted for in the parametric study.

4.2.4. Failure Criteria

Results from the SAFIR analysis were applied to evaluate failure and the time to failure was taken as fire resistance. For all parameters, except when the failure criterion is the focus, flexural strength limit state was applied to define failure. This limit state was selected for the parametric study because it represents the most probable and realistic failure mode for a PPC beam. No consideration was given to shear failure, as it assumed this failure mode is unlikely if adequate shear reinforcement is provided. A summary of the fire resistance times is provided in Table 4.2. Also included in this table are the fire resistance times from the prescriptive-based failure limit states, heat transmission (unexposed slab surface temperature) and critical strand temperatures, determined for the failure criteria parameter.

4.3. *Factors Governing Fire Resistance*

The literature review identified the critical factors that govern the fire resistance of PPC beams are fire scenario, concrete compressive strength, axial restraint, load intensity, aggregate type, and failure criteria. Based on these factors and the assumptions mentioned above, a set of numerical studies were carried out using SAFIR to study the influence of each of these factors on the fire resistance of PPC beams. The following sections present in-depth discussion on the various effects of each parameter on the fire resistance of PPC beams.

4.3.1. Effect of Fire Scenario

The effect of varying the fire scenario on fire resistance was evaluated by subjecting the 10DT24+2 and 12DT32+2 PPC beams to five different fire scenarios. Figure 4.3 shows two standard fires (ASTM E119 (2008) and ASTM E1529 (1993) hydrocarbon fire) and three parametric (design) fires used in the analysis. The current provisions for fire ratings are based on fire tests carried out under ASTM E119 (or ISO 834) fire exposure. There are many drawbacks with this standard fire exposure including the lack of a decay (cooling) phase.

In order to develop a wide range of realistic fire scenarios for the analysis, three additional parametric time–temperature relationships were generated through the guidelines provided in Eurocode 1 (2002). The fire scenario in a room is a function of fuel load and ventilation characteristics of a compartment. For generating these design fires, ventilation factors 0.03, 0.05, and 0.07 $m^{-1/2}$ (0.05, 0.09, and 0.13 $ft^{-1/2}$) and fuel loads 125, 200, and 400 MJ/m^2 (11,007, 17,611, and 35,222 Btu/ft^2), respectively, were assumed. The three different cases were selected to represent mild, medium, and severe fires, respectively. The medium and severe fires were selected to simulate a typical fire resulting from the burning of a passenger car in a parking garage. Typically, once a passenger car ignites in a parking garage, the fire rapidly grows to high temperatures due to the unlimited ventilation available in such an open structure. Therefore, the medium and severe fires were developed with rapidly rising temperatures which are greater than the ASTM E119 fire until the limiting fuel load causes the fire to die down. In contrast, the mild fire was selected to represent a minor fire, similar to a small compartment fire in a building. Literature (Feasey and Buchanan, 2002) indicates that the temperatures predicted by Eurocode design equations are slightly lower than realistic fires with similar fuel and ventilation conditions. Thus, a minor adjustment was made to the design equation to increase the temperature predictions (Feasey and Buchanan, 2002). These types of time–temperature scenarios can also be generated using a similar approach specified in a recently published SFPE Engineering Standard (2011).

The strand and unexposed slab temperatures predicted by SAFIR thermal analysis are plotted in Figure 4.4 for the 12DT32+2 PPC beam for different fire scenarios. Also shown in the figure are the limiting strand and slab temperatures, as prescribed in ASTM E119 (2008). The strand and slab temperature results follow similar trends as the actual fire scenarios. Initially, the strand and slab temperatures maintain a constant temperature until approximately 10 min into the fire due to effect of moisture. At this point in time, the free moisture has completely evaporated in the concrete surrounding the strands and the strand temperatures begin to rapidly rise analogously to its respective fire scenario. In contrast, the slab temperatures rise much slower in a linear fashion until approximately 70–80 min, depending on the fire scenario. This difference in temperature results is mainly due to the slabs' concrete mass retaining more free moisture, thus prolonging its insulating effect. Once all the free moisture has evaporated in the slab, the unexposed slab temperatures begin to follow a comparable trend with respect to its fire scenario, but these temperature results are much lower when compared to the temperatures in the strands. As the fire scenarios progress with time, a greater difference in temperature results can be seen. Neither the ASTM E1529 or E119 standard fire exposures include a decay phase; so the temperatures continue to rise throughout the duration of the fire. In contrast, the three design fire scenarios incorporate a decay phase and lead to a reduction in strand temperatures after about 120 min. Similar results can be seen in the slab temperatures, but the decay phase has less influence because of the concrete mass and exposure boundaries. Both the strand and slab temperature results indicate a significant difference in temperatures as a result of the decay phase. The greatest difference in temperature is apparent once the decay phase becomes a factor, especially with regards to the strand temperatures. These results indicate that fire scenario has a major impact on the strand and slab temperatures in a PPC double T-beam.

To further illustrate the effect of fire scenario on structural response, mid-span deflections predicted by SAFIR are plotted in Figure 4.5. The mid-span deflections for all fire scenarios follow a similar trend. Initially, the deflections for all fire scenarios, except ASTM E1529, remain constant during the first 5 min of exposure because the temperature increase within the cross-section is minimal. In the early stages of fire exposure, the beams camber upward and this is a direct result of relatively light loading and increase in temperatures within the concrete surrounding the strands. More specifically, as the temperatures rise, the concrete expands in the longitudinal direction, but the steel prestressing strands expand at a slower rate due to the reduction of temperatures near the center of the stem. This gradient of expansive forces induces a compressive force by the prestressing strands and leads to the exaggeration of the initial camber resulting from the light loading. A similar trend can be seen in the ASTM E1529 fire scenario, but this behavior begins at the early stages of fire exposure due to rapid rise in fire temperatures. The deflections turn negative after about 40 min, which can be attributed to substantial loss of stiffness of the beam due to increasing temperatures, particularly in strands.

The sagging of the PPC beam is further amplified just prior to failure, mainly due to high temperature creep. The deflection response indicates that fire scenario plays a key role in the structural behavior of a PPC double T-beam. A severe fire exposure, such as the ASTME E1529, leads to larger positive deflections that occur much sooner when compared to a less severe fire exposure.

The effect of fire scenario on fire resistance is tabulated in Table 4.2. The derived fire resistance is based on a strength failure criterion. For the 10DT24+2, fire resistance times are 61, 43, 56, 61, and 68 min for the ASTM E119, ASTM E1529, severe, medium, and mild fires, respectively. The corresponding fire resistance times for the 12DT32+2 are 85, 64, 79, 84, and 96 min. These results indicate that PPC beams fail sooner under a more severe fire, such as ASTM E1529 or severe design fire, rather than a moderate fire. One of the main reasons for attaining higher fire resistance under mild fires is the presence of a decay phase.

Results from the analysis indicate that fire scenario has a significant influence on the fire resistance of PPC double T-beams. Therefore, if a PPC beam is designed under the prescriptive approach and the ASTM E119 fire scenario does not represent the actual fire exposure, namely the severity or lack of a decay phase, then the beam may be over- or under-designed based on the actual fuel loads and ventilation conditions present. Unrealistic fire scenarios can limit the designer to costly and conservative designs, with no consideration for new and creative alternatives.

4.3.2. Effect of Concrete Compressive Strength

The effect of concrete compressive strength (f'_c) on the fire performance was investigated by analyzing two PPC beams with compressive strengths 40, 55, 70 MPa (5.8, 8, and 10.2 ksi) under an ASTM E119 (2008) standard fire. The concrete strengths were selected to represent a normal, intermediate, and HSC. Figure 4.6 illustrates the variation of mid-span deflection of 12DT32+2 for all three concrete strengths. The deflection patterns for all three concrete strengths are nearly identical with deflections initially increasing until the strands begin to gradually lose their stiffness leading to excessive sagging, and hence failure. These results indicate that concrete compressive strength has little influence on the fire resistance, with failure times approximately 61 and 85 min for the 10DT24+2 and 12DT32+2, respectively. It should be noted that in this analysis, fire-induced spalling is not taken into consideration as SAFIR cannot handle this phenomenon. A few studies, (Malhotra 1984 and Phan 1996) have indicated that higher strength concretes might be susceptible to spalling, especially under conditions such as rapidly rising fire intensity or high moisture content.

4.3.3. Effect of Restraint

According to the PCI Design Handbook (2004), PPC double T-beams are considered to be restrained when "potential thermal expansion of the floor or roof system is resisted by framing systems or the adjoining floor or roof construction." To model the effect of axial restraint levels, a truss element was introduced in the analysis. Figure 4.7(a) shows a generic schematic of the modified structural model. The truss element is intended to act as a spring with an axial stiffness of $\frac{E_S A_S}{l}$. Variable stiffness was applied through altering the cross-sectional area of the truss element, since the elastic modulus and length are constant. Various degrees of stiffness were simulated to determine the effect of restraint on the fire performance of PPC double T-beams. To quantify intermediate degrees of stiffness, it was necessary to establish a 'quasi' 100% axial stiffness. This upper limit can be visualized as similar to a pin–pin support condition. Although, the truss element cannot completely provide full axial restraint, this idealization is more realistic because no structure can provide infinite restraint.

The effect of axial restraint on the fire performance of PPC double T-beams is evaluated through applying 0, 25, 50, 75, and 100% axial restraint. Table 4.2 presents fire resistance times of the 10DT24+2 and 12DT32+2 beams. Results from analysis indicate that axial restraint increases the fire resistance of a PPC beam and the application of restraint improved fire resistance up to 6% and 10% for beams 10DT24+2 and 12DT32+2, respectively. This improvement results from the development of fire-induced axial forces due to the restraint offered by the support. The resultant axial force is eccentric to the beams' center of gravity (CG) as shown in Figure 4.7(b); hence a thermally induced moment is created. Therefore, the fire-induced restraint (moment) enhances the fire resistance by compensating for the loss of strength of the prestressing strand.

To illustrate the development of the axial restraint, the axial forces of the 12DT32+2 are plotted against time in Figure 4.8(a). As the beam tries to expand longitudinally, the fire-induced axial forces increase rapidly until they plateau at the level of axial restraint provided. The axial force eventually begins to decrease gradually as the degradation of prestressing strands causes a shift in the members' CG downward. Once the CG falls below the location of the restraining force, the axial restraint decreases the PPC beam's fire performance due to the reversal of moments. A similar trend can also be seen from the mid-span deflection of the 10DT24+2 PPC beam shown in Figure 4.8(b). Notice how the deflection of the axial restrained beam shifts gradually from positive to negative once the prestressing strands begin to lose significant stiffness. However, when the unrestrained beam starts to lose significant stiffness, there is no external effect to delay its failure. Thus, axial restraint can improve the fire resistance of PPC beams.

The above results suggest axial restraint can improve the fire resistance of a PPC double T-beam. However, it should be noted that these findings only represent a single type of support condition. In reality, numerous support configurations are possible in structural systems and this can influence the vertical location of the restraining force and ultimately the fire performance of a PPC beam. For instance, if the resultant restraining force is located at the deck of a PPC double T-beam, the thermally induced moment can have a negative effect and may lead to early failure. Also, each building is unique and exhibits variable stiffness characteristics. Such factors are not taken into consideration in the current approach of evaluating fire ratings. Another shortcoming of the current prescriptive fire provisions is the lack of a more specific definition to distinguish the difference between flexural and axial restrained beams. As reported in Dwaikat and Kodur (2008), these two restraint conditions exhibit different behaviors; the flexural restrained beams benefit from the redistribution of moments, while axial restrained beams rely on the location and magnitude of the restraining force. In order to accurately assess the effects of restraining forces of a PPC beam, the type of restraint, support condition (vertical location of support), and stiffness should be considered on a case-by-case basis.

4.3.4. Effect of Load Intensity

Previous studies (Gustaferro and Carlson 1962 and Selvaggio and Carlson 1964) have shown that load ratio has a significant influence on fire resistance of concrete members. The load ratio is defined as the ratio of the expected load effect (moments) under fire conditions to the nominal (flexural) capacity under ambient conditions.

The fire resistance analysis was carried out by subjecting the two PPC beams to three load ratios, namely 30%, 50%, and 70%. Results plotted in Figure 4.9(a) and tabulated in Table 4.2 show that fire resistance decreases with an increasing load ratio. The fire resistance times are 57, 54, and 45 min for the 10DT24+2 and 81, 78, and 64 min for the 12DT32+2, respectively. The effect of load intensity on fire response is further illustrated through a mid-span deflection plot for the PPC beam 10DT24+2 in Figure 4.9(b). It can be seen that the mid-span deflection of the 30% and 50% load ratio scenarios follow a similar trend to the previous results for an unrestrained member, because the loading is very similar. However, in the case of 70% load ratio, no cambering effects are noticed and the beams' deflections gradually decrease due to high level of load. These results indicate that the load intensity has a significant influence on the fire performance of PPC double T-beams. In spite of these trends, tabulated methods in codes and standards prescribe fire ratings of a structural member based on the sectional dimensions, concrete cover, and aggregate type, with no consideration for load intensity. Therefore, if tabulated approaches are utilized to prescribe a fire rating for highly loaded PPC beams, it may not lead to realistic designs.

4.3.5. Effect of Aggregate Type

The aggregate type used in the concrete mix has an influence on the fire resistance of concrete members. The two most common aggregates used in concrete are siliceous and carbonate aggregates. Siliceous aggregate mainly consists of quartzite, granite, and basalt, while carbonate aggregates are primarily composed of either limestone or dolomite. The fire resistance analysis is carried out by analyzing two PPC beams fabricated from siliceous and carbonate aggregate concrete under standard fire exposure. Results from the analysis indicate that carbonate aggregate concrete provides better fire resistance than siliceous aggregate concrete. For instance, the fire resistance of the 10DT24+2 increases from 56 to 61 min, while the 12DT32+2 beam fire resistance increases from 71 to 81 min.

The effect of aggregate type on fire response of PPC beams is illustrated in Figure 4.10, which shows the mid-span deflection as a function of time for a 12DT32+2 beam. For both types of aggregates, the deflection initially increases until the strands begin to gradually lose their stiffness, leading to excessive sagging and then failure. The deflections for a siliceous aggregate concrete beam produce larger camber effects and lead to sagging much sooner, hence a lower fire resistance. This difference in the beam's behavior is primarily due to the variation in high temperature properties of the two concrete types. Carbonate aggregate concrete has a much higher heat capacity than siliceous aggregate concrete in the 650–700°C (1202–1292°F) temperature range due to disassociation of dolomite as a result of an endothermic reaction. This reaction results in very high heat capacity, about 10 times higher than siliceous aggregate concrete, and is beneficial to fire resistance. In addition, carbonate aggregate has slightly lower thermal conductivity when compared to siliceous aggregates. Furthermore, carbonate aggregate concrete has lower thermal elongation and better resistance to strength loss. These properties of carbonate aggregates produce lower temperatures, deflections, and greater fire resistance. Both Eurocode and ASCE provisions recognize these differences in properties, but in a different manner. The Eurocode distinguishes these differences through mechanical properties, while ASCE relies on the thermal properties to make the distinction between the two aggregate types.

Therefore, the effect of aggregates must be taken into consideration when designing for the fire resistance of PPC beams.

4.3.6. Effect of Failure Criteria

ASTM E119 and other fire test standards specify three limiting criteria, namely, strength, heat transmission (unexposed slab surface temperatures), and critical strand temperatures for defining the failure of PPC beams. While the critical strand and unexposed slab temperatures represent prescriptive failure limit states, the strength limit state represents a realistic failure condition. These three failure criteria are applied to determine the fire resistance values of all analyzed PPC beams and the results are tabulated in Table 4.2.

The fire resistance results for the different failure criteria shown in Table 4.2 reveal that prescriptive limit states generally predict lower fire resistance than actual failure conditions. For instance, a lower fire resistance results for 10DT24+2 when the critical strand temperature criterion is applied, while the heat transmission criterion produces lower fire resistance in the case of a 12DT32+2 PPC beam. The only exception to this generalization is when load ratios equal to or greater than 50% are applied, at which time the strength criterion produces a lower fire resistance as can be seen from Table 4.2. Therefore, fire resistance of PPC beams is governed by prescriptive limit states, unless relatively large load levels are applied. The specific prescriptive limit state is dependent on the bulkiness of the beams' cross-section, as can be seen when an additional 13 to 25 mm (1/2 to 1 in.) of concrete cover thickness is provided to prestressing strands of 12DT32+2, resulting in lower temperatures in the prestressing strands and consequently altering its failure criterion from critical strand temperature to heat transmission.

The lower fire resistance produced by the prescriptive failure criteria, compared to actual failure conditions, should raise the question whether such limit states are viable considerations in evaluating fire resistance of PPC beams. To address one aspect of this question, recall that the intent of the heat transmission criterion is to maintain compartmentation within a structure. The necessity to prevent spread of fire beyond the first compartment indicates that this prescriptive limit state is a viable consideration. However, when considering the viability of the critical strand temperature limit state, it becomes clear that this simplified approach consistently underestimates the fire resistance of PPC beams, except when larger loads are applied, in which case it dangerously results in an overestimation. Therefore, the critical strand temperature failure criterion does not reflect a realistic limit state and may lead to under-prediction of the fire resistance of PPC beams.

4.4. Summary

Results from the parametric study revealed that critical factors that influence the fire resistance of PPC beams are fire scenario, axial restraint, load level, aggregate type, and failure criteria. Fire scenario proved to have significant influence on fire resistance of PPC beams and depending on the severity of a real fire, the ASTM E119 fire scenario can lead to over- or under-designed PPC beams. Axial restraint also has significant influence on fire resistance of PPC beams and the level of restraint is a function of type of restraint, support condition, and variable stiffness offered by adjoining members. Load level proved to be inversely proportional to fire resistance, while aggregate type has only a moderate influence on the fire resistance of PPC beams. However, carbonate aggregates do provide higher fire resistance than siliceous aggregate concrete. Failure criteria revealed that PPC beams are often governed by limiting strand temperatures for slender stems and heat transmission for bulkier stems where adequate cover thickness is provided. This parameter also identified that critical strand temperature limit state underestimates the actual failure of a PPC beam, unless high load levels are present and then it would actually over-estimate the fire resistance. In contrast to the other parameters, concrete compressive strength proved to have little to no effect on fire resistance of PPC beams. In conclusion, the parametric study provided insight in the fire resistance of PPC beams and exemplified the necessity to move from a prescriptive-based approach to performance-based approach to capture influence of fire scenarios, restraint, and load level.

Table 4.1 – Sectional Details and Material Properties of PPC Double T-beams 10DT24+2 and 12DT32+2 used in the Parametric Study.

Member			Prestressing Strand		
	10DT24+2	**12DT32+2**		**10DT24+2**	**12DT32+2**
A **(cm^2)**	4,445	6,310	***f_{pu}*** **(MPa)**	1,862	1,862
I **(cm^4)**	1,363,158	3,606,479	***f_{se}*** **(MPa)**	1,172	1,172
y_b **(mm)**	511	648	**Strand Pattern**†	88 - S	128 – S
y_t **(mm)**	150	216	***y_s*** **(mm)**	127	178
S_b **(mm^3)**	26,711	57,584	**Min. cover (mm)**	44	21
S_t **(mm^3)**	90,932	173,080	**Topping**		
Wt **(kN/m)**	0.98	1.38	***f'_c*** **(MPa)**	40	40
DL **(kN/m^2)**	3.44	4.07	**Span (m)**	12.2	15.2
V/S **(mm)**	34	43			
f'_c **(MPa)**	40	40			

†88-S refers to 8 - 12 mm (8/16 in.) diameter strands with a Straight profile; 128-S refers 12 - 12 mm (8/16 in.) diameter strands with a Straight profile.

Note: 1 in. = 25.4 mm; 1 ft = 0.3048 m; 1 lb = 4.448 N.

Table 4.2 – Results from Fire Resistance Analysis on PPC Double T-beams.

		Failure Criterion (minutes)					
		10DT24+2			12DT32+2		
		Strength	Heat Trans.	Strand Temp.	Strength	Heat Trans.	Strand Temp.
Fire Exposure	ASTM E119	61	78	57	85	81	82
	ASTM E1529	43	64	40	64	66	61
	Severe	56	74	36	79	63	76
	Medium	61	78	57	84	81	81
	Mild	68	84	64	96	87	92
Conc. Comp. Strength, MPa	40	61	78	57	85	81	82
	55	61	78	57	85	81	82
	70	61	78	57	85	81	82
Restraint	0	61	78	57	85	81	82
	25	64	78	57	94	81	82
	50	65	78	57	94	81	82
	75	65	78	57	95	81	82
	100	65	78	57	95	81	82
Load Ratio, %	30	65	78	57	96	81	82
	50	54	78	57	78	81	82
	70	45	78	57	64	81	82
Aggregate Type	Siliceous	56	68	52	78	71	75
	Carbonate	61	78	57	85	81	82

Note: 1 ksi = 6.89 MPa.

Figure 4.1 – Elevation and Cross-sectional Details of the 10DT24+2 PPC Double T-beam used in the Parametric Study

(a) Elevation

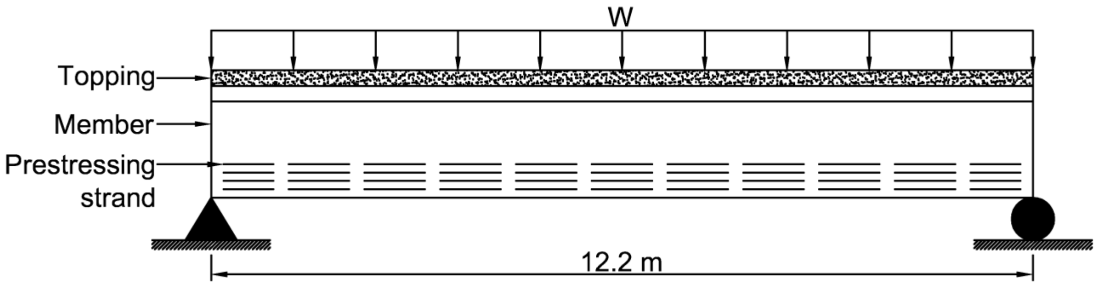

(b) Cross-section

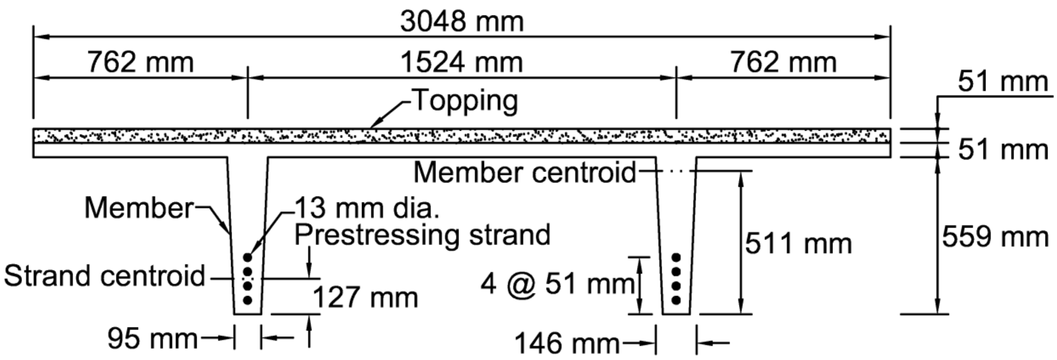

Figure 4.2 – Elevation and Cross-sectional Details of the 12DT32+2 PPC Double T-beam used in Parametric Study

(a) Elevation

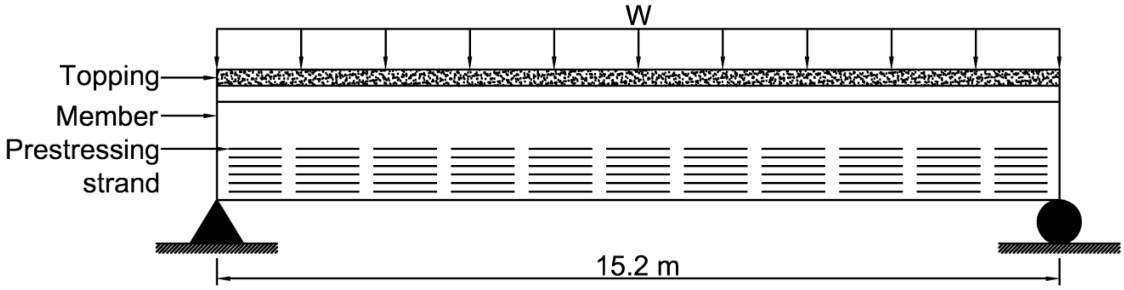

(b) Cross-section

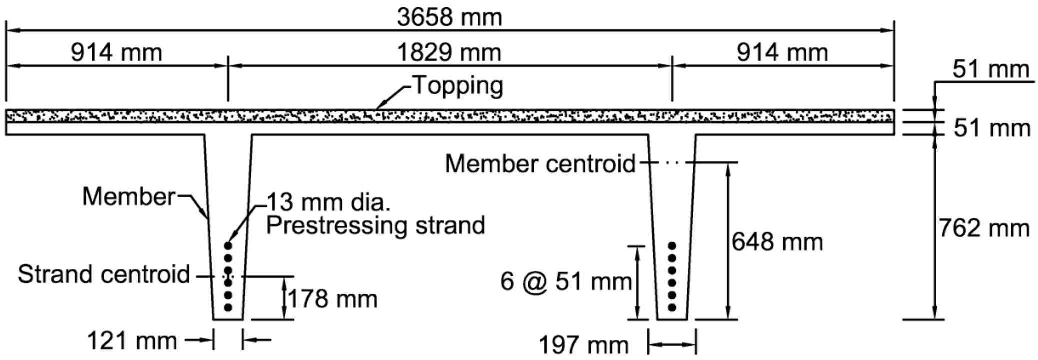

Figure 4.3 – Time-temperature Relationships for Various Fire Scenarios used in Parametric Study

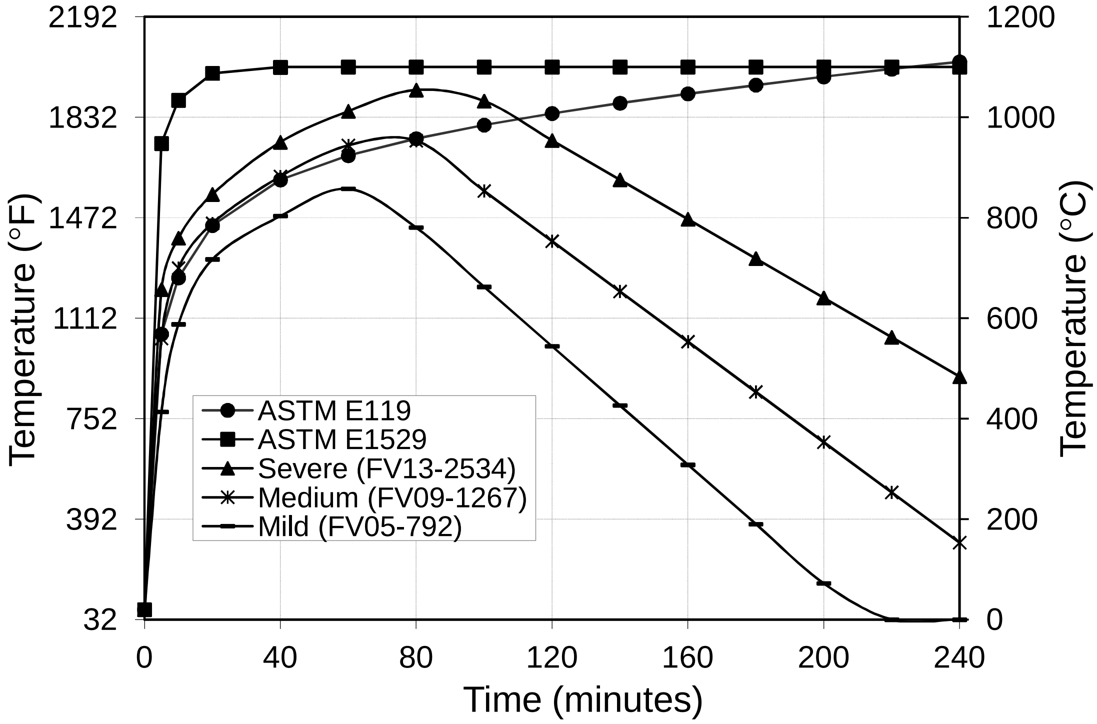

Figure 4.4 – Variation of Strand and Slab Temperatures as a Function of Time in PPC Beam 12DT32+2

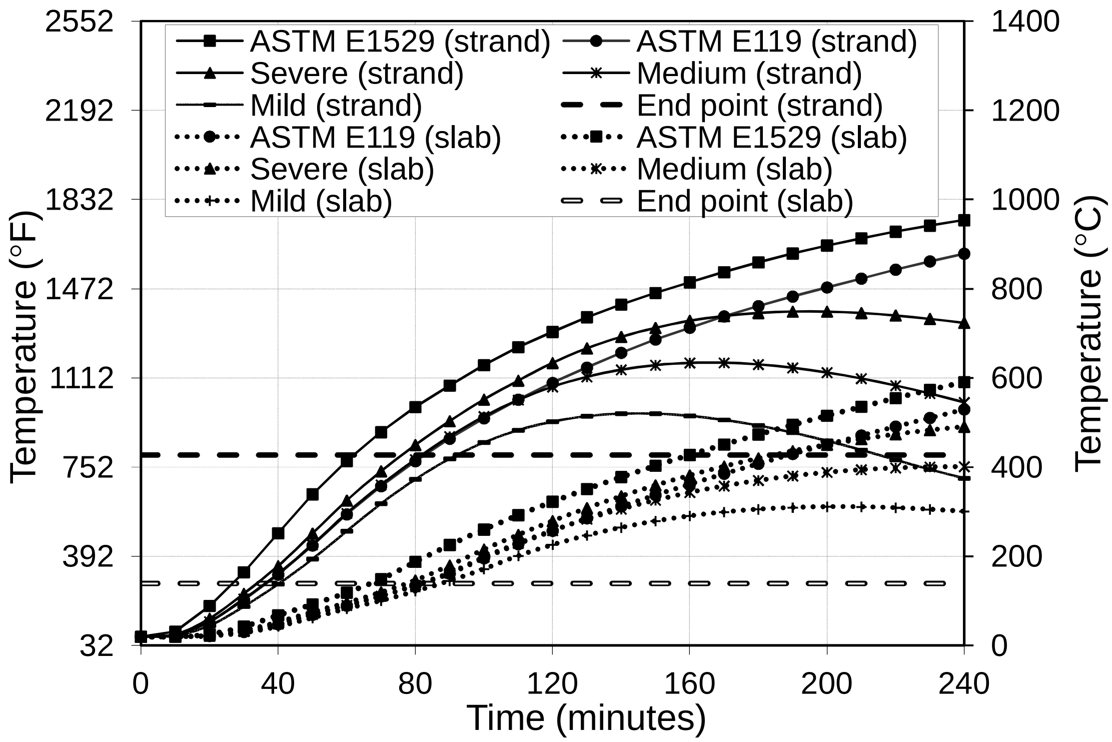

Figure 4.5 – Midspan Deflection as a Function of Time for PPC Beam 12DT32+2 under Various Fires Scenarios

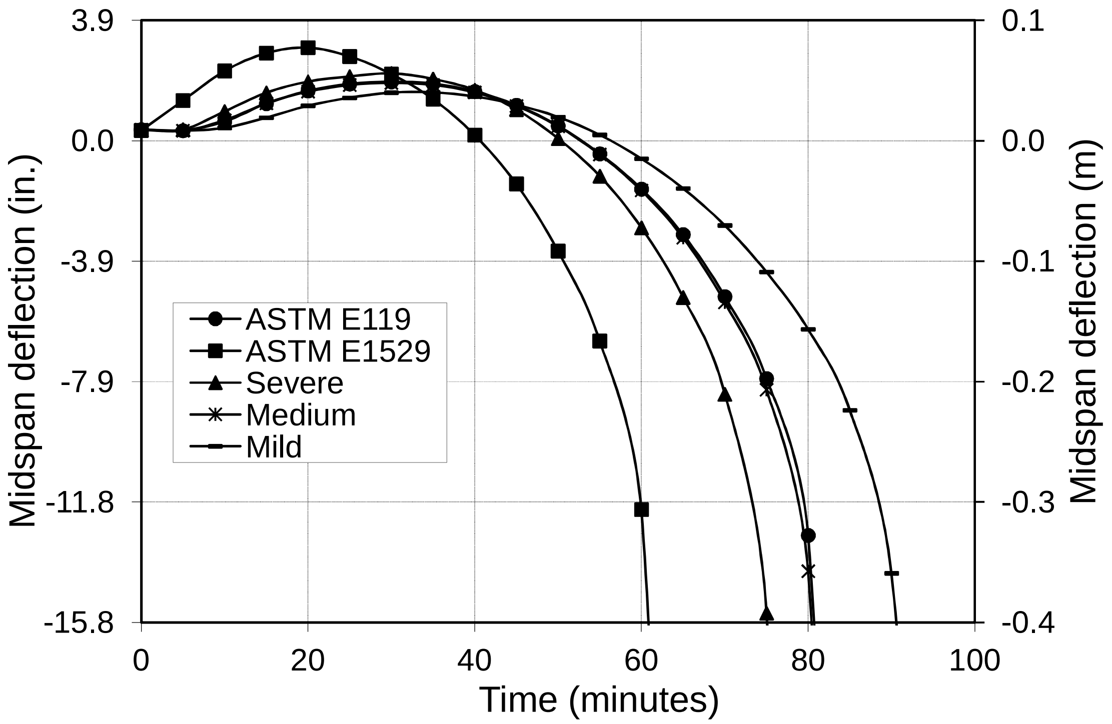

Figure 4.6 – Midspan Deflection as a Function of Time for PPC Beam 12DT32+2 with different Concrete Strengths

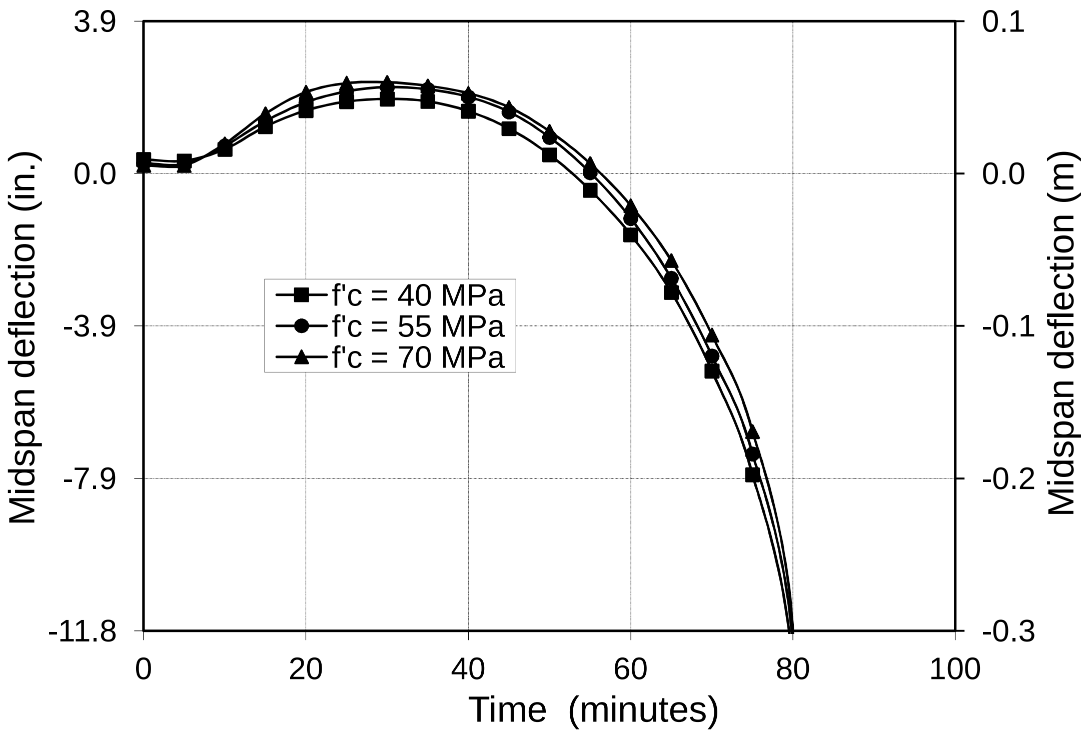

Figure 4.7 – Idealization of PPC Beam with Axial Restraint End Condition

(a) Elevation

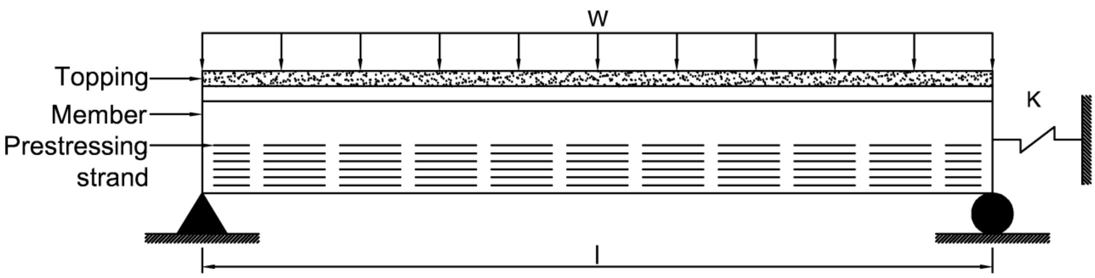

(b) Sectional Forces, Moments, and Strains

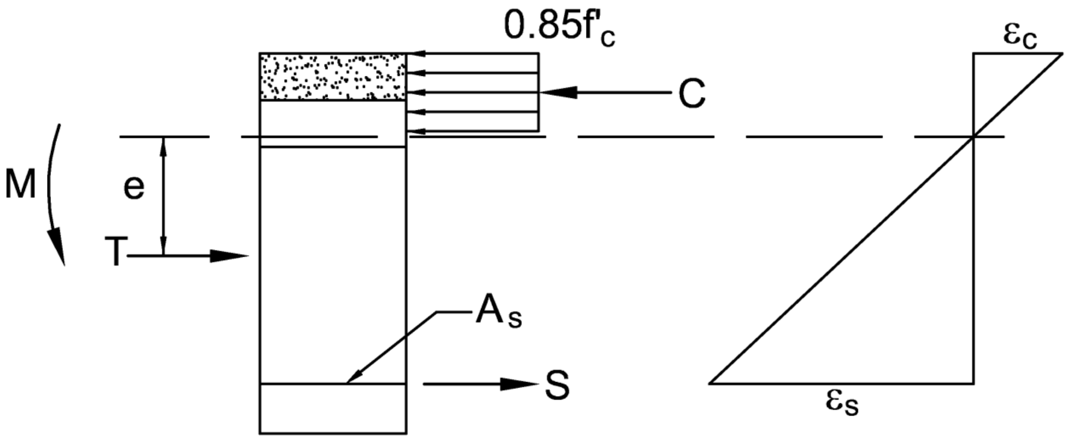

Figure 4.8 – Effect of Axial Restraint on Fire Response of 12DT32+2 PPC Beam

(a) Fire-induced Axial Force

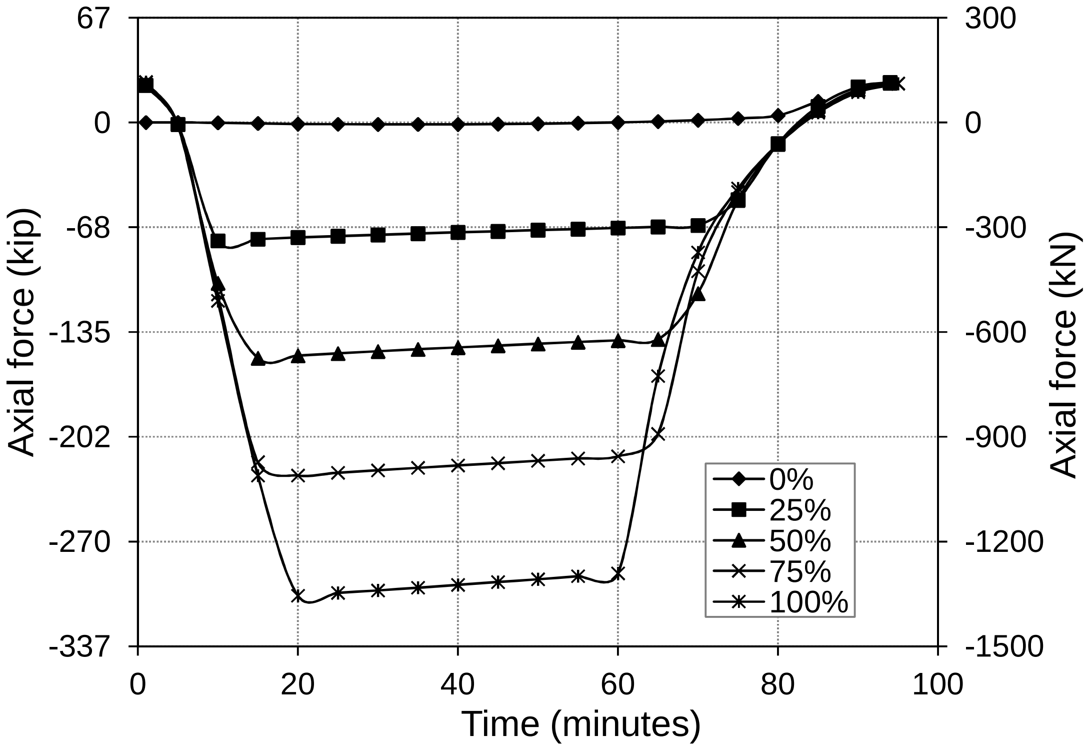

(b) Midspan Deflection

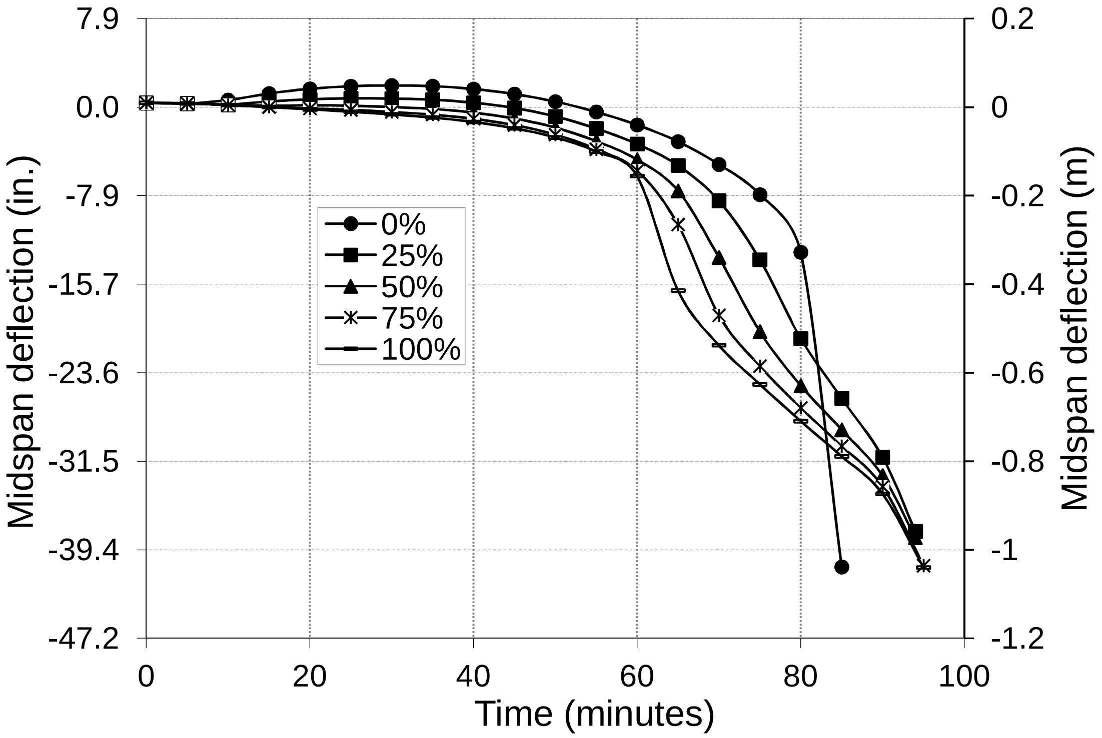

Figure 4.9 – Effect of Load Intensity on Fire Response of 10DT24+2 PPC Beam

(a) Fire Resistance

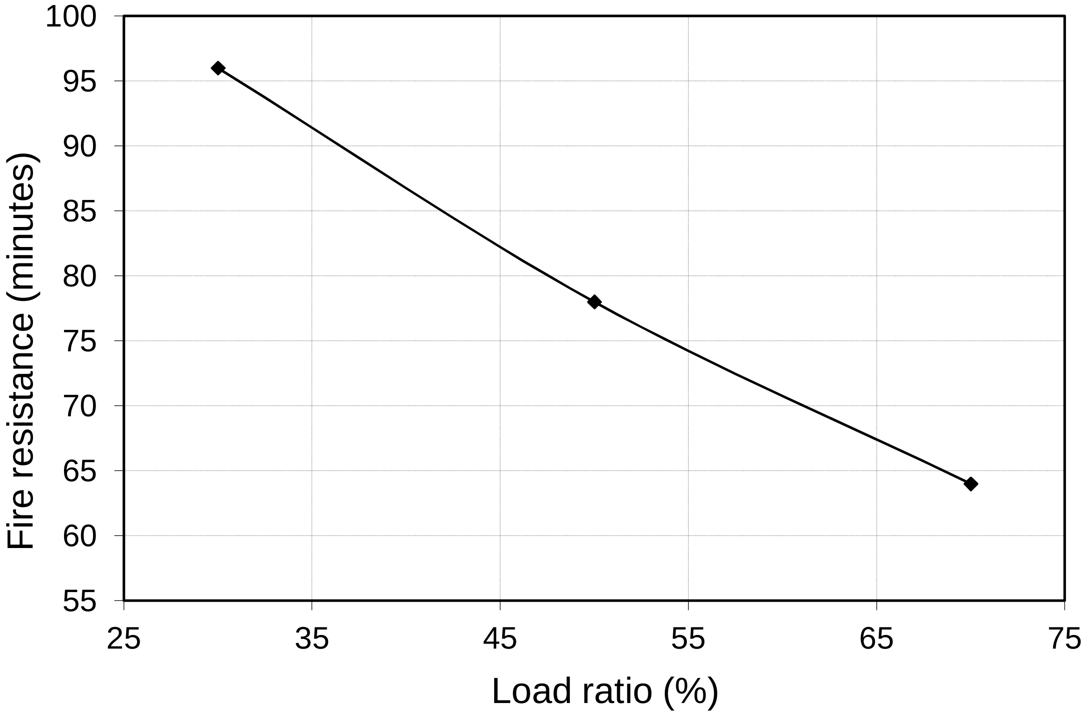

(b) Midspan Deflection

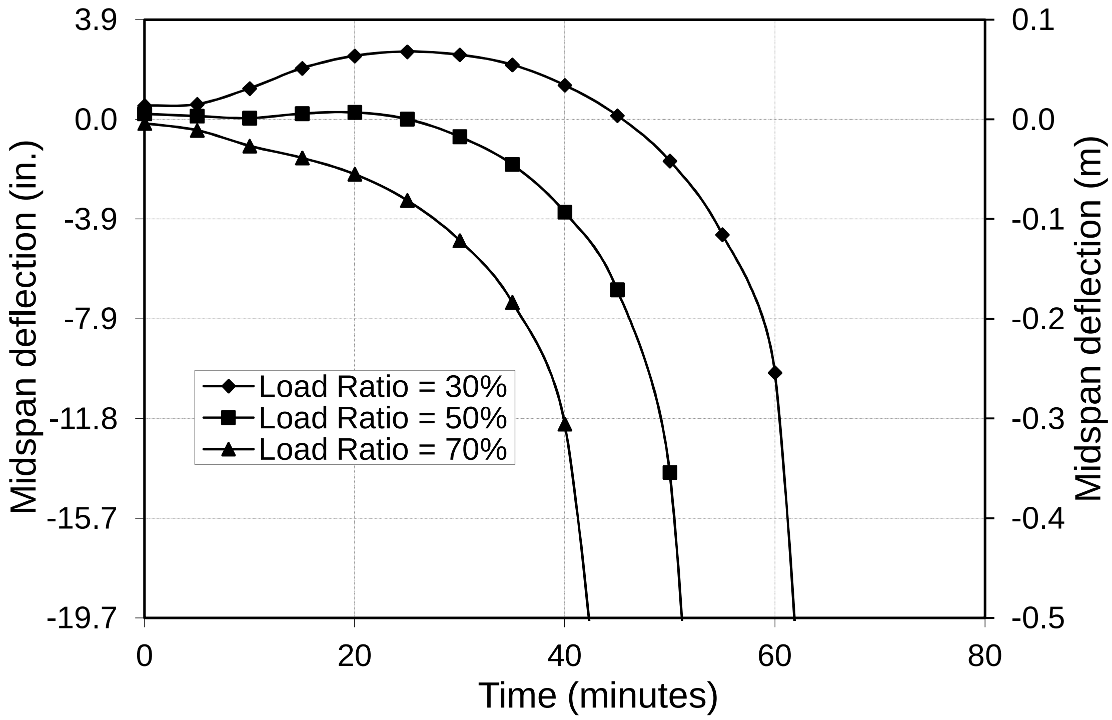

Figure 4.10 – Effect of Aggregate Type on Midspan Deflection of PPC Beam 12DT32+2

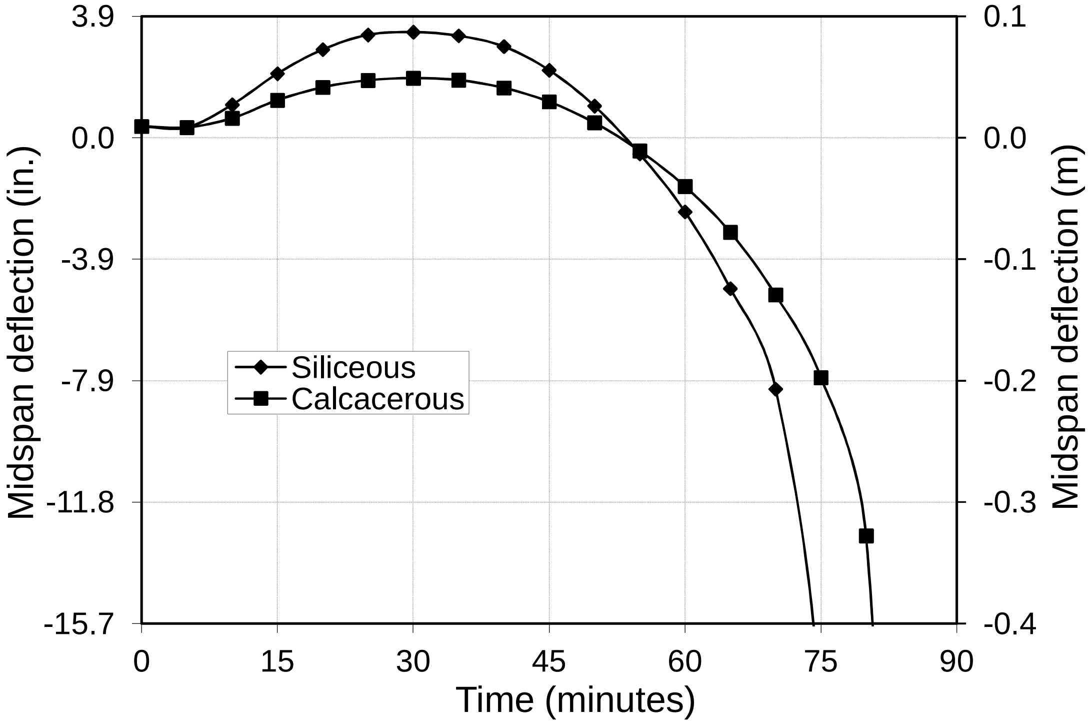

Chapter 5

5. Performance-Based Approach

5.1. General

In recent years, there has been a strong push by the fire research community to move towards a performance-based approach in fire safety provisions, in attempt to overcome the shortcomings of current prescriptive-based methods. Based on the findings of the literature review and parametric study presented in this thesis it is evident that the current approach does not account for realistic fire scenarios, load level, restraint, and failure criteria. These factors must be given due consideration to accurately predict the fire resistance of a precast/prestressed concrete (PPC) beam. Therefore, in effort to offer a rational and cost-effective approach, this chapter is dedicated to scripting a detailed approach for undertaking a performance-based approach for assessing the fire resistance of PPC beams.

5.2. Performance-Based Approach

The following performance-based approach is a rational calculation methodology that accounts for the critical factors (i.e. fire scenario, axial restraint, load level, aggregate type, and failure criteria) that influence fire resistance of PPC beams. This approach offers designers the flexibility to create innovation through design, construction, and materials. It also holds the potential to generate equal, if not improved fire safety than the current approach and maximizes the benefit/cost ratio potential. All of these advantages can be achieved through applying the following steps for evaluating fire resistance of PPC beams. The steps associated with the fire resistance assessment include:

1. Develop design fire and loading scenarios.
2. Select relevant high-temperature material properties.
3. Perform detailed thermal and structural analysis to generate fire response.
4. Apply relevant failure criteria.
5. Develop practical alternatives, as needed, to achieve required fire resistance.

5.2.1. Fire Scenario

To develop relevant fire scenarios for a compartment fire, parametric time–temperature relationships provided in Eurocode 1 (2002), by SFPE (2011), or design tables specified in the literature (Magnusson and Thelandersson 1970) can be used. For using these relationships, fuel load and ventilation characteristics are prescribed or estimated as input parameters. The fuel load can either be calculated based on fuel content, including wall and ceiling linings, or can be found directly from design tables in the literature based on compartment type (Parkinson and Kodur 2007). Likewise, the ventilation factor can be determined from the layout of windows and door openings (Feasey and Buchanan 2002) Figure 4.3 illustrates three design fires developed under the Eurocode provisions which were based on fuel loads and ventilation factors selected to represent mild, medium and severe fires.

5.2.2. Loading Scenario

The loading scenario selected for fire resistance calculations in a performance-based approach should reflect realistic conditions. A fire event is considered an extreme loading condition. In turn, this means there is a low probability that ambient temperature and extreme load combinations will occur simultaneously during a fire event. In fact, a reduction in live load is expected; as it is assumed that the occupants will be evacuated by the time temperature effects begin to significantly influence the structures' strength and stiffness. Dead loads should remain unaltered, as they are inherent characteristic of the structure. As for other types of loading, depending on the structures geographical and topographical location, snow and wind loads may also need to be considered. In general, some degree of wind load should be considered to assure lateral stability of the structure. Snow loads should also be included when considering roof elements in regions where snow loads are significant and frequent.

For checking the fire resistance of a structure or structural element (i.e. PPC beam) to withstand the effect of a fire event (i.e. extraordinary event), ASCE-07 (2005) design standard provides two load combinations $1.2D + (0.5L \text{ or } 0.2S)$ and $(0.9 \text{ or } 1.2)D + 0.2W$ that capture a realistic loading scenario for a fire event. The first load combination is intended to envelope the vertical demands on a structure or structural element, while the second load combination checks the lateral stability. It's noteworthy to mention, the term A_k, corresponding to loads from fire effects, are not included in these expressions, because they (temperature and restraint) are captured through boundary conditions and time-temperature relationships utilized in numerical model. Furthermore, these effects are multiplied by a factor of unity (1.0) due to uncertainty associated with this event and do not need to be modified.

5.2.3. High Temperature Material Properties

To predict the fire resistance of PPC beams with a numerical model, each material must be assigned a high temperature material model to define its fire response. The material models that are of interest for fire resistance analysis are thermal and mechanical properties and these properties vary with temperature. Numerous high-temperature material models are available to be utilized in the fire resistance calculations for a performance-based approach. However, to yield accurate results, it must be emphasized, that special precaution needs to be taken when selecting a material model. Two widely accepted material property models for concrete, prestressing steel, and reinforcing steel are present in Eurocode 2 (2004) and ASCE Manual of Practice No. 78 (1992). Both these models provide temperature dependent empirical relationships to define specific materials high temperature properties and these relationships are reproduced in Appendix B. For a detailed explanation of high temperature properties of these materials refer to Chapter 2. It should be noted, ASCE model does not provide high-temperature constitutive relationships for prestressing steel and in order to use this model for PPC beams an alternative stress-strain relationship is required such as relationship provided in Eurocode 2.

5.2.4. Thermal and Structural Analysis

The third step is to perform a thermo-mechanical analysis to predict the fire response of a PPC beam. The complexity involved in such an analysis requires the use of a finite element-based program, such as SAFIR (2004), ANSYS (2011) or ABAQUS (2011). These programs utilize heat transfer and mechanics principles to perform a coupled heat transfer/strain equilibrium analysis at incremental time steps. The analysis is carried out in three main steps: calculation of fire exposure temperature, calculation of temperature distribution within the PPC beam due to the fire exposure, and calculation of residual strength, internal forces, stresses, strains, and deflections. The estimated fire scenario, structural loads, as well as geometric and material properties form the input to these computer models. The critical component of the input is high-temperature constitutive models of concrete, reinforcing steel, and prestressing steel because these properties define the thermal and mechanical response of a material. These properties vary with temperature and have a significant influence on fire resistance predictions. In SAFIR, Eurocode properties are built into the computer program, but the ASCE recommended high temperature property relationships can also be coded into the program.

When selecting a finite-element based computer program to perform a thermo-mechanical analysis the following requirements must be satisfied to be deemed acceptable. For starters, the numerical formulation utilized in the thermal analysis must be based on fundamental heat transfer principals to generate temperatures accurately. Similarly, the mechanical analysis shall be based on mechanics principles to generate deflections, internal forces, and stresses. Another basic requirement is that the software program must be capable of performing a time-dependent analysis, so that results can be checked for failure at every time step. Furthermore, to obtain reliable results, the program must be capable of accounting for nonlinear high-temperature material properties, standard and user (i.e. design or parametric) defined fire scenarios, different concrete types, high temperature creep, second-order effects (i.e. P-delta), and failure criteria. The numerical model should also be able to handle multiple materials (i.e. concrete, prestressing steel, and reinforcing steel) in a model within a nonlinear geometry and to incorporate the effect of prestressing or residual stress. These requirements must be met to ensure the finite-element program is capable of yielding accurate fire resistance results.

5.2.5. Failure Criteria

Failure criteria to be selected for the performance-based approach are based on stability, insulation, and integrity requirements. The stability limit state, also known as strength limit state, defines failure as the time when a structural element can no longer maintain its load-bearing capacity and collapses. Flexure and shear are the two primary failure modes that must be considered for PPC beams. For each failure mode, respective limiting material strain is used to define failure. The latter two failure criteria, insulation and integrity, are intended to prevent the spread of fire. These failure criteria are of special importance for PPC beams, since the floor/roof systems must not only provide structural support, but also act as a barrier between compartments. The insulation (heat transmission) criterion defines failure when the unexposed temperature on the slab exceeds 181°C (325°F) at any one point or an average of 139°C (250°F). These limiting temperatures ensure compartmentation functionality and are based on the critical temperature required to ignite cotton waste. Lastly, the integrity criterion establishes failure as time when cracks or fissures form in the concrete slab, allowing flame or hot gasses to path through the assembly. This criterion can be very difficult to quantify, but should be met through either data from fire tests or calculations based assumptions regarding material loss. The main reason for this criterions existence is to assure engineers select materials and assemblies that can be relied upon to maintain integrity. Fire resistance shall be based on the lesser failure time of the three limits, when all three criteria are applicable.

5.2.6. Practical Alternatives

Results from the performance-based analysis can be utilized to develop practical alternatives for achieving required fire resistance in PPC beams. As an example, if the fire resistance of a PPC beam is just short of the required fire resistance by a few minutes, then one solution is to replace the siliceous aggregate in the concrete with carbonate aggregate to get additional fire resistance. Other options include changing sectional dimensions, increasing the slab depth, or modifying load level depending on the criteria governing the fire resistance of the PPC beam. Another option to improve fire resistance is to include the effects of axial restraint when appropriate. The fact that many of these options can be explained through numerical analysis, without the need for expensive fire tests, offers an attractive proposition for designers. These suggestions are just some of the several possibilities to improve the fire resistance of a PPC beam.

5.3. Summary

This chapter presented a performance-based approach to calculate the fire resistance of PPC beams. It was developed in attempt to overcome the shortcomings of the current prescriptive-based methods. It accounts for the critical factors, namely, realistic fire scenarios, load level, restraint, and failure criteria, which influence fire resistance of PPC beams. To undertake the fire resistance calculations, a step-by-step procedure is provided. At every step, a detailed discussion describing that steps goal, as well as suggestions on how it can be accomplished through readily available resources. As a result, this approach offers a rational and cost-effective calculation methodology for predicting the fire resistance of PPC beams. The performance-based approach offers designers the flexibility for innovation, potential to generate better fire safety, and opportunity to maximize benefit/cost ratio.

Chapter 6

6. Conclusions and Recommendations

6.1. General

This thesis presented results from numerical studies aimed at overcoming the current fire resistance limitations of precast/prestressed concrete (PPC) double T-beams. A performance-based approach was applied in the fire resistance analysis of two PPC double T-beams. A 10DT24+2 and 12DT32+2 PPC double T-beam were analyzed using SAFIR under different fire scenarios, loading and restraint. In the numerical studies high temperature material properties, various load and restraint levels, and material and geometric nonlinearity were accounted for, as well as realistic failure criterion were included to evaluate the fire response and determine failure. Prior to the analysis, SAFIR was validated using published fire test data from the Portland Cement Association (PCA) and Underwriters Laboratories (UL). The validation studies revealed, the temperatures, deflections, and fire resistance predicted with SAFIR show a strong correlation with the results of real fire tests. In addition, a sensitivity analysis was also undertaken to confirm that the level of refinement selected for discretization of the thermal and structural models were refined enough to produce accurate results. Next, the numerical model was used to conduct parametric studies to quantify the influence of various factors on fire response of PPC double T-beams. The critical factors influencing the fire resistance were found to be fire scenario, axial restraint, load level, aggregate type, and failure criterion. Based on the findings of the parametric studies, guidelines for a performance-based assessment approach were developed to offer a rational approach for determining the fire resistance of PPC double T-beams. The guidelines outline the specific requirements for the selection of the fire scenario, material model, numerical model, and failure criteria. The proposed design approach accounts for significant factors that influence the fire resistance of PPC double T-beams, and thus provides better fire resistance estimates as compared to current code provisions.

6.2. Conclusions

Based on the information presented in this thesis, the following conclusions can be drawn:

- Current approaches for evaluating the fire resistance of a PPC double T-beam are based on prescriptive methods and may not yield realistic fire resistance.
- The main factors that influence the fire response of PPC beams are load intensity, fire scenario, aggregate type, restraint, and cover thickness.
- Load intensity is inversely proportional to fire resistance of PPC beams and can drastically reduce the fire resistance for very high load levels. A 10% increase in load can decrease fire resistance by approximately 7 minutes.

- Fire scenario has a significant influence on the fire response of a PPC double T-beam. If a PPC beam is designed under the prescriptive approach, then the beam may be over- or under-designed when compared to the actual fuel loads and ventilation conditions present.
- The type of aggregate used in concrete has a moderate influence on fire resistance of PPC beams. Carbonate aggregate concrete provide higher fire resistance (about 10% in most cases) than siliceous aggregate concrete.
- Axial restraint can improve fire resistance of PPC double T-beams by up to 12%, but the level of restraint depends on the type of restraint, support condition, and variable stiffness offered by the adjoining members.
- Fire resistance of PPC beams is often governed by limiting strand temperatures for slender stems and heat transmission for bulkier stems where adequate cover thickness is provided.
- Performance-based fire design can be used to develop rational and innovative solutions by introducing realistic fire scenarios, load intensity, and restraint conditions.

6.3. Recommendations for Future Research

While herein lies a state-of-the-art approach for assessing the fire resistance of PPC beams; more research is still needed to develop a better understanding of the subtle nuances and other scenarios not considered in this study with respect to the fire resistance of PPC beams. Below is a list of recommendations for future research in attempt to achieve this goal:

- The effects of restraint presented in this manuscript could be expanded upon by performing a comprehensive stand-alone study that would investigate numerous support conditions, types of restraint (axial, moment, and membrane action), and varying degrees of stiffness found in building applications. This research would lay the ground work for future design provisions and additional insight into the beneficial or detrimental effects of restraint.

- The high temperature constitutive relationships presented in this study revealed several discrepancies between the models and in the case of prestressing steel, even a lack of information. Therefore, future research should focus on further developing and confirming the high temperature material properties for new and existing types of concrete, reinforcing steel, and especially prestressing steel. To assure the accuracy of these models special consideration should be given to capture high temperature creep and in the case of concrete only, transient strains.
- Physical properties, such as fire-induced spalling of concrete and bond loss between prestressing steel and concrete under fire conditions need to be further studied. These properties can have the potential to be catastrophic on the fire resistance of PPC beams and subsequent collapse of an entire structure. As seen in the literature review, little is understood about the nature of either these physical properties and to date, neither property has been developed to a point where it can be predicted under fire conditions.
- A series of fire tests must be undertaken to validate results from numerical models utilized in a performance-based approach. These fire tests will help the performance based approach gain acceptance and instill confidence amongst the engineering community so that one day it will no longer be necessary to perform costly fire tests.
- The influence of a localized fire or thermal gradient about the cross-sectional depth and/or along the length of the PPC beam due to the dynamics of a real fire. These two

fire exposure scenarios to need to be considered to give insight into the potential for shear failure or potential for issues regarding principal stresses when developing guidelines for the fire design of PPC beams.

APPENDICES

Appendix A

A.1 Code Fire Resistance Rating Calculations

This appendix provides fire resistance rating calculations for the 10DT24+2 and 12DT32+2 PPC double T-beams per US, Canadian and European fire provisions. Each countries fire provisions are applied to determine a fire rating based on tabulated data, simplified calculations, and heat transmission failure criteria. Refer to Figures 4.1 and 4.2 for cross-sectional dimensions and details of 10DT24+2 and 12DT32+2 PPC beams, respectively. Refer to Table 4.1 for material and section properties for each PPC beam.

A.1.1 US Fire Provisions

The ACI 318 (2008) and PCI Design Handbook (2004) were selected to illustrate how US fire provisions determine the fire resistance of PPC beams. The following calculations assume a normal weight concrete composed of carbonate aggregates.

Tabulated Data:

<u>10DT24+2</u>

Effective flange width for a T-beam per ACI 318 Section 8.10.2

$$b_{eff} = 3*(AverageStemWidth) = 3*(\frac{95mm+146mm}{2}) = 362mm$$

Effective area of a single stem

$$A_{eff} = 362mm*102mm + 559mm*\frac{(95mm+146mm)}{2} = 104{,}284mm^2 = 10.4cm^2$$

$$\therefore A_{eff} \Rightarrow 9.6 < A_{eff} < 19.4cm^2$$

Concrete cover to prestressing strands

$$c_{bottom}(provided) = 51mm - 13mm * \frac{1}{2} = 45mm$$

$$c_{side}(provided) = \frac{95mm}{2} + \frac{127mm}{559mm} * \frac{(146mm - 95mm)}{2} - \frac{13mm}{2} = 47mm$$

Minimum concrete cover to prestressing strand

$$c_{\min} \cong 45mm$$

Tabulated fire resistance ratings based on restraint condition, aggregate type, beam area, and minimum concrete cover to prestressing strands per Table 9.3.7.1(5) of the PCI Design Handbook.

Minimum required concrete cover to prestressing strands for 1 1/2 hr fire resistance rating

$$c_{req} = 44mm$$

$$FRR = 1\frac{1}{2}\,hr$$

12DT32+2

Effective flange width for a T-beam per ACI 318 Section 8.10.2

$$b_{eff} = 3 * (AverageStemWidth) = 3 * (\frac{197mm + 121mm}{2}) = 477mm$$

Effective area of a single stem

$$A_{eff} = 476mm * 102mm + 762mm * \frac{(197mm + 121mm)}{2} = 169{,}710mm^2 = 17.0cm^2$$

$$\therefore A_{eff} \Rightarrow 9.6 < A_{eff} < 19.4cm^2$$

Concrete cover to prestressing strands

$$c_{bottom}(provided) = 51mm - 13mm * \frac{1}{2} = 45mm$$

$$c_{side}(provided) = \frac{146mm}{2} + \frac{178mm}{762mm} * \frac{(197mm - 121mm)}{2} - \frac{13mm}{2} = 75mm$$

Minimum concrete cover to prestressing strand

$$c_{\min} \cong 45mm$$

Tabulated fire resistance ratings based on restraint condition, aggregate type, beam area, and minimum concrete cover to prestressing strands per Table 9.3.7.1(5) of the PCI Design Handbook.

Minimum required concrete cover to prestressing strands for 1 1/2 hr fire resistance rating

$$c_{req} = 44mm$$

$$FRR = 1\tfrac{1}{2}\,hr$$

Simplified Calculations:

A single set of detailed calculations to determine the moment capacity at 1 hr of fire exposure is provided below for each PPC beam. A complete set of results are provided in Tables A1.1.1 and A1.1.2 for the 10DT24+2 and 12DT32+2, respectively.

<u>10DT24+2</u>

Depth to strand centroid

$$u = 127mm$$

Stem width at strand centroid

$$b = 95mm + \frac{127mm}{559mm} * \frac{(146mm - 95mm)}{2} * 2 = 107mm$$

Strand temperature increase based on width and depth to centroid per Table 9.3.7.6 of the PCI Design Handbook.

$T = 342°C$

Strength reduction per Figure 9.3.7.2 of the PCI Design Handbook

$STR\_red = 66\%$

Ultimate tensile strength in prestressing strand after 1 hr of fire exposure

$f_{pu\theta} = 0.66 * 1862 MPa = 1229 MPa$

Factor based on type of prestressing strand per section 18.7.2 of ACI 318

Since $\frac{f_{py}}{f_{pu}} > 0.8 \Rightarrow \gamma_p = 0.4$

Compressive stress block factor per section 4.2.1.1 of PCI Design Handbook

$\beta_1 = 0.76$

Stress in prestressing strand at nominal strength after 1 hr of fire exposure

$$f_{ps\theta} = f_{pu\theta}[1 - \frac{\gamma_p A_{ps} f_{pu\theta}}{\beta_1 b d f'_c}] = 1{,}229 MPa * [1 - \frac{0.4 * 1{,}013 mm^2 * 1{,}229 MPa}{0.76 * 3{,}048 mm * 533 mm * 40 MPa}] = 1217 MPa$$

Depth of equivalent rectangular compression stress block

$$a_\theta = \frac{A_{ps} f_{ps\theta}}{0.85 f'_c b} = \frac{1{,}013 mm^2 * 1{,}217 MPa}{0.85 * 40 MPa * 3{,}048 mm} = 12 mm$$

Moment capacity after 1 hr of fire exposure

$$M_{n\theta} = A_{ps} f_{ps\theta}(d_p - \frac{a_\theta}{2}) = 1{,}013 mm^2 * 1{,}217 MPa * (533 mm - \frac{12 mm}{2}) = 650 kNm$$

Table A1.1.1 – Simplified Calculation Results for 10DT24+2 According to US Fire Provisions

	1 hr	2 hr	3 hr	4 hr
Temperature (°C)	342	609	703	709
Strength reduction (%)	66	14	6	5
$f_{pu\theta}$ (MPa)	1,229	261	112	93
$f_{ps\theta}$ (MPa)	1,217	255	110	90
a_{θ} (mm)	12	3	1	1
$M_{n\theta}$ (kNm)	650	137	59	49

Selfweight of PPC Beam

$$D = 3.45\,kPa * 3.048\,m = 10.5\,kN/m$$

Live load for a parking garage/building per ASCE 7-05 (2005) design loads for a parking garage/building

$$L = 2.39\,kPa * 3.048\,m = 7.3\,kN/m$$

Load combination

$$w = 1.2D + 0.5L = 1.2 * 10.5\,kN/m + 0.5 * 7.3\,kN/m = 16.3\,kN/m$$

Factored moment demands

$$M = \frac{wl^2}{8} = \frac{16.3\,kN/m * (12.192\,m)^2}{8} = 302\,kNm$$

Determine moment capacity for 1 ½ hr fire rating from Table A1.1.1:

$$M_{n\theta} = \frac{(650\,kNm + 138\,kNm)}{2} = 394\,kNm$$

Since $394\,kNm > 302\,kNm \Rightarrow FRR = 1\,{}^{1}\!/_{2}\,hrs$

12DT32+2

Depth to strand centroid

$$u = 178mm$$

Stem width at strand centroid

$$b = 121mm + \frac{178mm}{762mm} * \frac{(197mm - 121mm)}{2} * 2 = 139mm$$

Strand temperature increase based on width and depth to centroid per Table 9.3.7.6 of the PCI Design Handbook.

$$T = 198°C$$

Strength reduction per Figure 9.3.7.2 of the PCI Design Handbook

$$STR\_red = 93\%$$

Ultimate tensile strength in prestressing strand after 1 hr of fire exposure

$$f_{pu\theta} = 0.93 * 1862MPa = 1{,}732MPa$$

Factor based on type of prestressing strand per section 18.7.2 of ACI 318

Since $\frac{f_{py}}{f_{pu}} > 0.8 \Rightarrow \gamma_p = 0.4$

Compressive stress block factor per section 4.2.1.1 of PCI Design Handbook

$$\beta_1 = 0.76$$

Stress in prestressing strand at nominal strength after 1 hr of fire exposure

$$f_{ps\theta} = f_{pu\theta}[1 - \frac{\gamma_p A_{ps} f_{pu\theta}}{\beta_1 bdf'_c}] = 1{,}732MPa * [1 - \frac{0.4 * 1{,}523mm^2 * 1{,}732MPa}{0.76 * 3{,}658mm * 686mm * 40MPa}] = 1{,}708MPa$$

Depth of equivalent rectangular compression stress block

$$a_\theta = \frac{A_{ps} f_{ps\theta}}{0.85 f'_c b} = \frac{1{,}523mm^2 * 1{,}732MPa}{0.85 * 40MPa * 3{,}658mm} = 21mm$$

Moment capacity after 1 hr of fire exposure

$$M_{n\theta} = A_{ps} f_{ps\theta}(d_p - \frac{a_\theta}{2}) = 1{,}523mm^2 * 1{,}732MPa * (686mm - \frac{21mm}{2}) = 1{,}782kNm$$

Table A1.1.2 – Simplified Calculation Results for 12DT32+2 According to Canadian Fire Provisions

	1 hr	2 hr	3 hr	4 hr
Temperature (°C)	198	431	576	592
Strength reduction (%)	93	45	18	16
$f_{pu\theta}$ (MPa)	1,732	838	335	298
$f_{ps\theta}$ (MPa)	1,708	832	334	297
a_θ (mm)	21	10	4	4
$M_{n\theta}$ (kNm)	1,782	863	348	309

Selfweight of PPC Beam

$$D = 4.08kPa * 3.6576\,m = 14.9kN\,/\,m$$

Live load for a parking garage/building per ASCE 7-05 (2005) design loads for a parking garage/building

$$L = 2.39kPa * 3.6576\,m = 8.7kN\,/\,m$$

Load combination

$$w = 1.2D + 0.5L = 1.2 * 14.9kN\,/\,m + 0.5 * 8.7kN\,/\,m = 22.2kN\,/\,m$$

Factored moment demands

$$M = \frac{wl^2}{8} = \frac{22.2kN\,/\,m * (15.24m)^2}{8} = 645kNm$$

Since $863\,kNm > 645\,kNm \Rightarrow FRR = 2hrs$

Heat Transmission:

<u>10DT24+2</u>

Slab thickness

$h = flange + topping = 51mm + 51mm = 102\,mm$

Heat transmission fire resistance rating based on type of concrete and slab thickness per Table 9.3.6.1 of the PCI Design Handbook.

$FRR = 1hr$

<u>12DT32+2</u>

Slab thickness

$h = flange + topping = 51mm + 51mm = 102\,mm$

Heat transmission fire resistance rating based on type of concrete and slab thickness per Table 9.3.6.1 of the PCI Design Handbook.

$FRR = 1hr$

A.1.2 Canadian Fire Provisions

The National Building Code of Canada (2005) and CPCI Design Manual (2007) were selected to illustrate how Canadian fire provisions determine the fire resistance of PPC beams. The following calculations assume a normal weight concrete (Type N) composed of calcareous (carbonate) aggregates.

Tabulated Data:

<u>10DT24+2</u>

Effective flange width for a T-beam per CAN3-D-2.10

$$b_{eff} = 12t_f = 12*102mm = 1,224mm$$

$$b_{eff} = \frac{1}{2}(ClearDist.) = \frac{1}{2}*(1,524mm - 95mm) = 715mm$$

$$b_{eff} = \frac{1}{5}(Span) = \frac{1}{5}(12,192mm) = 2,438mm$$

$$\therefore b_{eff} = 714mm$$

Effective area of a single stem

$$A_{eff} = 102mm*714mm + 559mm*121mm = 140,000mm^2 = 1,400cm^2$$

$$\therefore A_{eff} \Rightarrow 970 < A_{eff} < 1,940cm^2$$

Concrete cover to prestressing strands

$$c_{bottom}(provided) = 45mm$$

$$c_{side}(provided) = 47mm$$

Average concrete cover to prestressing strands

$$c_{avg} = \frac{(45mm + 47mm)}{2} = 46mm$$

Tabulated fire resistance ratings based on restraint condition, aggregate type, beam area, and average concrete cover to prestressing strands per Table D-2.10.1 of National Building Code of Canada.

Minimum required concrete cover to prestressing strands for 1 1/2 hr fire resistance rating

$$c_{req} = 45mm$$

$$FRR = 1\,{}^{1}\!/_{2}\,hr$$

<u>12DT32+2</u>

Effective flange width for a T-beam per CAN3-D-2.10

$$b_{eff} = 12t_f = 12*102mm = 1{,}224mm$$

$$b_{eff} = \frac{1}{2}(ClearDist.) = \frac{1}{2}*(1{,}829mm - 121mm) = 854mm$$

$$b_{eff} = \frac{1}{5}(Span) = \frac{1}{5}(15{,}240mm) = 3{,}048mm$$

$$\therefore b_{eff} = 854mm$$

Effective area of a single stem

$$A_{eff} = 102mm*854mm + 762mm*171mm = 217{,}410mm^2 = 2{,}174cm^2$$

$$\therefore A_{eff} \Rightarrow A_{eff} > 1{,}940cm^2$$

Concrete cover to prestressing strands

$$c_{bottom}(provided) = 45mm$$

$$c_{side}(provided) = 76mm$$

Average concrete cover to prestressing strands

$$c_{avg} = \frac{(45mm + 76mm)}{2} = 61mm$$

Tabulated fire resistance ratings based on restraint condition, aggregate type, beam area, and average concrete cover to prestressing strands per Table D-2.10.1 of National Building Code of Canada.

Minimum required concrete cover to prestressing strands for 2 hr fire resistance rating

$$c_{req} = 50mm$$

$$FRR = 2hr$$

Simplified Calculations:

A single set of detailed calculations to determine the moment capacity at 1 hr of fire exposure is provided below for each PPC beam. A complete set of results are provided in Tables A1.2.1 and A1.2.2 for the 10DT24+2 and 12DT32+2, respectively. Note, the CPCI Design Manual only provides a 2 hour temperature profile to determine the strand temperatures. Therefore, Table 9.3.7.6, 9.3.7.8, and 9.3.7.9 from the PCI Design Handbook were used to assess the fire temperatures for the 1, 3, and 4 hour moment capacity calculation.

<u>10DT24+2</u>

Depth to strand centroid

$$u = 127mm$$

Stem width at strand centroid

$$b = 107mm$$

Strand temperature increase based on width and depth to centroid per Table 9.3.7.6 of the PCI Design Handbook (Figure 6.3.10 of CPCI Design Manual for 2 hr temperature).

$$T = 342°C$$

Strength reduction per Figure 6.3.7 of CPCI Design Manual

$$STR\_red = 66\%$$

Ultimate tensile strength in prestressing strand after 1 hr of fire exposure

$$f_{pu\theta} = 0.66 * 1{,}860MPa = 1{,}228MPa$$

Ratio of average stress in rectangular compression block to specified concrete strength per section 3.3.1 of CPCI Design Manual

$$\alpha_1 = \min(0.67, 0.85 - 0.0015 * f'_c) = \min(0.67, 0.85 - 0.0015 * 40MPa) = 0.79$$

Ratio of depth to rectangular compression block to depth to the neutral axis

$$\beta_1 = \min(0.67, 0.97 - 0.0025 * f'_c) = \min(0.67, 0.97 - 0.0025 * 40MPa) = 0.87$$

Distance from extreme compression fiber to centroid of stressed reinforcement

$$d_p = 533mm$$

Minimum effective web width within depth *d*

$$b_w = 3{,}048mm$$

$$\frac{c}{d_p} = \frac{A_{ps} f_{pu\theta}}{\alpha_1 f'_c b_w d_p \beta_1} = \frac{1{,}013mm^2 * 1{,}228MPA}{0.79 * 40MPa * 3{,}048mm * 533mm * 0.87} = 0.0279$$

Coefficient accounting for the shape of tendon stress-strain curve (low relaxation strand of wire)

$$k_p = 0.28$$

Stress in prestressing strand at nominal strength after 1 hr of fire exposure

$$f_{pr\theta} = f_{pu\theta}[1 - k_p \frac{c}{d_p}] = 1{,}228MPa * [1 - 0.28 * (0.0279)] = 1{,}218MPa$$

Depth of equivalent rectangular compression stress block

$$a_\theta = \frac{A_{ps} f_{pr\theta}}{\alpha_1 b_w f'_c} = \frac{1{,}013mm^2 * 1{,}218MPa}{0.79 * 3{,}048mm * 40MPa} = 13mm$$

Moment capacity after 1 hr of fire exposure

$$M_{n\theta} = A_{ps} f_{pr\theta}(d_p - \frac{a_\theta}{2}) = 1{,}013mm^2 * 1{,}218MPa * (533mm - \frac{13mm}{2}) = 650kNm$$

Table A1.2.1 – Simplified Calculation Results for 10DT24+2 According to Canadian Fire Provisions

	1 hr	2 hr	3 hr	4 hr
Temperature (°C)	342	610	703	709
Strength reduction (%)	66	12	4	4
$f_{pu\theta}$ (MPa)	1,228	223	74	74
c/d_p	0.0279	.0051	0.0017	0.0017
$f_{pr\theta}$ (MPa)	1,218	223	74	74
a_θ (mm)	13	2	1	1
$M_{n\theta}$ (kNm)	650	120	40	40

Selfweight of PPC Beam

$$D = 3.45\,kPa * 3.048\,m = 10.5\,kN/m \backslash$$

Live load for a parking garage/building per ASCE 7-05 (2005) design loads for a parking garage/building

$$L = 2.39\,kPa * 3.048\,m = 7.3\,kN/m$$

Load combination

$$w = D + L = 10.5\,kN/m + 7.3\,kN/m = 17.8\,kN/m$$

Factored moment demands

$$M = \frac{wl^2}{8} = \frac{17.8\,kN/m * (12.192\,m)^2}{8} = 331\,kNm$$

Determine moment capacity for 1 ½ hr fire rating from Table A1.2.1

$$M_{n\theta} = \frac{(650\,kNm + 120\,kNm)}{2} = 385\,kNm$$

Since $385\,kNm > 331\,kNm \Rightarrow FRR = 1\,{}^1\!/_2\ hrs$

12DT32+2

Depth to strand centroid

$u = 178mm$

Stem width at strand centroid

$b = 138mm$

Strand temperature increase based on width and depth to centroid per Table 9.3.7.6 of the PCI Design Handbook (Figure 6.3.10 of CPCI Design Manual for 2 hr temperature).

$T = 198°C$

Strength reduction per Figure 6.3.7 of CPCI Design Manual

$STR\_red = 94\%$

Ultimate tensile strength in prestressing strand after 1 hr of fire exposure

$f_{pu\theta} = 0.94 * 1{,}860MPa = 1{,}748MPa$

Ratio of average stress in rectangular compression block to specified concrete strength per section 3.3.1 of CPCI Design Manual

$\alpha_1 = \min(0.67, 0.85 - 0.0015 * f'_c) = \min(0.67, 0.85 - 0.0015 * 40MPa) = 0.79$

Ratio of depth to rectangular compression block to depth to the neutral axis

$\beta_1 = \min(0.67, 0.97 - 0.0025 * f'_c) = \min(0.67, 0.97 - 0.0025 * 40MPa) = 0.87$

Distance from extreme compression fiber to centroid of stressed reinforcement

$d_p = 686mm$

Minimum effective web width within depth *d*

$b_w = 3{,}658mm$

$$\frac{c}{d_p} = \frac{A_{ps} f_{pu\theta}}{\alpha_1 f'_c b_w d_p \beta_1} = \frac{1{,}013 mm^2 * 1{,}748 MPA}{0.79 * 40 MPa * 3{,}658 mm * 686 mm * 0.87} = 0.0257$$

Coefficient accounting for the shape of tendon stress-strain curve (low relaxation strand of wire)

$$k_p = 0.28$$

Stress in prestressing strand at nominal strength after 1 hr of fire exposure

$$f_{pr\theta} = f_{pu\theta}[1 - k_p \frac{c}{d_p}] = 1{,}748 MPa * [1 - 0.28 * (0.0257)] = 1{,}735 MPa$$

Depth of equivalent rectangular compression stress block

$$a_\theta = \frac{A_{ps} f_{pr\theta}}{\alpha_1 b_w f'_c} = \frac{1{,}013 mm^2 * 1{,}735 MPa}{0.79 * 3{,}658 mm * 40 MPa} = 15 mm$$

Moment capacity after 1 hr of fire exposure

$$M_{n\theta} = A_{ps} f_{pr\theta}(d_p - \frac{a_\theta}{2}) = 1{,}013 mm^2 * 1{,}735 MPa * (686 mm - \frac{15 mm}{2}) = 1{,}192 kNm$$

Table A1.2.2 – Simplified Calculation Results for 12DT32+2 According to Canadian Fire Provisions

	1 hr	2 hr	3 hr	4 hr
Temperature (°C)	198	460	703	709
Strength reduction (%)	94	35	15	13
$f_{pu\theta}$ (MPa)	1,748	651	279	242
c/d_p	0.0257	.0096	0.0041	0.0036
$f_{pr\theta}$ (MPa)	1,735	649	279	242
a_θ (mm)	15	6	2	2
$M_{n\theta}$ (kNm)	1,192	449	194	168

Selfweight of PPC Beam

$$D = 4.08 kPa * 3.6576 m = 14.9 kN / m$$

Live load for a parking garage/building per ASCE 7-05 (2005) design loads for a parking garage/building

$$L = 2.39\,kPa * 3.6576\ m = 8.7\,kN\ /\ m$$

Load combination

$$w = D + L = 14.9\,kN\ /\ m + 8.7\,kN\ /\ m = 23.6\,kN\ /\ m$$

Factored moment demands

$$M = \frac{wl^2}{8} = \frac{23.6\,kN/m * (15.24\,m)^2}{8} = 685\,kNm$$

Determine moment capacity for 1 ½ hr fire rating from Table A1.2.2

$$M_{n\theta} = \frac{(1{,}192\,kNm + 449\,kNm)}{2} = 821\,kNm$$

Since $821\,kNm > 685\,kNm \Rightarrow FRR = 1\,{}^1\!/_2\ hrs$

Heat Transmission:

<u>10DT24+2</u>

Slab thickness

$$h = flange + topping = 51mm + 51mm = 102\,mm$$

Heat transmission fire resistance rating based on type of concrete and slab thickness per Table D-2.2.1.A of the National Building Code of Canada.

$$FRR = 1hr$$

12DT32+2

Slab thickness

$$h = flange + topping = 51mm + 51mm = 102\,mm$$

Heat transmission fire resistance rating based on type of concrete and slab thickness per Table D-2.2.1.A of the National Building Code of Canada.

$$FRR = 1hr$$

A.1.3 Eurocode Fire Provisions

Eurocode 1 Part 1-2 (2002), Eurocode 2 Part 1-1 (2004), and Eurocode 2 Part 1-2 (2004) were selected to illustrate how Eurocode fire provisions determine the fire resistance of PPC beams.

Tabulated Data:

10DT24+2

Vertical distance to centroid of bottom prestressing strand

$$a = 51mm$$

Modification to axis distance for prestressing wire per section 5.2(5) of Eurocode 2 Part 1-2 to account for critical temperature of 350 °C

$$a_{\mathrm{mod}} = 51mm + 15mm = 66mm$$

Side distance to centroid of prestressing strand

$$a_{sd} = 47mm$$

Modification to axis distance for prestressing wire per Table 5.5 of Eurocode 2 Part 1-2

$$a_{sd,\mathrm{mod}} = 47mm + 10mm = 57mm$$

Stem width at strand centroid

$b = 107mm$

Tabulated fire resistance ratings based on minimum of either the combination of the average axis distance and width of beam or web thickness per Table 5.5 of Eurocode 2 Part 1-2. Assume web thickness is based on a Class WB (tapered web).

Web thickness controls

$b_w = 100mm$

$FRR = 1\frac{1}{2} hr$

<u>12DT32+2</u>

Vertical distance to centroid of bottom prestressing strand

$a = 51mm$

Modification to axis distance for prestressing wire per section 5.2(5) of Eurocode 2 Part 1-2 to account for critical temperature of 350 °C

$a_{\mathrm{mod}} = 51mm + 15mm = 66mm$

Side distance to centroid of prestressing strand

$a_{sd} = 59mm$

Modification to axis distance for prestressing wire per Table 5.5 of Eurocode 2 Part 1-2

$a_{sd,\mathrm{mod}} = 47mm + 10mm = 69mm$

Stem width at strand centroid

$b = 138mm$

Tabulated fire resistance ratings based on minimum of either the combination of the average axis distance and width of beam or web thickness per Table 5.5 of Eurocode 2 Part 1-2. Assume web thickness is based on a Class WB (tapered web).

Web thickness controls

$b_w = 120mm$

$FRR = 2hr$

Simplified Calculations:

A single set of detailed calculations to determine the moment capacity at 1 hr of fire exposure is provided below for each PPC beam. A complete set of results are provided in Tables A1.3.1 and A1.3.2 for the 10DT24+2 and 12DT32+2, respectively. Note, the Eurocode 2 Part 1-2 only provides temperature profiles for rectangular cross-sections. To accurately predict the temperatures within a stemmed cross-section, the temperature profiles provided in Tables 9.3.7.6 to 9.3.7.9 of the PCI Design Handbook are used.

<u>10DT24+2</u>

Depth to strand centroid

$u = 127mm$

Stem width at strand centroid

$b = 107mm$

Strand temperature increase based on width and depth to centroid per Table 9.3.7.6 of the PCI Design Handbook.

$T = 342°C$

Strength reduction per Figure 5.1 of Eurocode 2 Part 1-2

$$k_p(\theta) = 1.0 - 0.45(\theta - 100)/250 = 1.0 - 0.45(342°C - 100)/250 = 0.56$$

Ultimate tensile strength in prestressing strand after 1 hr of fire exposure

$$\sigma_{pr\theta} = k_p(\theta)\sigma_{pu} = 0.56 * 1{,}860MPa = 1{,}042MPa$$

Effective strength factor per section 3.1.7 of the Eurocode Part 1-1

$$\eta = 1.0$$

Area of prestressing steel strand

$$A_{s,provided} = 1{,}013mm^2$$

Depth of equivalent rectangular compression stress block after 1 hour of fire exposure

$$a_\theta = \frac{A_{ps}\sigma_{pr\theta}}{\eta f_{ck} b} = \frac{1{,}013mm^2 * 1{,}042MPa}{1.0 * 40MPa * 3{,}048mm} = 9mm$$

Depth of equivalent rectangular compression stress block at ambient temperatures

$$a = \frac{A_{ps}\sigma_{pu}}{\eta f_{ck} b} = \frac{1{,}013mm^2 * 1{,}860MPa}{1.0 * 40MPa * 3{,}048mm} = 15mm$$

Distance from extreme compression fiber to centroid of stressed reinforcement

$$d_p = 533mm$$

Selfweight of PPC Beam

$$G_k = 3.45kPa * 3.048m = 10.5kN/m$$

Live load for a parking garage/building per ASCE 7-05 (2005) design loads for a parking garage/building

$$Q_k = 2.39kPa * 3.048m = 7.3kN/m$$

Load combination

$$w_{Ed,fi} = G_k + 0.9Q_k = 10.5kN/m + 0.9*7.3kN/m = 17.1kN/m \backslash$$

Factored moment demands

$$M_{Ed,fi} = \frac{w_{Ed,fi} l_{eff}^2}{8} = \frac{17.1kN/m*(12.192m)^2}{8} = 318kN\_m$$

Required area of prestressing steel

$$A_{s,req} = \frac{M_{Ed,fi}}{\sigma_p(d_p - \frac{a}{2})} = \frac{318kN\_m}{1{,}860MPa*(533mm - \frac{15mm}{2})} = 325mm^2$$

Partial factor for prestressing steel under accidental design situations per Table 2.1N of Eurocode 2 Part 1-1

$$\gamma_S = 1.0$$

Partial factor for prestressing steel under persistent and transient design situations per Table 2.1N of Eurocode 2 Part 1-1

$$\gamma_{s,fi} = 1.15$$

Ratio o f provided to required reinforcement shall not be taken greater than 1.3 per annex E.2(4) of Eurocode 2 Part 1-2

$$\frac{A_{s,provided}}{A_{s,req}} = \min(\frac{A_{s,provided}}{A_{s,req}}, 1.3) = \min(\frac{1013mm^2}{325mm^2}, 1.3) = \min(3.11, 1.3) = 1.3$$

Moment capacity after 1 hr of fire exposure

$$M_{Rd,fi} = \left(\frac{\gamma_s}{\gamma_{s,fi}}\right) k_s(\theta)\sigma_{pr\theta}\left(\frac{A_{s,provided}}{A_{s,req}}\right) = \left(\frac{1.0}{1.15}\right)*(0.56)*(1{,}042MPa)*(1.3) = 660kNm$$

Table A1.3.1 – Simplified Calculation Results for 10DT24+2 According to Eurocode Fire Provisions

	1 hr	2 hr	3 hr	4 hr
Temperature (°C)	342	609	703	709
k_p	0.56	0.09	0.08	0.08
σ_{pr} (MPa)	1,042	167	149	149
a_θ (mm)	9	1	1	1
$M_{Rd,fi}$ (kNm)	660	17	13	13

Determine moment capacity for 1 ½ hr fire rating from Table A1.2.1

$$M_{n\theta} = \frac{(660kNm + 17kNm)}{2} = 339kNm$$

Since $339\,kNm > 318\,kNm \Rightarrow FRR = 1\,{}^1\!/_2\,hrs$

<u>12DT32+2</u>

Depth to strand centroid

$$u = 178mm$$

Stem width at strand centroid

$$b = 138mm$$

Strand temperature increase based on width and depth to centroid per Table 9.3.7.6 of the PCI Design Handbook.

$$T = 198°C$$

Strength reduction per Figure 5.1 of Eurocode 2 Part 1-2

$$k_p(\theta) = 1.0 - 0.45(\theta - 100)/250 = 1.0 - 0.45(198°C - 100)/250 = 0.82$$

Ultimate tensile strength in prestressing strand after 1 hr of fire exposure

$$\sigma_{pr\theta} = k_p(\theta)\sigma_{pu} = 0.82 * 1{,}860MPa = 1{,}525MPa$$

Effective strength factor per section 3.1.7 of the Eurocode Part 1-1

$$\eta = 1.0$$

Area of prestressing steel strand

$$A_{s,provided} = 1{,}520 mm^2$$

Depth of equivalent rectangular compression stress block after 1 hour of fire exposure

$$a_\theta = \frac{A_{ps}\sigma_{pr\theta}}{\eta f_{ck} b} = \frac{1{,}520mm^2 * 1{,}525MPa}{1.0 * 40MPa * 3{,}658mm} = 16mm$$

Depth of equivalent rectangular compression stress block at ambient temperatures

$$a = \frac{A_{ps}\sigma_{pu}}{\eta f_{ck} b} = \frac{1{,}520mm^2 * 1{,}860MPa}{1.0 * 40MPa * 3{,}658mm} = 19mm$$

Distance from extreme compression fiber to centroid of stressed reinforcement

$$d_p = 686mm$$

Selfweight of PPC Beam

$$G_k = 4.08 kPa * 3.6576 m = 14.9 kN / m$$

Live load for a parking garage/building per ASCE 7-05 (2005) design loads for a parking garage/building

$$Q_k = 2.39 kPa * 3.6576 m = 8.7 kN / m$$

Load combination

$$w_{Ed,fi} = G_k + 0.9Q_k = 14.9kN/m + 0.9 * 8.7kN/m = 22.7kN/m$$

Factored moment demands

$$M_{Ed,fi} = \frac{w_{Ed,fi} l_{eff}^2}{8} = \frac{22.7kN/mt * (15.24m)^2}{8} = 659kN\_m$$

Required area of prestressing steel

$$A_{s,req} = \frac{M_{Ed,fi}}{\sigma_p(d_p - \frac{a}{2})} = \frac{659kN\_m}{1{,}860MPa * (686mm - \frac{19mm}{2})} = 524mm^2$$

Partial factor for prestressing steel under accidental design situations per Table 2.1N of Eurocode 2 Part 1-1

$$\gamma_s = 1.0$$

Partial factor for prestressing steel under persistent and transient design situations per Table 2.1N of Eurocode 2 Part 1-1

$$\gamma_{s,fi} = 1.15$$

Ratio o f provided to required reinforcement shall not be taken greater than 1.3 per annex E.2(4) of Eurocode 2 Part 1-2

$$\frac{A_{s,provided}}{A_{s,req}} = \min(\frac{A_{s,provided}}{A_{s,req}}, 1.3) = \min(\frac{1{,}520mm^2}{521mm^2}, 1.3) = \min(2.92, 1.3) = 1.3$$

Moment capacity after 1 hr of fire exposure

$$M_{Rd,fi} = \left(\frac{\gamma_s}{\gamma_{s,fi}}\right) k_s(\theta)\sigma_{pr\theta}\left(\frac{A_{s,provided}}{A_{s,req}}\right) = \left(\frac{1.0}{1.15}\right) * (0.82) * (1{,}525MPa) * (1.3) = 1{,}414kNm$$

Table A1.3.2 – Simplified Calculation Results for 12DT32+2 According to Eurocode Fire Provisions

	1 hr	2 hr	3 hr	4 hr
Temperature (°C)	198	431	576	592
k_p	0.82	0.37	0.10	0.09
$\sigma_{pr\theta}$ (MPa)	1,525	688	186	167
a_θ (mm)	16	7	2	2
$M_{Rd,fi}$ (kNm)	1,414	288	21	17

Determine moment capacity for 1 ½ hr fire rating from Table A1.2.1

$$M_{n\theta} = \frac{(1{,}414kNm + 288kNm)}{2} = 851kNm$$

Since $851kNm > 659kNm \Rightarrow FRR = 1\,{}^{1}\!/_{2}\,hrs$

Heat Transmission:

<u>10DT24+2</u>

Slab thickness

$h = \text{ } flange + topping \text{ } = 51mm + 51mm = 102\,mm$

Heat transmission fire resistance rating based on thickness of concrete per Table 5.8 of the Eurocode 2 Part 1-2.

$$FRR = 1\,{}^{1}\!/_{2}\,hr$$

<u>12DT32+2</u>

Slab thickness

$h = \text{ } flange + topping \text{ } = 51mm + 51mm = 102\,mm$

Heat transmission fire resistance rating based on thickness of concrete per Table 5.8 of the Eurocode 2 Part 1-2.

$$FRR = 1\,{}^{1}\!/_{2}\,hr$$

Appendix B

B.1 High Temperature Material Property Relationships

Table B.1 – Constitutive Relationships for High Temperature Properties of Normal Strength Concrete

		Eurocode 2 (2004)
Volumetric Specific Heat (J/m^3°C)	***All Types***	Specific heat (J/kg°C) $c = 900$ $for\ 20\,°C \le T \le 100\,°C$ $c = 900 + (T - 100)$ $for\ 100\,°C < T \le 200\,°C$ $c = 1000 + (T - 200)/2$ $for\ 200\,°C < T \le 400\,°C$ $c = 1100$ $for\ 400\,°C < T \le 1200\,°C$ Density (kg/m^3) $\rho = \rho(20\,°C)$ $for\ 20\,°C \le T \le 100\,°C$ $\rho = \rho(20\,°C)(1 - 0.02(T - 115)/85)$ $for\ 115\,°C < T \le 200\,°C$ $\rho = \rho(20\,°C)(0.98 - 0.03(T - 200)/200)$ $for\ 200\,°C < T \le 400\,°C$ $\rho = \rho(20\,°C)(0.95 - 0.07(T - 400)/800)$ $for\ 400\,°C < T \le 1200\,°C$ $Volumetric\ Specific\ Heat = \rho c$
Thermal Conductivity (W/m°C)	***All Types***	Upper limit $k_c = 2 - 0.2451(T/100) + 0.0107(T/100)^2$ $for\ 20\,°C \le T \le 1200\,°C$ Lower limit $k_c = 1.36 - 0.136(T/100) + 0.0057(T/100)^2$ $for\ 20\,°C \le T \le 1200\,°C$

Table B.1 (cont'd) – Constitutive Relationships for High Temperature Properties of Normal Strength Concrete

		Eurocode 2 (2004)
Thermal Strain	***Carbonate Aggregates***	$\varepsilon_{th} = -1.2x10^{-4} + 6x10^{-6}T + 2.3x10^{-11}T^3$ $for\ 20\,°C \le T \le 700\,°C$ $\varepsilon_{th} = 14x10^{-3}$ $for\ 700\,°C \le T \le 1200\,°C$
	Siliceous Aggregates	$\varepsilon_{th} = -1.2x10^{-4} + 6x10^{-6}T + 1.4x10^{-11}T^3$ $for\ 20\,°C \le T \le 805\,°C$ $\varepsilon_{th} = 12x10^{-3}$ $for\ 805\,°C \le T \le 1200\,°C$
Stress-strain relationships (MPa)	***All Types***	$\sigma_c(\theta) = \dfrac{3\varepsilon f'_{c,\theta}}{\varepsilon_{c1,\theta}\left(2 + \left(\dfrac{\varepsilon}{\varepsilon_{c1,\theta}}\right)^3\right)}$ $\quad for\ \varepsilon \le \varepsilon_{c1,\theta}$ *For numerical purposes a descending branch should be adopted. Linear or nonlinear models are permitted.* $\quad for\ \varepsilon_{c1,\theta} < \varepsilon \le \varepsilon_{cu1,\theta}$ (For the variables in this equation refer to Table B.2.)

Table B.1 (cont'd) – Constitutive Relationships for High Temperature Properties of Normal Strength Concrete

		ASCE Manual (1992)	
Volumetric Specific Heat (J/m^3°C)	***Carbonate Aggregates***	$\rho c = 2.566$ $\rho c = 0.1765T - 68.034$ $\rho c = 25.00671 - 0.05043T$ $\rho c = 2.566$ $\rho c = 0.01603T - 5.44881$ $\rho c = 0.16635T - 100.90225$ $\rho c = 176.07343 - 0.22103T$ $\rho c = 2.566$	$for\ 20\,°C \le T \le 400\,°C$ $for\ 400\,°C < T \le 410\,°C$ $for\ 410\,°C < T \le 445\,°C$ $for\ 445\,°C < T \le 500\,°C$ $for\ 500\,°C < T \le 635\,°C$ $for\ 635\,°C < T \le 715\,°C$ $for\ 715\,°C < T \le 785\,°C$ $for\ T > 785\,°C$
	Siliceous Aggregates	$\rho c = 0.005T + 1.7$ $\rho c = 2.7$ $\rho c = 0.013T - 2.5$ $\rho c = 10.5 - 0.013T$ $\rho c = 2.7$	$for\ 20\,°C \le T \le 200\,°C$ $for\ 200\,°C < T \le 400\,°C$ $for\ 400\,°C \le T \le 500\,°C$ $for\ 500\,°C < T \le 600\,°C$ $for\ T > 600\,°C$
Thermal Conductivity (W/m°C)	***Carbonate Aggregates***	$k_c = 1.355$ $k_c = -0.001241T + 1.7162$	$for\ 20\,°C \le T \le 293\,°C$ $for\ T > 293\,°C$
	Siliceous Aggregates	$k_c = -0.000625T + 1.5$ $k_c = 1.0$	$for\ 20\,°C \le T \le 800\,°C$ $for\ T > 800\,°C$

Table B.1 (cont'd) – Constitutive Relationships for High Temperature Properties of Normal Strength Concrete

		ASCE Manual (1992)
Thermal Conductivity (cont.) (W/m°C)	***Pure Quartz Aggregates***	$k_c = -0.00085T + 1.9 \quad for\ 0\,°C \le T \le 800\,°C$ $k_c = 1.22 \quad for\ T > 800\,°C$
	Expanded Shale Aggregates	$k_c = -0.00039583T + 0.925 \quad for\ 20\,°C \le T \le 600\,°C$ $k_c = 0.6875 \quad for\ T > 600\,°C$

Table B.1 (cont'd) – Constitutive Relationships for High Temperature Properties of Normal Strength Concrete

		ASCE Manual (1992)
Thermal Strain	***All Types***	$\varepsilon_{th} = (0.008T + 6)x10^{-6}$ $for\ 20\,°C < T \leq 1200\,°C$
Stress-strain relationships (MPa)	***All Types***	Stress $\sigma_c = f'_{c,T}\left[1 - \left(\frac{\varepsilon - \varepsilon_{max,T}}{\varepsilon_{max,T}}\right)^2\right]$ $for\ \varepsilon \leq \varepsilon_{max,T}$ $\sigma_c = f'_{c,T}\left[1 - \left(\frac{\varepsilon_{max,T} - \varepsilon}{3\varepsilon_{max,T}}\right)^2\right]$ $for\ \varepsilon > \varepsilon_{max,T}$ *Compressive Strength* (MPa) $f'_{c,T} = f'_c$ $for\ 20\,°C < T \leq 450\,°C$ $f'_{c,T} = f'_c\left[2.011 - 2.353\left(\frac{T-20}{1000}\right)\right]$ $for\ 450\,°C < T \leq 874\,°C$ $f'_{c,T} = 0$ $for\ T < 874\,°C$ Strain $\varepsilon_{max,T} = 0.0025 + \left(6.0T + 0.04T^2\right)x10^{-6}$

Table B.2 – Values for Main Parameters of Stress-strain Relationships of Normal Strength Concrete at Elevated Temperatures (Eurocode 2, 2004)

Temperature, °C	Siliceous			Carbonate		
	$\frac{f'_{c,\theta}}{f'_{c,20}}$	$\varepsilon_{c1,\theta}$	$\varepsilon_{cu1,\theta}$	$\frac{f'_{c,\theta}}{f'_{c,20}}$	$\varepsilon_{c1,\theta}$	$\varepsilon_{cu1,\theta}$
20	1.00	0.0025	0.0200	1.00	0.0025	0.0200
100	1.00	0.0040	0.0225	1.00	0.0040	0.0225
200	0.95	0.0055	0.0250	0.97	0.0055	0.0250
300	0.85	0.0070	0.0275	0.91	0.0070	0.0275
400	0.75	0.0100	0.0300	0.85	0.0100	0.0300
500	0.60	0.0150	0.0325	0.74	0.0150	0.0325
600	0.45	0.0250	0.0350	0.60	0.0250	0.0350
700	0.30	0.0250	0.0375	0.43	0.0250	0.0375
800	0.15	0.0250	0.0400	0.27	0.0250	0.0400
900	0.08	0.0250	0.0425	0.15	0.0250	0.0425
1000	0.04	0.0250	0.0450	0.06	0.0250	0.0450
1100	0.01	0.0250	0.0475	0.02	0.0250	0.0475
1200	0.00	–	–	0.00	–	–

Table B.3 – Constitutive Relationships for High Temperature Properties of Prestressing Steel Reinforcement

<table>
<tr><th></th><th>Eurocode 2 (2004)</th></tr>
<tr><td>Thermal Strain</td><td>$$\varepsilon_{th} = -2.016x10^{-4} + 1.0x10^{-5}T + 0.4x10^{-8}T^2$$ $$for\ 20\,°C < T \leq 1200\,°C$$</td></tr>
<tr><td>Stress-strain relationships (MPa)</td><td>Stress
$\sigma_p = \varepsilon_p E_{p,\theta}$ $for\ \varepsilon_p \leq \varepsilon_{pp,\theta}$
$\sigma_p = f_{pp,\theta} - c + (b/a)\left[a^2 - (\varepsilon_{py,\theta} - \varepsilon_p)^2\right]^{0.5}$ $for\ \varepsilon_{pp,\theta} < \varepsilon_p \leq \varepsilon_{py,\theta}$
$\sigma_p = f_{py,\theta}$ $for\ \varepsilon_{py,\theta} < \varepsilon_p \leq \varepsilon_{pt,\theta}$
$\sigma_p = f_{py,\theta}\left[1 - \left(\varepsilon_p - \varepsilon_{pt,\theta}\right)/\left(\varepsilon_{pu,\theta} - \varepsilon_{pt,\theta}\right)\right]$ $for\ \varepsilon_{pt,\theta} < \varepsilon_p \leq \varepsilon_{pu,\theta}$
$\sigma_p = 0.0$ $for\ \varepsilon_p = \varepsilon_{pu,\theta}$

Parameters
$\varepsilon_{pp,\theta} = f_{pp,\theta}/E_{p,\theta}$ $\varepsilon_{py,\theta} = 0.02$

Functions
$$a^2 = \left(\varepsilon_{py,\theta} - \varepsilon_{pp,\theta}\right)\varepsilon_{py,\theta} - \varepsilon_{pp,\theta} + \frac{c}{E_{p,\theta}}$$ $$b^2 = c\left(\varepsilon_{py,\theta} - \varepsilon_{pp,\theta}\right)E_{p,\theta} + c^2$$ $$c = \frac{\left(f_{py,\theta} - f_{pp,\theta}\right)^2}{\left(\varepsilon_{py,\theta} - \varepsilon_{pp,\theta}\right)E_{p,\theta} - 2\left(f_{py,\theta} - f_{pp,\theta}\right)}$$
(Values for $f_{py,\theta}$, $f_{pp,\theta}$, $E_{p,\theta}$, $\varepsilon_{pt,\theta}$ and $\varepsilon_{pu,\theta}$ can be found from Table B.4)</td></tr>
</table>

Table B.4 – Values for Main Parameters of Stress-strain Relationships of Prestressing Steel Reinforcement at Elevated Temperatures (Eurocode 2, 2004)

Temperature (°C)	$\frac{f_{py,\theta}}{\beta f_{yk}}$	$\frac{f_{pp,\theta}}{\beta f_{yk}}$	$\frac{E_{p,\theta}}{E_p}$	$\varepsilon_{pt,\theta}$	$\varepsilon_{pu,\theta}$
20	1.00	1.00	1.00	0.050	0.100
100	0.99	0.68	0.98	0.050	0.100
200	0.87	0.51	0.95	0.050	0.100
300	0.72	0.32	0.88	0.055	0.105
400	0.46	0.13	0.81	0.060	0.110
500	0.22	0.07	0.54	0.065	0.115
600	0.10	0.05	0.41	0.070	0.120
700	0.08	0.03	0.10	0.075	0.125
800	0.05	0.02	0.07	0.080	0.130
900	0.03	0.01	0.03	0.085	0.135
1000	0.00	0.00	0.00	0.090	0.140
1100	0.00	0.00	0.00	0.095	0.145
1200	0.00	0.00	0.00	0.100	0.150

Table B5. –Values for Ultimate Strength of Prestressing Steel at Elevated Temperatures (PCI, 2004)

Temperature (°C)	Strength Loss
20	1.00
93	1.00
149	0.98
238	0.90
260	0.86
304	0.78
371	0.64
460	0.42
582	0.20
627	0.14
716	0.06
749	0.04

Table B.6 – Constitutive Relationships for High Temperature Properties of Reinforcing Steel

	Eurocode 2 (2004)
Thermal Strain	$\varepsilon_{th} = -2.416x10^{-4} + 1.2x10^{-5}T + 0.4x10^{-8}T^2 \quad for\ 20\,°C < T \leq 750\,°C$ $\varepsilon_{th} = 11x10^{-3} \quad for\ 750\,°C < T \leq 860\,°C$ $\varepsilon_{th} = -6.2x10^{-3} + 2x10^{-5}T \quad for\ 860\,°C < T \leq 1200\,°C$
Stress-strain relationships (MPa)	Stress $\sigma_s = \varepsilon_s E_{s,\theta} \quad for\ \varepsilon_s \leq \varepsilon_{sp,\theta}$ $\sigma_s = f_{sp,\theta} - c + (b/a)\left[a^2 - (\varepsilon_{sy,\theta} - \varepsilon_s)^2\right]^{0.5} \quad for\ \varepsilon_{sp,\theta} < \varepsilon_s \leq \varepsilon_{sy,\theta}$ $\sigma_s = f_{sy,\theta} \quad for\ \varepsilon_{sy,\theta} < \varepsilon_s \leq \varepsilon_{st,\theta}$ $\sigma_s = f_{sy,\theta}[1 - (\varepsilon_s - \varepsilon_{st,\theta})/(\varepsilon_{su,\theta} - \varepsilon_{st,\theta})] \quad for\ \varepsilon_{st,\theta} < \varepsilon_s \leq \varepsilon_{su,\theta}$ $\sigma_s = 0.0 \quad for\ \varepsilon_s = \varepsilon_{su,\theta}$ Parameters $\varepsilon_{sp,\theta} = f_{sp,\theta}/E_{s,\theta} \quad \varepsilon_{sy,\theta} = 0.02 \quad \varepsilon_{st,\theta} = 0.15 \quad \varepsilon_{su,\theta} = 0.20$ Functions $a^2 = \left(\varepsilon_{sy,\theta} - \varepsilon_{sp,\theta}\right)\varepsilon_{sy,\theta} - \varepsilon_{sp,\theta} + \frac{c}{E_{s,\theta}}$ $b^2 = c\left(\varepsilon_{sy,\theta} - \varepsilon_{sp,\theta}\right)E_{s,\theta} + c^2$ $c = \frac{\left(f_{sy,\theta} - f_{sp,\theta}\right)^2}{\left(\varepsilon_{sy,\theta} - \varepsilon_{sp,\theta}\right)E_{s,\theta} - 2\left(f_{sy,\theta} - f_{sp,\theta}\right)}$ (Values for $f_{sy,\theta}$, $f_{sp,\theta}$ and $E_{s,\theta}$ can be found from Table B.7)

Table B.6 (cont'd) – Constitutive Relationships for High Temperature Properties of Reinforcing Steel

	ASCE Manual (1992)
Thermal Strain	$\varepsilon_{th} = [0.004(T^2 - 400) + 12(T - 20)x10^{-6}$ $\quad for\ T < 1000\,°C$ $\varepsilon_{th} = [16(T - 20)]x10^{-6}$ $\quad for\ T \geq 1000\,°C$
Stress-strain relationships (MPa)	Stress $f_s = \frac{f(T, 0.001)}{0.001}\varepsilon_p$ $\quad for\ \varepsilon_s \leq \varepsilon_p$ $f_s = \frac{f(T, 0.001)}{0.001}\varepsilon_p + f[T, (\varepsilon_s - \varepsilon_p + 0.001)] - f(T, 0.001)$ $\quad for\ \varepsilon_s \geq \varepsilon_p$ Functions $f(T, 0.001) = (50 - 0.04T)x\left\{1 - \exp\left[(30 + 0.03T)\sqrt{(0.001)}\right]\right\}x6.9$ $\varepsilon_p = 4x10^{-6}f_{yo}$ $f[T, (\varepsilon_s - \varepsilon_p + 0.001)] = (50 - 0.04T)x$ $\left\{1 - \exp\left[(-30 + 0.03T)\sqrt{(\varepsilon_s - \varepsilon_p + 0.001)}\right]\right\}x6.9$

Table B.7 –Values for Main Parameters of Stress-strain Relationships of Reinforcing Steel at Elevated Temperatures (Eurocode 2, 2004)

Temperature (°C)	$\frac{f_{sy,\theta}}{f_{yk}}$	$\frac{f_{sp,\theta}}{f_{yk}}$	$\frac{E_{s,\theta}}{E_s}$
20	1.00	1.00	1.00
100	1.00	1.00	1.00
200	1.00	0.81	0.90
300	1.00	0.61	0.80
400	1.00	0.42	0.70
500	0.78	0.36	0.60
600	0.47	0.18	0.31
700	0.23	0.05	0.13
800	0.11	0.04	0.09
900	0.06	0.02	0.07
1000	0.04	0.01	0.04
1100	0.02	0.00	0.02
1200	0.00	0.00	0.00

Appendix C

C.1 Eurocode High Temperature Material Properties

Figure C.1 – Variation of Specific Heat of Concrete as a Function of Temperature for Different Moisture Contents by Weight

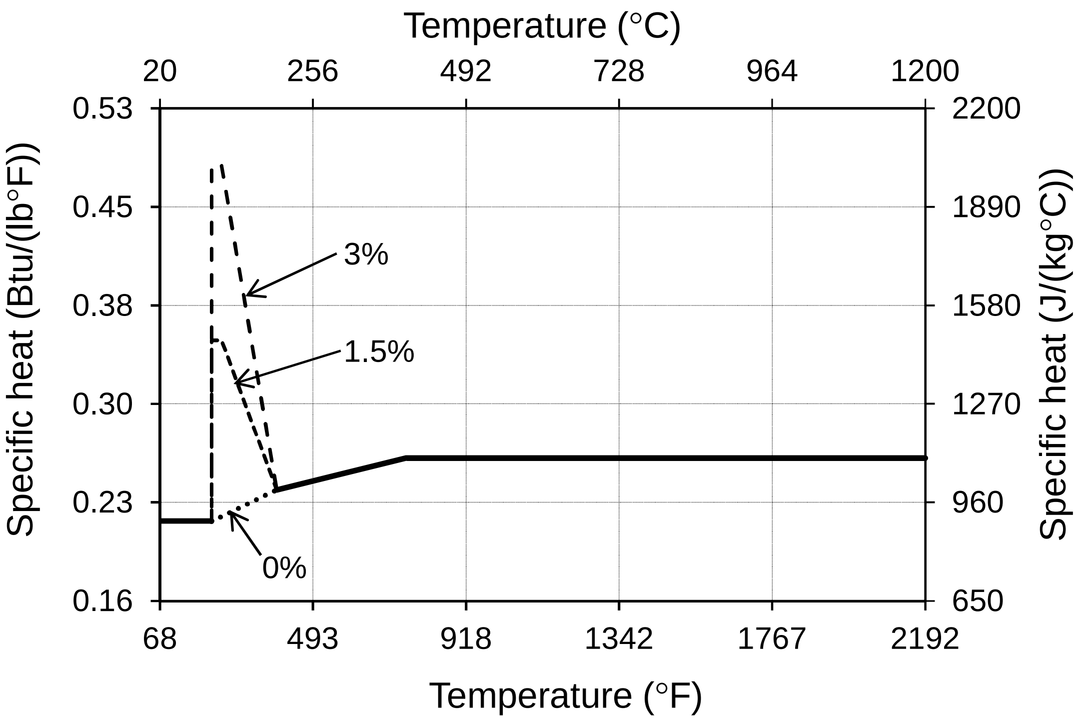

Figure C.2 – Variation of Volumetric Specific Heat of Concrete as a Function of Temperature for Different Moisture Contents by Weight

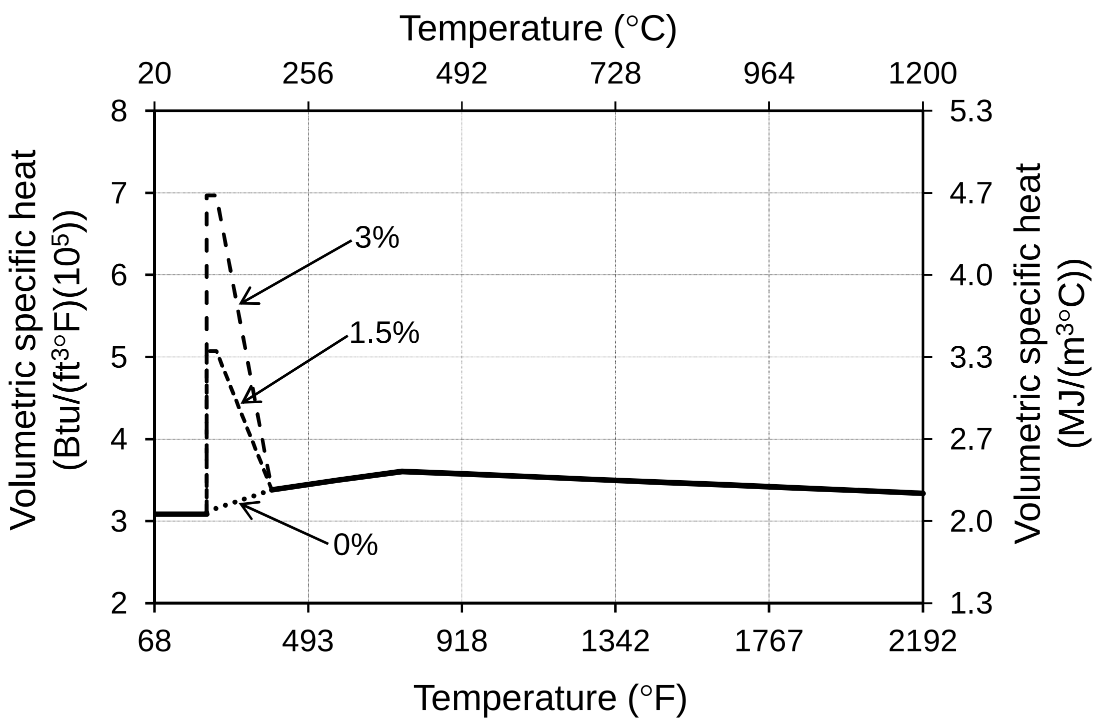

Figure C.3 – Variation of Thermal Conductivity of Concrete as a Function of Temperature

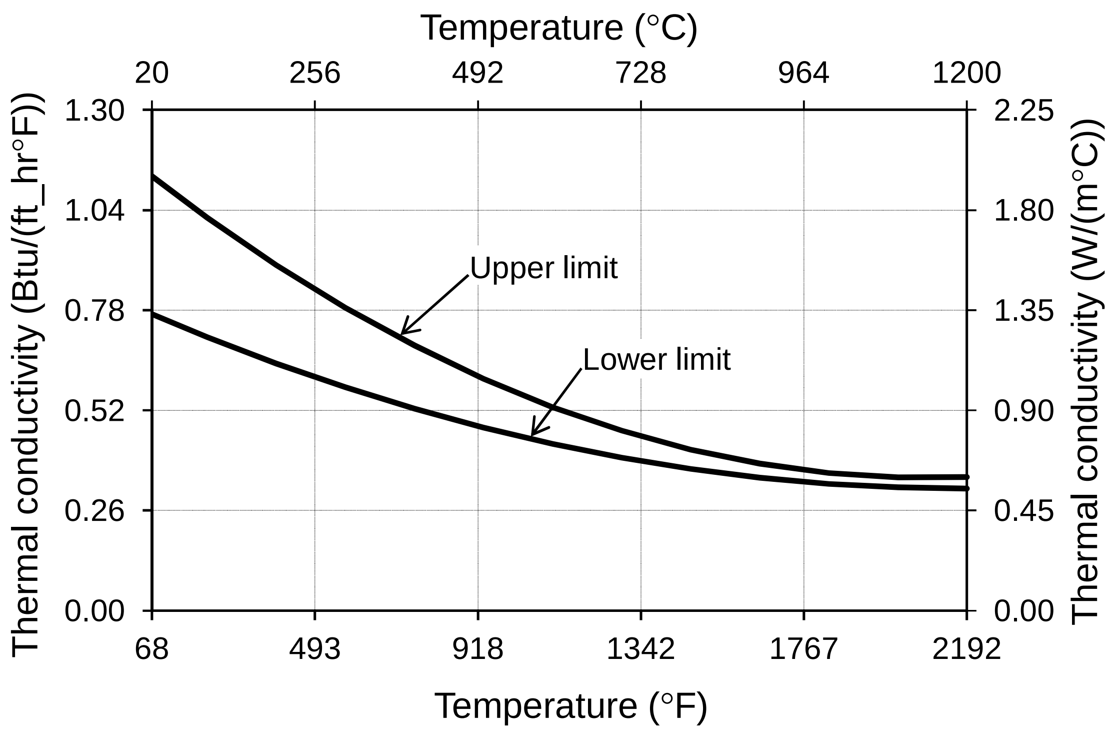

Figure C.4 – Variation of Concrete Density as a Function of Temperature

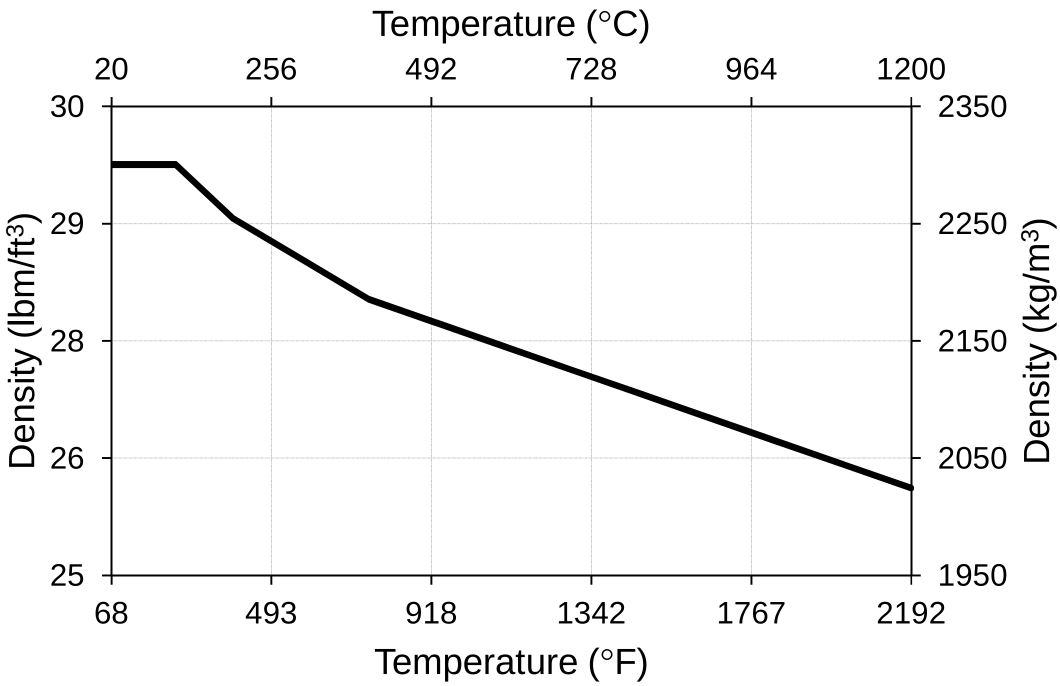

Figure C.5 – Variation of Concrete Thermal Elongation as a Function of Temperature for Siliceous and Carbonate Aggregates

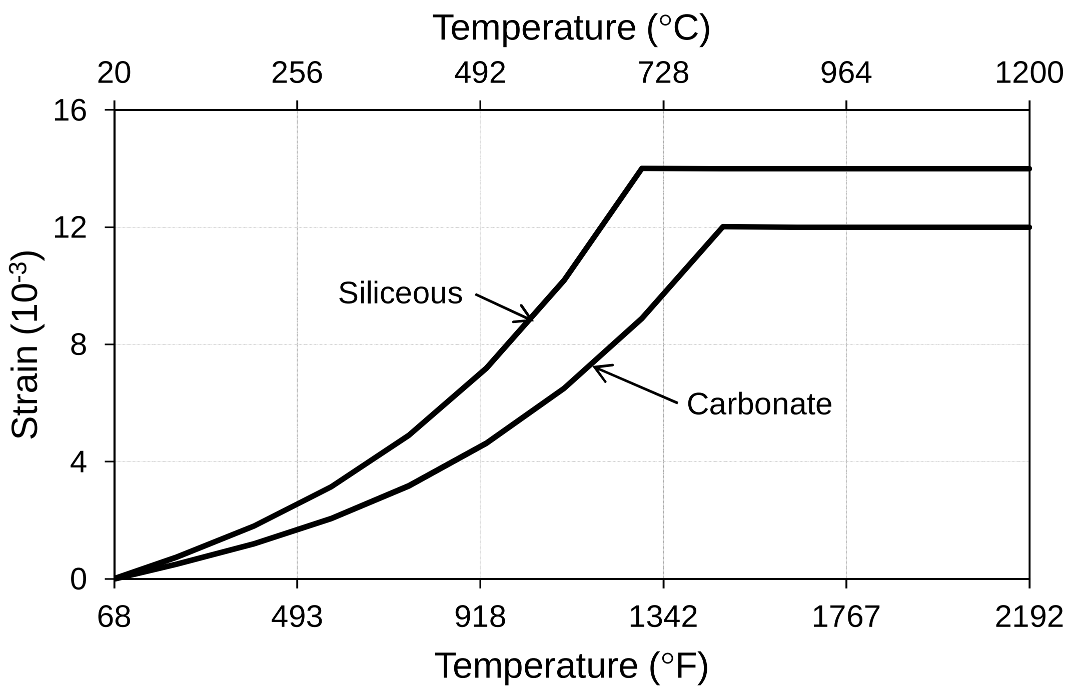

Figure C.6 – Variation of Concrete Tensile Strength as a Function of Temperature

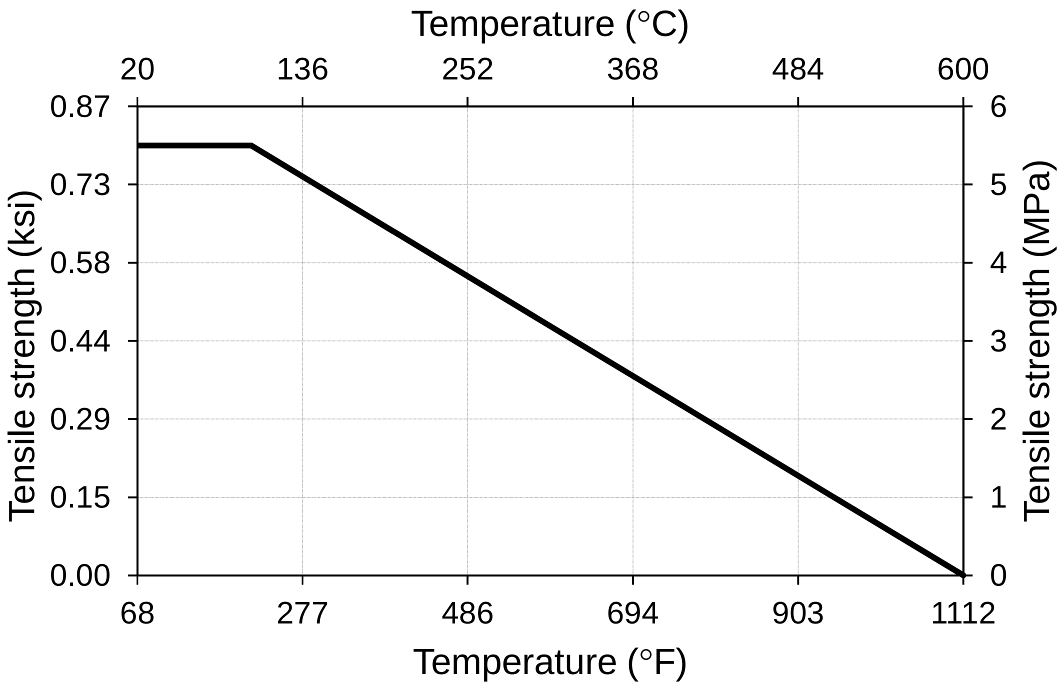

Figure C.7 – Variation of Stress-strain Curve of Concrete as a Function of Temperature

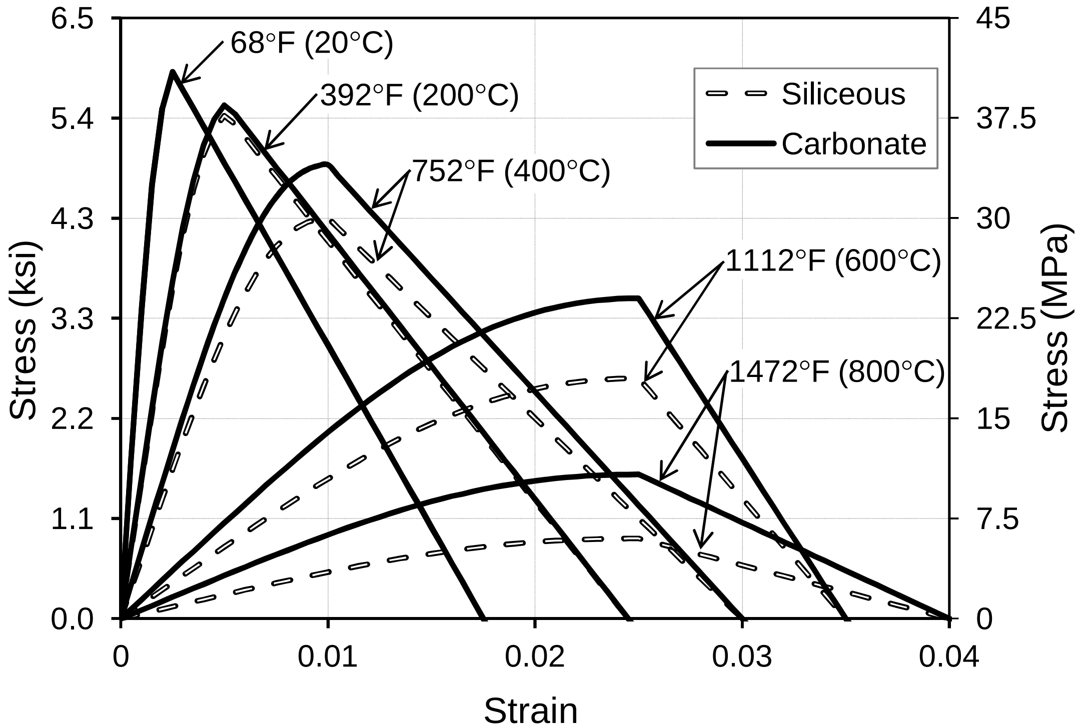

Figure C.8 – Variation of Prestressing Steel Thermal Elongation as a Function of Temperature

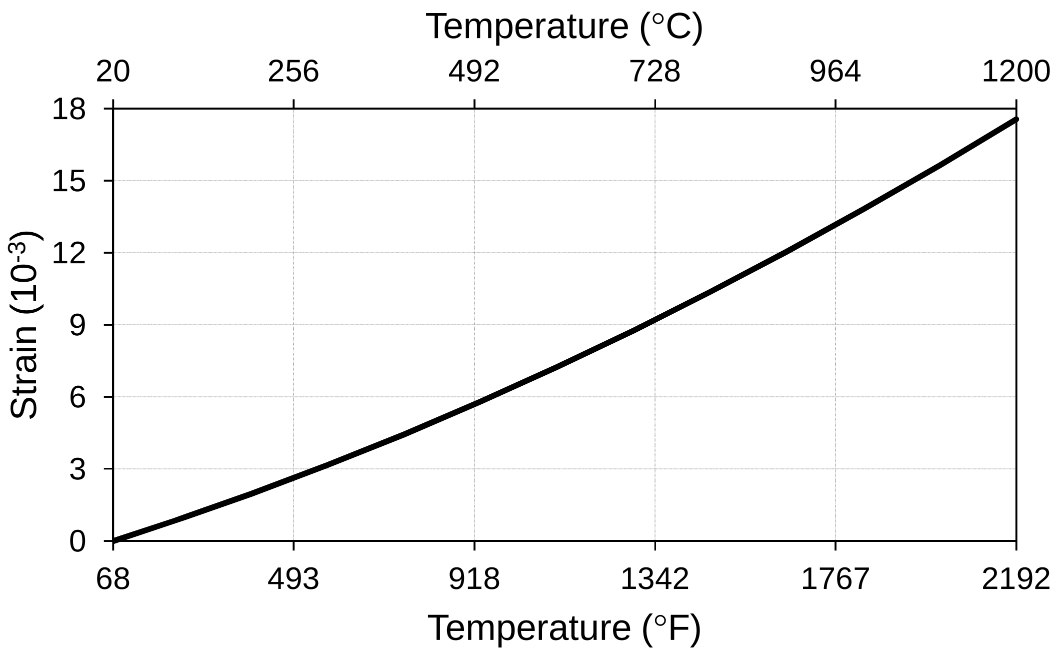

Figure C.9 – Variation of Stress-strain Curve of Prestressing Steel as a Function of Temperature

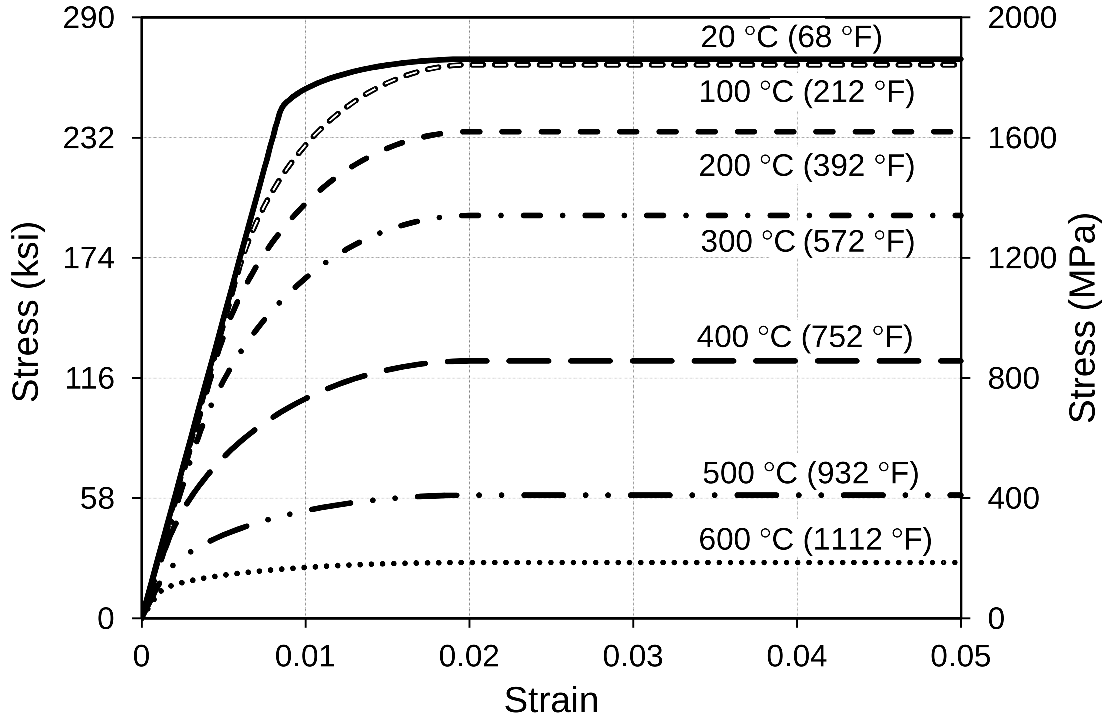

Appendix D

D.1 Moment Capacity and Load Ratio Calculations

The following calculations are provided to illustrate how the ambient moment capacity and load ratio were determined for the 10DT24+2 and 12DT32+2 PPC beams. Note, moment capacity calculations are based on the provisions specified in PCI Design Handbook (2004). Refer to Figures 4.1 and 4.2 for cross-sectional dimensions and details of 10DT24+2 and 12DT32+2 PPC beams, respectively. Refer to Table 4.1 for material and section properties for each PPC beam.

Moment Capacity:

<u>10DT24+2</u>

Concrete compressive strength

$$f'_c = 40MPa$$

Ultimate tensile stress of prestressing steel

$$f_{pu} = 1860MPa$$

Area of prestressing steel

$$A_{ps} = 1{,}013mm^2$$

Span length

$$l = 12.192\,m$$

Effective stress in prestressing steel after losses, assume

$$f_{se} = 1172MPa$$

Coefficient based on concrete compressive stress per Figure 4.12.3

$$C = 1.13 - \frac{1.13 - 1.06}{41.4MPa - 34.5MPa} * (41.4MPa - 40MPa) = 1.12$$

Beam width

$$b = 3{,}048\,mm$$

Distance from extreme compression fiber to centroid of stressed reinforcement

$$d_p = 533mm$$

Mild reinforcement (positive and negative) ratio

$$\omega = \omega' = 0$$

Relationship used to determine the stress in prestressed reinforcement at nominal strength of member

$$c\omega_{pu} = C\frac{A_{ps} f_{pu}}{bd_p f'_c} + \frac{d}{d_p}(\omega - \omega') = \frac{1.12 * 1{,}013mm^2 * 1{,}860MPa}{3{,}048mm * 533mm * 40MPa} = 0.032$$

Stress in prestressing steel at nominal strength per Figure 4.12.3

$$f_{ps} = 1{,}848MPa$$

Depth of equivalent rectangular compression stress block

$$a = \frac{A_{ps} f_{ps}}{0.85 f'cb} = \frac{1{,}013mm^2 * 1{,}848MPa}{0.85 * 40MPa * 3{,}048mm} = 18mm$$

Compressive stress block factor per section 4.2.1.1

$$\beta_1 = 0.76$$

$$c/d_t = a/\beta_1 d_p = \frac{18mm}{0.76 * 533mm} = 0.04$$

Strength reduction factor per Figure 4.2.1.3

$$\theta = 0.65 + \frac{0.9 - 0.65}{0.6 - 0.375} * 0.04 = 0.69$$

Nominal moment capacity

$$\theta M_n = \theta A_{ps} f_{ps}(d_p - \frac{a}{2}) = 0.69 * 1{,}013mm^2 * 1{,}848MPa * (533mm - \frac{18mm}{2}) = 679kNm$$

Selfweight of PPC Beam

$$D = 3.45\,kPa * 3.048\,m = 10.5kN / m$$

Live load for a parking garage/building per ASCE 7-05 (2005) design loads for a parking garage/building

$$L = 2.39\,kPa * 3.048\,m = 7.3kN / m$$

Load combination

$$w = 1.2D + 1.6L = 1.2 * 10.5kN / m + 1.6 * 7.3kN / m = 24.3kN / m$$

Factored moment demands

$$M = \frac{wl^2}{8} = \frac{24.3kN / m * (12.192\,m)^2}{8} = 452\,kNm$$

Check nominal moment capacity against factored demands

$$\theta M_n > M \therefore OK$$

<u>12DT32+2</u>

Concrete compressive strength

$$f'_c = 40MPa$$

Ultimate tensile stress of prestressing steel

$$f_{pu} = 1860MPa$$

Area of prestressing steel

$$A_{ps} = 1{,}523 mm^2$$

Span length

$$l = 15.24 m$$

Effective stress in prestressing steel after losses, assume

$$f_{se} = 1172 MPa$$

Coefficient based on concrete compressive stress per Figure 4.12.3

$$C = 1.13 - \frac{1.13 - 1.06}{41.4MPa - 34.5MPa} * (41.4MPa - 40MPa) = 1.12$$

Beam width

$$b = 3{,}658 mm$$

Distance from extreme compression fiber to centroid of stressed reinforcement

$$d_p = 686 mm$$

Mild reinforcement (positive and negative) ratio

$$\omega = \omega' = 0$$

Relationship used to determine the stress in prestressed reinforcement at nominal strength of member

$$c\omega_{pu} = C\frac{A_{ps} f_{pu}}{bd_p f'_c} + \frac{d}{d_p}(\omega - \omega') = \frac{1.12 * 1{,}523mm^2 * 1{,}860MPa}{3{,}658mm * 686mm * 40MPa} = 0.032$$

Stress in prestressing steel at nominal strength per Figure 4.12.3

$$f_{ps} = 1{,}848 MPa$$

Depth of equivalent rectangular compression stress block

$$a = \frac{A_{ps} f_{ps}}{0.85 f'cb} = \frac{1{,}523mm^2 * 1{,}848MPa}{0.85 * 40MPa * 3{,}658mm} = 23mm$$

Compressive stress block factor per section 4.2.1.1

$$\beta_1 = 0.76$$

$$c/d_t = a/\beta_1 d_p = \frac{23mm}{0.76 * 686mm} = 0.04$$

Strength reduction factor per Figure 4.2.1.3

$$\theta = 0.65 + \frac{0.9 - 0.65}{0.6 - 0.375} * 0.04 = 0.69$$

Nominal moment capacity

$$\theta M_n = \theta A_{ps} f_{ps}(d_p - \frac{a}{2}) = 0.69 * 1{,}523mm^2 * 1{,}848MPa * (686mm - \frac{23mm}{2}) = 1{,}310kNm$$

Selfweight of PPC Beam

$$D = 4.08\,kPa * 3.6576\,m = 14.9kN/m$$

Live load for a parking garage/building per ASCE 7-05 (2005) design loads for a parking garage/building

$$L = 2.39\,kPa * 3.6576\,m = 8.7kN/m$$

Load combination

$$w = 1.2D + 1.6L = 1.2 * 14.9kN/m + 1.6 * 8.7kN/m = 31.8kN/m$$

Factored moment demands

$$M = \frac{wl^2}{8} = \frac{31.8kN/m * (15.24m)^2}{8} = 923kNm$$

Check nominal moment capacity against factored demands

$$\theta M_n > M \therefore OK$$

Load Ratio:

Calculations for a load ratio of 30, 50, and 70% are provided below for both PPC double T-beams. In addition, each section starts with a load ratio calculation for the standard loading used in the parametric study. Note, results from the ambient moment calculations from above are utilized below.

<u>10DT24+2</u>

Strength reduction factor under ambient conditions

$$\theta_C = 0.69$$

Strength reduction factor under ambient conditions

$$\theta_f = 1.0$$

Moment capacity under ambient conditions

$$R_C = 984 kNm$$

Service Conditions:

Selfweight of PPC Beam

$$D = 3.45 kPa * 3.048 m = 10.5 kN / m$$

Live load for a parking garage/building per ASCE 7-05 (2005) design loads for a parking garage/building

$$L = 2.39 kPa * 3.048 m = 7.3 kN / m$$

Load combination for fire conditions

$$w_f = 1.2D + 0.5L = 1.2*10.5kN/m + 0.5*7.3kN/m = 16.3kN/m$$

Factored moment demands

$$R_{fire} = \frac{wl^2}{8} = \frac{16.3kN/m*(12.192m)^2}{8} = 303kNm$$

Load ratio under service conditions

$$r_L = \left(\frac{\Phi_f R_{fire}}{\Phi_c R_{cold}}\right) = \frac{1.0*303kNm}{0.69*984kNm} \cong 0.45 = 65\%$$

30% Load Ratio:

Load ratio

$$r_L = \left(\frac{\Phi_f R_{fire}}{\Phi_c R_{cold}}\right) = 30\% = 0.30$$

Moment demands based on a load ratio of 30%

$$R_f = \frac{\Phi_c R_{cold} * r_L}{\Phi_f} = \frac{0.69*984kNm*0.3}{1.0} = 203.7kNm$$

Distributed load based on a 30% load ratio for a simply supported beam

$$w_f = \frac{8*R_f}{l^2} = \frac{8*203.7kNm}{(12.192m)^2} = 10{,}963N/m$$

50% Load Ratio:

Load ratio

$$r_L = \left(\frac{\Phi_f R_{fire}}{\Phi_c R_{cold}}\right) = 50\% = 0.50$$

Moment demands based on a load ratio of 50%

$$R_f = \frac{\Phi_c R_{cold} * r_L}{\Phi_f} = \frac{0.69 * 984 kNm * 0.5}{1.0} = 339.5 kNm$$

Distributed load based on a 50% load ratio for a simply supported beam

$$w_f = \frac{8 * R_f}{l^2} = \frac{8 * 339.5 kNm}{(12.192m)^2} = 18{,}272 N/m$$

70% Load Ratio:

Load ratio

$$r_L = \left(\frac{\Phi_f R_{fire}}{\Phi_c R_{cold}} \right) = 70\% = 0.70$$

Moment demands based on a load ratio of 70%

$$R_f = \frac{\Phi_c R_{cold} * r_L}{\Phi_f} = \frac{0.69 * 984 kNm * 0.7}{1.0} = 475.3 kNm$$

Distributed load based on a 70% load ratio for a simply supported beam

$$w_f = \frac{8 * R_f}{l^2} = \frac{8 * 475.3 kNm}{(12.192m)^2} = 25{,}580 N/m$$

<u>12DT32+2</u>

Strength reduction factor under ambient conditions

$$\theta_c = 0.69$$

Strength reduction factor under ambient conditions

$$\theta_f = 1.0$$

Moment capacity under ambient conditions

$$R_c = 1{,}899 kNm$$

Service Conditions:

Selfweight of PPC Beam

$$D = 4.08\,kPa * 3.6576\,m = 14.9\,kN / m$$

Live load for a parking garage/building per ASCE 7-05 (2005) design loads for a parking garage/building

$$L = 2.39\,kPa * 3.6576\,m = 8.7\,kN / m$$

Load combination for fire conditions

$$w_f = 1.2D + 0.5L = 1.2 * 14.9kN / m + 0.5 * 8.7kN / m = 22.2kN / m$$

Factored moment demands

$$R_{fire} = \frac{wl^2}{8} = \frac{22.2kN / m * (15.24m)^2}{8} = 645\,kNm$$

Load ratio under service conditions

$$r_L = \left(\frac{\Phi_f R_{fire}}{\Phi_c R_{cold}}\right) = \frac{1.0 * 645kNm}{0.69 * 1{,}899kNm} \cong 0.49 = 49\%$$

30% Load Ratio:

Load ratio

$$r_L = \left(\frac{\Phi_f R_{fire}}{\Phi_c R_{cold}}\right) = 30\% = 0.30$$

Moment demands based on a load ratio of 30%

$$R_f = \frac{\Phi_c R_{cold} * r_L}{\Phi_f} = \frac{0.69 * 1{,}899kNm * 0.3}{1.0} = 393.1kNm$$

Distributed load based on a 30% load ratio for a simply supported beam

$$w_f = \frac{8 * R_f}{l^2} = \frac{8 * 393.1kNm}{(15.24m)^2} = 13{,}540N / m$$

50% Load Ratio:

Load ratio

$$r_L = \left(\frac{\Phi_f R_{fire}}{\Phi_c R_{cold}}\right) = 50\% = 0.50$$

Moment demands based on a load ratio of 50%

$$R_f = \frac{\Phi_c R_{cold} * r_L}{\Phi_f} = \frac{0.69 * 1{,}899 kNm * 0.5}{1.0} = 655.2 kNm$$

Distributed load based on a 50% load ratio for a simply supported beam

$$w_f = \frac{8 * R_f}{l^2} = \frac{8 * 655.2 kNm}{(15.24 m)^2} = 22{,}568 N/m$$

70% Load Ratio:

Load ratio

$$r_L = \left(\frac{\Phi_f R_{fire}}{\Phi_c R_{cold}}\right) = 70\% = 0.70$$

Moment demands based on a load ratio of 70%

$$R_f = \frac{\Phi_c R_{cold} * r_L}{\Phi_f} = \frac{0.69 * 1{,}899 kNm * 0.7}{1.0} = 917.2 kNm$$

Distributed load based on a 70% load ratio for a simply supported beam

$$w_f = \frac{8 * R_f}{l^2} = \frac{8 * 917.2 kNm}{(15.24 m)^2} = 31{,}593 N/m$$

Appendix E

E.1 SAFIR Input Files

E.1.1 Thermal Input

Sample thermal input file for SAFIR
ASTME119 12DT24+2
Thermal input file for SAFIR2004
PCI 12DT32+2
2 in. normal weight topping
ASTME119 (3 sided exposure)

```
NPTTOT         1
NNODE          1209
NDIM           2
NDIMMATER      1
NDDLMAX        1
EVERY_NODE     1
END_NDDL
TEMPERAT
TETA           0.9
TINITIAL       20.0
MAKE.TEM
LARGEUR11      43145
LARGEUR12      1
NORENUM
ASTM.tem
NMAT           3
ELEMENTS
SOLID          1078
NG             2
NVOID          0
END_ELEM
NODES
NODE   1 0.0000   0.0000
NODE   2 0.0000   0.0056
NODE   3 0.0000   0.0184
NODE   4 0.0000   0.0311
NODE   5 0.0000   0.0438
NODE   6 0.0000   0.0565
NODE   7 0.0000   0.0603
NODE   8 0.0113   0.0000
NODE   9 0.0113   0.0056
```

```
NODE 10  0.0000   0.0184
…………
NODE   1199   0.8636   0.7657
NODE   1200   0.8636   0.7806
NODE   1201   0.8636   0.7954
NODE   1202   0.8636   0.8103
NODE   1203   0.8636   0.8252
NODE   1204   0.8636   0.8400
NODE   1205   0.8636   0.8549
NODE   1206   0.8636   0.8698
NODE   1207   0.8636   0.8847
NODE   1208   0.8636   0.8995
NODE   1209   0.8636   0.9144
NODELINE     0.6480    0.
YC_ZC          0.6480    0.
FIXATIONS
END_FIX
NODOFSOLID
ELEM       1      1      2      9      8      1    0.
GELEM      6      6      7      14     13     1    0.              1
ELEM       7      7      5      14     0      1    0.
ELEM       8      8      9      17     16     1    0.
GELEM      14     14     15     23     22     1    0.              1
REPEAT     7      8             2
ELEM       29     32     33     41     40     2    1172000000     0.
ELEM       30     33     34     42     41     1    0.
GELEM      35     38     38     47     46     1    0.              1
ELEM       36     40     41     49     48     1    0.
GELEM      42     46     47     55     54     1    0.              1
REPEAT     7      8                                                3
…………
ELEM       558    615    631    630    0      1    0.
ELEM       559    616    617    683    682    1    0.
GELEM      623    680    681    747    746    1    0.              1
REPEAT     65     66                                               3
ELEM       819    880    881    947    946    3    0.
GELEM      883    944    945    1011   1010   3    0.              1
REPEAT     65     66                                               3
FRONTIER
F       1  ASTME119            NO       NO       NO
GF      7  ASTME119            NO       NO       NO      1
F      14             NO  ASTME119      NO       NO
GF  119               NO  ASTME119      NO       NO      7
F    127  ASTME119             NO       NO       NO
…………
F    529  ASTME119             NO       NO       NO
```

```
F    543  ASTME119              NO       NO       NO
F    558  ASTME119              NO       NO       NO
F    574  ASTME119              NO       NO       NO
GF  623  ASTME119              NO       NO       NO       1
END_FRONT
SYMMETRY
REALSYM    1  1144
END_SYM
PRECISION     1.E-3
MATERIALS
CALCONCEC2
       46.  25.  9.    .56
PSTEELA16
       25.  9.    .50
CALCONCEC2
       46.  25.  9.    .56
TIME
       60.      14400.
END_TIME
IMPRESSION
TIMEPRINT
        60.     14400.
END_TIMEPR
```

E.1.2 Structural Input

Sample structural input file for SAFIR

```
Structural input file for SAFIR2004
PCI 12DT32+2
2 in. normal weight topping
ASTM E-119 Temperature Exposure
Simply supported
Uniformly Distributed Load

NPTTOT          86240
NNODE           41
NDIM            2
NDIMMATER       1
NDDLMAX         3
EVERY_NODE      3
END_NDDL
STATIC   PURE_NR
NLOAD           1
OBLIQUE         0
COMEBACK        1
LARGEUR11       544
LARGEUR12       6
NORENUM
NMAT            3
ELEMENTS
BEAM            20   1
NG              2
NFIBER          2156
END_ELEM
NODES
NODE     1      0.0000     0.0000
GNODE    41     15.2400    0.0000     1
FIXATIONS
BLOCK    1      F0   F0   NO
BLOCK    41     NO   F0   NO
END_FIX
NODOFBEAM
ASTM_55.TEM
TRANSLATE   1   1
TRANSLATE   2   2
TRANSLATE   3   3
END_TRANS
ELEM     1    1    2    3    1
ELEM     2    3    4    5    1
ELEM     3    5    6    7    1
```

```
ELEM      4    7    8    9    1
ELEM      5    9    10   11   1
ELEM      6    11   12   13   1
ELEM      7    13   14   15   1
ELEM      8    15   16   17   1
ELEM      9    17   18   19   1
ELEM      10   19   20   21   1
ELEM      11   21   22   23   1
ELEM      12   23   24   25   1
ELEM      13   25   26   27   1
ELEM      14   27   28   29   1
ELEM      15   29   30   31   1
ELEM      16   31   32   33   1
ELEM      17   33   34   35   1
ELEM      18   35   36   37   1
ELEM      19   37   38   39   1
ELEM      20   39   40   41   1
PRECISION    1.E-4
LOADS
FUNCTION FLOAD
DISTRBEAM    1    0    -11120    0
DISTRBEAM    2    0    -11120    0
DISTRBEAM    3    0    -11120    0
DISTRBEAM    4    0    -11120    0
DISTRBEAM    5    0    -11120    0
DISTRBEAM    6    0    -11120    0
DISTRBEAM    7    0    -11120    0
DISTRBEAM    8    0    -11120    0
DISTRBEAM    9    0    -11120    0
DISTRBEAM    10   0    -11120    0
DISTRBEAM    11   0    -11120    0
DISTRBEAM    12   0    -11120    0
DISTRBEAM    13   0    -11120    0
DISTRBEAM    14   0    -11120    0
DISTRBEAM    15   0    -11120    0
DISTRBEAM    16   0    -11120    0
DISTRBEAM    17   0    -11120    0
DISTRBEAM    18   0    -11120    0
DISTRBEAM    19   0    -11120    0
DISTRBEAM    20   0    -11120    0
END_LOAD
MATERIALS
CALCONCEC2
    0.25   55E6    46E5    0
PSTEELA16
    1.9995E11     0.3  1.772E9
```

```
CALCONCEC2
      0.25    55E6      46E5      0
TIME
       60.     14400.
END_TIME
LARGEDISPL
EPSTH
IMPRESSION
TIMEPRINT
       60.     14400.
END_TIMEPR
PRINTMN
PRINTREACT
```

REFERENCES

References

1. ABAQUS (2011), *ABAQUS 6.11 Analysis User's Manual*, DCS Simulia.

2. Abrams M.S. and Cruz C.R. (1961), "The Behavior at High Temperature of Steel Strand for Prestressed Concrete", *Journal of the Portland Cement Association Research and Development Laboratories*, 3(3), pp. 8 – 19.

3. Abrams M.S. and Gustaferro A.H. (1972), "Fire Endurance of Prestressed Concrete Unit Coated with Spray-Applied Insulation", *Prestressed Concrete Institute*,17(1), pp. 82 – 103.

4. Abrams M.S., Gustaferro A.H., and Salse E.A.B. (1971), "Fire Tests of Concrete Joist Floors and Roofs", *R&D Bulletin RD006B*, Portland Cement Association, Skokie, IL, USA.

5. ACI Committee 216 (2007). "Standard Method for Determining Fire Resistance of Concrete and Masonry Construction Assemblies", American Concrete Institute, Detroit, MI, USA.

6. ACI Committee 318 (2008). "Building Code Requirements for Reinforced Concrete", *ACI 318-08 and Commentary,* American Concrete Institute, Detroit, Michigan, USA.

7. Anderberg, Y. and Thelandersson, S. (1976). "Stress and Deformation Characteristics of Concrete at High Temperatures – Experimental Investigation and Material Behavior Model", *Bulletin 54,* Division of Structural Mechanics and Concrete Construction, Lund Institute of Technology, Lund, Sweden.

8. Anderberg Y. (2008), "The Impact of Various Material Models on Structural Fire Behavior Prediction", *Proceedings of Fifth International Conference on Structures in Fire*, Singapore, pp. 12.

9. Anderberg Y. (1986), "Modeling Steel Behaviour", *Report LUTVDG,* Division of Building Fire Safety and Technology, Lund Institute of Technology, Lund, Sweden.

10. ANSYS (2011), *Structural Analysis Guide,* ANSYS, Inc.

11. *Proceedings of International Conference on High Performance Materials in Bridges,* Kona, HI, USA, pp. 21 – 33.

12. Anderson N.E. and Laurisden D.H. (1999), "TT-roof slabs", *Technical Report X52650, Part 1*, Danish Institute of Fire Technology, København, Denmark.

13. Arioz O. (2007), "Effects of Elevated Temperatures on Properties of Concrete", *Fire Safety Journal*, 42(8), pp. 516 – 522.

14. ASCE 7-05 (2005). "Minimum Design Loads for Buildings and Other Structures", American Society of Civil Engineers, Reston, VA, USA.

15. ASCE Manual of Practice No. 78 (1992). "Structural Fire Protection", ASCE Committee on Fire Protection, Structural Division, American Society of Civil Engineers, NY, USA.

16. ASCE/SEI 7-05 (2005). "Minimum Design Loads for buildings and Other Structures", American Society of Civil Engineers, Reston, VA, USA.

17. ASCE/SEI/SFPE 29-05 (2007), "Standard Calculation Methods for Structural Fire Protection", American Society of Civil Engineers, Reston, VA, USA.

18. ASTM E119 (2008), "Standard Methods of Fire Test of Building Construction and Materials", American Society for Testing and Materials, West Conshohocken, PA, USA .

19. ASTM E1529 (1993), "Standard Test Methods for Determining Effects of Large Hydrocarbon Pool Fires on Structural Members and Assemblies", American Society for Testing and Materials, West Conshohocken, PA, USA.

20. Atienza J.M. and Elices M. (2009), "Behavior of Prestressing Steels After a Simulated Fire: Fire-induced Damages", *Construction and Building Materials*, 23(8), pp. 2932 – 2940.

21. Bastami, M. and Aslani, F. (2010), "Preloaded High-Temperature Constitutive Models and Relationships for Concrete", *Scientia Iranica*, 17(1), pp. 11-25.

22. Boon J. and Monnier T. (1976), "Calculation of the Fire Resistance of Prestressed Concrete Beams", *Heron*, 21(1), pp. 37 – 44.

23. Canadian Standards Association (2005), "Code for the Design of Concrete Structures for Buildings", *CAN3-D-2.10*, Rexdale, Canada.

24. Cook R.A., Fagundo F.E., and Richarson D. (1997). "Effect of External Elevated Temperatures on the Bond Performance of Epoxy-Coated Prestressing Strands", *Prestressed Concrete Institute*, 42(1), pp. 68-75.

25. Canadian Precast and Prestressed Concrete Institute (2007), "Design Manual: Precast and Prestressed Concrete", 4th ed., Ottawa, Canada.

26. Dwaikat, M.B. and Kodur, V.K.R. (2007), "A Numerical Approach for Modeling the Fire Induced Restraint Effects in Reinforced Concrete Beams", *Fire Safety Journal*, 43(4), pp. 291-307.

27. Dilek, U., Caldwell T., Sharpe F.E., and Leming M. (2003), "Fire Damage Assessment, Prestressed Concrete Double-Tees at Parking Deck", *Proceedings of the Third Concgress*, San Diego, CA, USA, pp. 247 – 258.

28. Dorn, J.E. (1955), "Some Fundamental Experiments on High-Temperature Creep", *Journal of the Mechanics and Physics of Solids*, 3, pp. 85 – 116.

29. Dwaikat M.B. and Kodur V.K.R. (2008) "Effect of Fire Induced Spalling on the Response of Reinforced Concrete Beams", *International Journal of Concrete Structures and Materials*, 2(2), pp. 71-81.

30. Elghazouli, A.Y., Cashell, K.A., and Izzuddin, B.A. (2009), "Experimental Evaluation of the Mechanical Properties of Steel Reinforcement at Elevated Temperature", *Fire Safety Journal,* 44, pp. 909-919.

31. Eurocode 1 (2002), "EN 1991-1-2: Actions on Structures. Part 1-2: General Actions – Actions on Structures Exposed to Fire", European Committee for Standardization, Brussels, Belgium.

32. Eurocode 2 (2004), "EN 1992-1-1: Design of Concrete Structures. Part 1-1: General Rules and Rules for Building", European Committee for Standardization, Brussels, Belgium.

33. Eurocode 2 (2004), "EN 1992-1-2: Design of Concrete Structures. Part 1-2: General Rules – Structural Fire Design", European Committee for Standardization, Brussels, Belgium.

34. Falkner H. and Gerritzen D. (2005), The Continued Use of Pre-tensioned Concrete Parts After Exposure to Fire", *Betonwerk und Fertigteik/Concrete Precasting Plant and Technology*, 71(2), pp. 178 – 179.

35. Feasey R. and Buchanan A.H. (2002), "Post Flash-Over Fires for Structural Design", *Fire Safety Journal*, 37(1), pp. 83 – 105.

36. Fellinger J.H.H., Starck, J.W.B., and Warave J.C. (2001), "Bond Model for Prestressed Strands in Fire Exposed Concrete", *Proceedings of International Conference on High Performance Materials in Bridges*, Kona, HI, USA, pp. 21 – 33.

37. Fletcher, I.A., Welch, S., Torero, J.L., Carvel, R.O., and Usmani, A. (2007). "The Behaviour of Concrete Structures under Fire", *Thermal Science*, 11(2), pp. 37-52.

38. Franssen J.M. and Bruls A. (1997), "Design and Tests of Prestressed Concrete Beams", *Proceedings of the 5th International Symposium on Fire Safety Science*, Melbourn, Australia, pp. 1081 – 1092.

39. Franssen J.M., Kodur V.R., and Mason, J. (2004), *User Manual for SAFIR*, University of Liege, Belgium.

40. Gales J., Bisby, L.A., MacDougall C., and MacLean K. (2009) "Transient High-Temperature Stress Relaxation of Prestressing Tendons in Unbonded Construction", *Fire Safety Journal*, 44(4), pp. 570-579.

41. Gernay, T. and Franssen, J.M. (2011), "A Comparison Between Explicit and Implicit Modeling of Transient Creep Strain in Concrete Uniaxial Constitutive Relationships", *Proceedings of the Fire and Materials 2011 Conference"*, San Francisco, USA.

42. Gustaferro A.H. and Carlson C.C. (1962), "An Interpretation of Results of Fire Tests of Prestressed Concrete Building Components", *Prestressed Concrete Institute*, 7(1), pp. 14 – 43.

43. Harmathy T.Z. (1988), "Properties of Building Materials", *The SFPE Handbook of Fire Protection Engineering*, (1)26, p. 378 – 391.

44. Harmathy T.Z. (1967), "A Comprehensive Creep Model", *Journal of Basic Engineering Transaction of the ASME*, (89), pp. 496-502.

45. Harmathy T.Z. and Stanzak W.W. (1970), "Elevate-Temperature Tensile and Creep Properties of Some Structural and Prestressing Steels", *Special Technical Publication 464*, American Society for Testing and Materials, West Conshohocken, PA, USA.

46. Hill, A.W. and Ashton A.L. (1957), "The Fire Resistance of Prestressed Concrete", *Civil Engineering an Public Works Review*, 52(617), pp. 1249-1253.

47. Holmes M., Anchor R.D., Cook G.M.E., and Crook R.N. (1982), "Effects of Elevated Temperatures of the Strength Properties of Reinforcing and Prestressing Steel", *Structural Engineer*, 60B(1), pp. 7 – 13.

48. Husem M. (2006), "The Effects of High Temperature on Compressive and Flexural Strengths of Ordinary and High-Performance Concrete", *Fire Safety Journal*, 41(2), pp. 155-163.

49. International Code Council (2006), "International Building Code", Falls Church, VA, USA.

50. Industry Handbook Committee (2004), "PCI Design Handbook: Precast and Prestressed Concrete Institute", 6th ed., *PCI MNL 120-04*, Skokie, IL, USA.

51. ISO 834 (1975), "Fire Resistance Tests – Elements of Building Construction. International Organization for Standardization".

52. Jansson R. (2008). "Material Properties of Fire Spalling of Concrete", *Rep. No. TVBM-3143*, Division of Building Fire Safety and Technology, Lund Institute of Technology, Lund University, Sweden.

53. Kodur V.K.R. and Dwaikat M.D. (2008) "Effect of Fire Induced Spalling on the Response of Reinforced Concrete Beams", *International Journal of Concrete Structures and Materials*, 2(2), pp. 71 – 81.

54. Kodur V.K.R., Dwaikat M.M.S., and Dwaikat M.B. (2008), "High Temperature Properties of Concrete for Fire Resistance Modeling of Structures", *ACI Material Journal*, 105(5), pp. 517 – 527.

55. Kodur V. R. and Harmathy T.Z. (2008), "Properties of building materials" Editor: DiNenno P.J., *SFPE Handbook of Fire Protection Engineering*, 4th ed., National Fire Protection Association, Quincy, MA, pp. 1.167-1.195.

56. Kodur V.K.R. and Sultan M.A. (2003), “ Effect of Temperature on Thermal and Properties of High Strength Concrete”, *Journal of Materials in Civil Engineering*, 15(2), pp. 101 – 107.

57. Khoury, G.A. and Anderberg, Y. (2000), “Concrete Spalling – Review, *Fire Safety Design,* Report Submitted to Swedish National Road Administration, Borlange, Sweden .

58. LeClair P.J. and Shaikh A.F. (1996), “Effect of Elevated Temeprature on Bond Strength of Epoxy-Coated Prestressing Strand”, *Prestressed Concrete Institute*, 41(4), pp. 54 – 60.

59. Li M., Qian C.X., and Sun W. (2004), “Mechanical Properties of High-Strength Concrete After Fire”, *Cement and Concrete Research*, 34(6), pp. 1001 – 1005.

60. Lier G. (1983), “Creep of Structural Steel Fire: Analytical Expressions.” *Fire and Materials*, 7(2), pp. 73-78.

61. Lin T.D., Gustaferro A.H., and Abrams M.S. (1981), “Fire Endurance of Continuous Reinforced Concrete Beams”, *R&D Bulletin RD006B*, Portland Cement Association, Skokie, IL, USA.

62. MacLean K. (2007), “Post-fire Assessment of Unbonded Post-tensioned Concrete Slabs: Strand Deterioration and Prestress Loss”, M.S. Thesis, Department of Civil Engineering, Queens University, Kingston, Ontario, Canada.

63. Magnusson S.E. and Thelandersson S. (1970), “Temperature-time Curves of Complete Process of Fire Development. Theoretical Study of Wood Fuel Fires in Enclosed Spaces”, *Acta Polytechnica Scandanavia Civil Engineering and Building Construction*, 65(1), pp. 1 – 181.

64. Malhorta H.L. (1984), “Spalling of Concrete in Fires”, *Technical Note No. 118*, Construction Industry Research and Information Association, London, England.

65. Naus, D. G. (2005). “The Effect of Elevated Temperature on Concrete Materials and Structures – A Literature Review”, NRC Fin No. Y6741, U.S. Nuclear Regulatory Commission, Oak Ridge, TN, USA.

66. Neves I.C., Rodrigues J.P.C., and Loureiro A.D.P. (1996), "Mechanical Properties of Reinforcing and Prestressing Steel After Heating", *Journal of Materials in Civil Engineering*, 8(4), pp. 189 – 194.

67. Parkinson D.L. and Kodur V.K.R. (2007), "Performance-Based Design of Structural Steel for Fire Conditions – A Calculation Methodology", *International Journal of Steel Structures*, 7(3), pp. 219 – 226.

68. Pettersson, O. (1965). "Structural fire engineering research today and tomorrow." Acta Polytechnica Scandinavica, Civil Engineering and Building Construction Series No. 33, Stockholm, pp. 42-55.

69. Phan L.T. (1996), "Fire Performance of High-strength concrete. A Report of the State-of-the-Art", *NISTIR 5934*, National Institute of Standards and Technology, Gaithersburg, MD, USA.

70. Saad M., Abo-El-Enein S.A., Hanna G.B., and Kotkata M.F. (1996), "Effect of Temperature on Physical and Mechanical Properties of Concrete Containing Silica Fume", *Cement and Concrete Research*, 26(5), pp. 669 – 675.

71. Saito, H. (1965). "Explosive spalling of prestressed concrete in fire." BRI Occasional Report No. 22, Building Research Institute, Ministry of Construction, Tokyo, pp. 18.

72. Schneider, U., Diedrichs, U., and Ehm, C. (1981), "Effect of Temperature on Steel and Concrete for PCRV's", *Nuclear Engineering and Design*, 67, pp. 245-258.

73. Shin K.Y., Kim S.B., Kim J.H., and Jung P.S. (2002), "Thermo-Physical Properties and Transient Heat Transfer of Concrete at Elevated Temperatures", *Nuclear Engineering and Design*, 212(1-3), pp. 233-241.

74. Selvaggio S.L. and Carlson C.C. (1963), "Effect of Restraint on Fire Resistance of Prestressed Concrete", *Special Technical Publication 344*, American Society for Testing and Materials, West Conshohocken, PA, USA.

75. Selvaggio S.L. and Carlson C.C. (1964), "Fire Resistance of Prestressed Concrete Beams Study: Influence of Aggregate and Load Intensity", *Prestressed Concrete Institute*, 6(4), pp. 10 – 25.

76. Society of Fire Protection Engineers (2011), "SFPE Standard on Calculating Fire Exposures to Structures", Bethesda, MD, USA.

77. UL Fire Resistance Directory (1996), "Online Certification Directory BXUV.J945-J947," Underwriters Laboratories Inc, Camas, WA, USA.

78. Wang T.C., Cheng F.P. and Kodur V.K.R. (2004), "Predicting the Fire Resistance Behavior of High Strength Concrete Columns", *Cement and Concrete Composites*, 26(2), pp. 141 – 153.

79. Wenzhong, Z., Qiong, H., and Haoyu, Z. (2007), "Experimental Research on the Mechanical Property of Prestressing Wire During and After Heating", *Frontiers of Architecture and Civil Engineering in China*, 1(2), pp. 247-254.

80. Woods H. (1960), "Research on Fire Resistance of Prestressed Concrete", *Journal of Structural Division, Proceedings of the American Society of Civil Engineers*, 86(11), pp. 53 – 56.

81. Yafei, S., Yongjun, T., Jing, S., and Dongjie, N. (2009), "Effect of Temperature and Composition on Thermal Properties of Carbon Steel", *Proceedings of the 21st Annual International Conference on Chinese Control and Decision Conference"*, Guilin, China, pp. 3756-3760.

82. Zheng W., Hu Q., and Zhang H. (2007), "Experimental Research on the Mechnaical Property of Prestressing Steel Wire During and After Heating", *Frontiers of Architecture and Civil Engineering in China*, 1(2), pp. 247 – 254.

83. Zollman C.C. and Garavaglia M.G. (1960), "Prestressed Concrete Resists Fire Damage", *Civil Engineering, 30(12), pp. 36 – 41*.